Microfluidic capillary systems for microarraying and diagnostic applications

Roozbeh (Hosseinali) Safavieh

Doctor of Philosophy

Department of Biomedical Engineering

McGill University

Montreal, Quebec, Canada

A thesis submitted to McGill University in partial fulfillment of the requirements of

the degree of Doctor of Philosophy

July 2013

"There is no duty more indispensable than that of returning a kindness". Cicero

Acknowledgement

I am thankful to my supervisor, Prof. David Juncker, for his exceptional patience, technical guidance, extraordinary leadership, and support throughout my PhD. With his help, I learnt how to think outside the box, and not to be scared of taking risks. I am also very grateful of him for giving me the opportunity to attend in various conferences and present the results of my research.

Also, I would like to express my gratitude to my committee members Profs. Hanadi Sleiman, David Sinton and Henrietta Galiana for their technical advice and help.

Dr. Mateu Pla-Roca was my mentor during the first year of my PhD. I am very thankful of him. He supported and taught me a lot. Additionally, I would like to acknowledge Prof. Elizabeth Jones for providing me the access to the microscope facilities in her lab.

My special thanks go to the past and present members of my research group, and my friends, in particular, Mohammad Ameen Qasaimeh, Dr. Maryam Mirzaei, Setareh Ghorbanian, Dr. Nikola Perkas, Dr. Ali Tamayol, Dr. Tohid Fetanat, Dr. Babak Khorsandi, Dr. Payam Mousavi, Dr. Mohammad Malekian and

Dedication

I dedicate this thesis to my parents,

who always valued education and taught me tenacity, hard work, and honesty.

There was a door to which I found no Key:

There was a veil past which I could not see:

Some little talk awhile of me and thee

There seem'd - and then no more of thee and me.

Omar Khayyám

راست چون سوسن و گل از اثر صحبت پاک

بر زبان بود مرا آن چه تو را در دل بود

حافظ

Contributions of authors

This thesis is organized as a collection of articles written by the candidate with the contributions from the co-authors. Chapters 1&2 present research objectives and the background knowledge of the thesis. As for the results of chapters 3-6, each chapter was published or submitted in a peer-reviewed scientific journal. Finally, chapter 7 concludes the thesis by providing a summary of our findings and presenting the future prospects of this work. In all the articles the candidate designed and performed the experiments, analysed the experimental data, and developed a theoretical models for most of the experiments. My supervisor, Dr. David Juncker, appears as the co-author of the papers to acknowledge his leadership in the research projects, efforts in defining the questions needed to be investigated, helping to analyse the data, as well as his involvement in writing the manuscripts. On the third chapter, Dr. Mateu Pla-roca, Dr. Maryam Mirzaei, and Dr. Mohammad Ameen Qasaimeh appear as the co-authors. Dr. Mateu Pla-roca helped me to learn microfabrication, and thought how to functionalize the surface of the pins. Also Dr. Maryam Mirzaei and Mohammad Ameen Qasaimeh contributed on preparing the manuscript. On the forth chapter, Gina Zhou appears as the co-author of the paper to acknowledge her contribution on taking micrographs of the fibers and preparing the manuscript. Last, Dr. Ali Tamayol

appears as the co-author on chapter 5 to acknowledge his contribution on manuscript preparation.

Table of contents

viii

List of tables

List of figures

Abstract

Microfluidic capillary systems are devices, in which the liquid is driven and controlled only by surface tension (capillarity) forces. These devices are self-powered and self-regulated, as the energy required to drive and control the liquid is structurally and chemically encoded in the microscale conduits. The objective of this thesis is to develop materials and propose novel architectures to expand the functionalities of these systems in the context of microarray spotting and diagnostic applications.

Silicon and steel pins are popularly used for microarray spotting; however, these pins are expensive, and in the case of silicon, brittle, and can damage the substrate during the printing process. To solve these issues, we optimize the design and propose a new fabrication process to make miniaturized quill pins out of a negative tone epoxy-based photoresist, SU-8. These pins are inexpensive, easy to fabricate and robust, and may be used as disposable pins for spotting microarrays.

For global health applications, microfluidic systems need to be very low cost, which is difficult to achieve with microfabricated systems. Here, we present cotton yarns as a new material for making ultra-low cost microfluidic devices, which can transport minute amount of liquids by capillarity. We study the flow properties of yarn and demonstrate using knots for splitting, mixing and merging

of fluid streams. We also show that the knot topology can be used to control the mixing ratio between two inlets and two outlets. Finally, we build a serial dilutor by iterative combining of mixing and splitting of fluids using a knotted web, and analyze the fluid distribution using network analysis concepts developed for electrical circuit analysis, and compare the theoretical and experimental results.

One of the major challenges in capillary systems is to make circuits which can perform complex fluidic operations. To enhance the capabilities of these systems, we introduce novel architectures of capillary pumps for precisely pumping liquids and metering samples as well as valves for switching between liquids and timing the reactions. We then combine these elements with other capillary elements, which had already been developed such as flow resistors and capillary retention valves, to build a capillary circuit that following sample addition, autonomously delivers a defined sequence of multiple chemicals according to a preprogrammed and predetermined flow rate and time. We illustrate that as in electronics, complex capillary circuits may be built by combining simple capillary elements. We define such circuits as "capillarics". As a proof of concept we use such a circuit for measuring the concentration of C-reactive protein down to 100 ng/mL in 5 mins.

Last, we summarize our findings, and propose some of the future works that offer exciting prospects for the future research.

Résumé

Les systèmes capillaires microfluidiques sont des dispositifs dans lesquels un liquide est conduit et contrôlé uniquement par des forces de tension superficielle (capillarité). Ces appareils sont autoalimentés et autorégulés, car l'énergie requise pour conduire et contrôler le liquide est structurellement et chimiquement encodée dans les microconduits. L'objectif de cette thèse est de développer des matériaux et de proposer de nouvelles architectures dans le but d'élargir les fonctionnalités de ces systèmes dans le contexte de repérage de micromatrices et dans des applications de diagnostic.

Les broches de silicium et d'acier sont utilisées fréquemment dans les micromatrices; cependant, ces broches en silicium sont dispendieuses et fragiles, et peuvent endommager le substrat durant le processus d'impression. Pour résoudre ces problèmes, nous avons optimisé la conception et proposons un nouveau procédé permettant de fabriquer des broches miniaturisées à partir de résine photosensible négative de type époxyde SU-8. Ces broches sont peu coûteuses, faciles à fabriquer, robustes, et peuvent être utilisées comme broches jetable pour le repérage de micromatrices.

Afin d'être utilisés dans des applications de santé à l'échelle globale, les systèmes microfluidiques doivent être peu coûteux, ce qui est difficile à réaliser pour les systèmes élaborés par des techniques de microfabrication. Ici, nous

présentons le fils de coton comme un nouveau matériau dans la fabrication d'appareils microfluidiques à très faible coût qui peuvent transporter d'infimes quantités de liquide par capillarité. Nous étudions et démontrons ici les propriétés rhéologiques du fil en utilisant des nœuds pour la division, le mélange, et la fusion de flux de liquides. Nous démontrons également que la topologie du nœud peut être utilisée pour contrôler le rapport de mélange entre deux entrées et deux sorties. Finalement, nous fabriquons un dilueur en série par combinaison itérative de mélange et division de fluides en utilisant une toile nouée, et analysons la distribution des liquides à l'aide de concepts d'analyse de réseau développés pour l'analyse de circuits électriques, et comparons les résultats théoriques et expérimentaux.

L'un des défis majeurs dans les systèmes capillaires est de faire des circuits pouvant performer des opérations fluidiques complexes. Pour améliorer la capacité de ces systèmes, nous introduisons de nouvelles architectures de pompes capillaires pour le pompage de liquides et la mesure d'échantillons plus précis, ainsi que des valves pour la commutation des liquides et la mesure du temps de réaction. Nous combinons ensuite ces éléments à d'autres éléments capillaires qui ont déjà été développés, tels que les résistances au flux et les valves de rétention capillaire, pour construire un circuit capillaire qui, après l'addition de l'échantillon, délivre de façon autonome une séquence définie de

multiples produits chimiques selon un débit et un temps préprogrammés et prédéfinis. Nous illustrons que tout comme ce que l'on observe dans les circuits électriques, des circuits capillaires complexes peuvent être bâtis en combinant de simples éléments capillaires. Nous définissons ces circuits en tant que « capillarics ». Nous avons utilisé un tel circuit pour mesurer la concentration de la protéine C réactive jusqu'à 100ng/ml en cinq minutes en tant que preuve de principe.

Finalement, nous résumons nos découvertes, et proposons quelques-uns des travaux futurs qui offrent des perspectives excitantes pour la recherche future.

Chapter 1: Introduction

1.1 Background

In vitro diagnostics are a significant part of clinical practice. These bioassays use bodily fluids such as blood, urine, and saliva to detect, monitor or even prevent medical conditions. However, these analyses often involve time-consuming protocols and expensive reagents. Miniaturization of conventional bioassays may provide many advantages. For example, the evaluation of diagnostic markers can be performed using small quantities of sample and reagents. In addition, since the miniaturization of the assay increases the surface-to-volume ratio, this would accelerate mass transfer limited reactions, and thus increase the speed of the assay. Moreover, it renders the diagnostic devices portable and easy to use. Microfluidic capillary systems, in which all the actions required to manipulate the liquids are performed solely using capillary forces, do not need external pumps and valves to regulate and drive the liquids. As a result, these systems are being increasingly exploited for making self-powered and low-cost biological tests.

Microarray spotters and point-of-care (POC) diagnostic devices are important tools that are commonly used to perform bioassays and have the advantage of portability and convenience of capillary systems.

Microarray spotters print an array of micro-size spots on a glass slide or other substrates such as nitrocellulose.[1] The main advantage of microarray spotting is that hundreds of different biomolecules can be printed simultaneously in a dense array of small spots using a minute volume of solution. These spots usually consist of proteins or DNAs. Protein microarrays are employed to analyze protein-protein or protein-ligand (DNA, lipid, drug) interactions following an immunoassay. DNA microarrays are used to measure gene expression levels in a sample.[2] To print and pattern the array of spots, pin spotting is commonly used.[3] This process first involves dipping an array of pins into a 96- or 384-well microtiter plate containing spotting solutions. This will cause the solutions to spontaneously fill the slits of the pins by capillarity. Then, by contacting the tip of these pins onto a hydrophilic surface (i.e. glass slide), the solutions are printed from the pins to the surface. The liquid transfer is a result of the balance between the wettability of the liquid-pin and liquid-substrate interfaces. The efficiency of the microarray spotting depends on spot uniformity and density. It would therefore be beneficial to develop slit-pins, which may be inexpensive and ideally disposable, to prevent solution contamination and, at the same time, print spots uniformly in a dense array.

POC devices are portable diagnostic tests that can directly evaluate a patient's condition without requiring a central laboratory.[4] The World Health Organization (WHO)[5] has established benchmark criteria, termed the ASSURED (Affordable, Sensitive, Specific, User-friendly, Rapid and robust, Equipment-free and Deliverable to end users) criteria, for evaluating ideal POC devices.[6]

POC devices consist of a liquid handling mechanism and, in some cases, an interface. The POC interface is designed for either sample preparation (i.e. assays using Polymerase Chain Reaction (PCR)), signal quantification, and recording and reporting of the assay results. The liquid handler is designed to autonomously change the concentration of reagents over a local region (i.e. capture zone) with respect to time. In central laboratories, this process is commonly performed using an automated liquid handling system (i.e. pipettes and giant robotic systems).[7] Thus, the challenge for an ideal POC liquid-handler is to operate these functions while meeting ASSURED criteria.

1.2 Research Objective

Our objective is to develop novel enabling technologies to enhance the functionality of microfluidic capillary systems. The first technology described here is a fabrication process for making polymeric pins for microarray spotting.

Currently, silicon (Si) and steel pin spotters are used for printing DNA and protein microarrays. These pins are expensive and may be brittle (as is the case for Si), thus damaging the substrate during the printing process. Therefore, our main goal is to replace these commonly used pins with ones made out of an SU-8 UV cross-linked polymer. This is accomplished through introducing a novel fabrication process, which eliminates the residual stress formed during the fabrication of SU-8 structures. This process allows for making 30mm-long straight pins without bending significantly. The SU-8 pins are resilient and can buckle without damage during the printing process.

The second technology described here employs sewing yarn and knots as the building blocks for making capillary driven microfluidic circuits. Miniaturization of fluidic channels can reduce sample consumption and enable multiplexing of the assays. However, these devices often require costly photolithography equipment or printing facilities. Thus, the goal of this work is to develop a low-cost and scalable solution to manipulate and regulate minute liquid volumes by capillary forces using yarn and knots. In particular, we aim to introduce basic capillary driven microfluidic elements, including flow routers, mixers, resistors, and pumps using knotted yarn. These knotted microfluidic elements can then be assembled using knots to make microfluidic circuits.

The final goal of this thesis is to enhance the capabilities of autonomous microfluidic capillary (AMC) systems by developing novel functional elements such as capillary encoded pumps (CPs) and capillary valves. First, we develop two novel CPs. These pumps avoid bubble trapping by guiding the progression of the liquid filling front. We also explore the filling behavior of such CPs and study how the flow resistance and capillary pressure of a CP vary as it is being filled. In addition, we present a novel capillary trigger valve (TV) and programmable retention burst valves (RBVs). The TV enables the liquid to stop passively, and can then be triggered when needed. RBVs facilitate pre-programmed switching between liquids using only capillary forces. By selectively assembling these elements, we demonstrate a capillary circuit that can autonomously meter samples and switch between liquids at programmed flow rates without any need for external pumps or valves. This circuit is suitable for numerous assays or chemical reactions that require appropriate flow control of liquids and reagents. AMC systems are commonly applied in rapid point-of-care (POC) immunodiagnostic devices, where miniaturization of immunoassays and portability are required. Thus, as a proof of concept, we employ the circuit to perform a one-step sandwich immunoassay to measure the concentration of C-reactive protein. To do so, all reagents are preloaded in the circuit and, upon introducing the sample, the concentration of the analyte is quantified by

5

measuring the intensity of the fluorescent dye using fluorescence microscopy. Advancement of these AMC circuits may lead to in vitro diagnostics that can perform highly sensitive, quantitative assays within a short time and at an affordable cost.

1.3 Thesis Overview

This thesis covers our work on the development of various platforms of microfluidic capillary systems and is organized as follows:

In Chapter 2, we introduce dominant physical phenomena in microfluidics, including laminar flow, liquid surface tension, wetting, and capillary pressure. We also provide a historical review of the inventions that lead to the evolution of microfluidics from 1947 onwards. Subsequently, we present examples of microfluidic liquid handling devices with the main focus on capillary systems. Finally, we provide an overview of immunoassays and various detection systems which can be integrated with microfluidic immunoassays.

Chapter 3 is dedicated to the development of straight SU-8 pins for microarray spotting. We present a novel fabrication process for making miniaturized straight quill pins out of polymer SU-8. These pins each contains a slit, which is filled by

surface tension forces and can be arrayed to spot multiple proteins at once. Since residual stress forms during the fabrication of SU-8 structures, we developed an annealing method that relieves SU-8 from its internal stress, and allows for making straight pins 30 millimeters in length without measurable bending. The low processing cost of these pins could lead to disposable microarray systems, rendering the technique of bio-molecular microarray analysis more affordable, faster, and more accessible to the scientific community. Chapter 4 demonstrates the development of an ultra-low-cost microfluidic capillary system made out of yarn and knots. We describe the methods used to characterize and modify basic fluidic properties of the yarn, and give examples using cotton yarn to construct autonomous passive microfluidics that transport fluids according to a predetermined sequence. We also modify the surface property of the cotton to improve its hydrophilicity, and then measure the flow resistance of the yarn. Subsequently, we employ knots to control the flow resistance and to make various microfluidic elements, such as passive splitters, blenders and mixers, out of yarn. We also quantify the mixing ratios of the proposed knotted mixers, and show that topologically different knots can confer different mixing ratios. Finally, we make a web of knots, which can be used as a serial dilutor.

Chapter 5 introduces two novel architectures of capillary pumps (CPs). These pumps consist of arrays of hydrophilic posts, providing precise capillary pressure with small flow resistance. We show that these platforms prevent the entrapment of bubbles by controlling the propagation of the filling front. We then demonstrate the flexibility and robustness of the design using CPs with different filling angles. Moreover, we calculate the flow resistance of a CP as it is being filled using a pore network modelling approach, and validate our calculations experimentally. Finally, we develop a CP with a gradient of capillary pressure in which the liquid flow rate can be regulated with respect to the position of the liquid filling front.

Chapter 6 discusses the development of pre-programmed capillary circuits using a limited number of capillary elements as their building elements. We call this concept *capillarics* as an analogy to electronics, in which complicated electronic circuits can be made out of a number of electrical elements. We first introduce robust capillary trigger valves and retention burst valves, and then combine these building elements with other capillary-based elements to develop a capillary circuit that has the ability to autonomously meter the sample, switch between liquids, and time the reactions. Finally, as a proof of concept, we employ the capillary circuit to perform a one-step sandwich immunoassay for measuring the concentration of a C-reactive protein.

Chapter 7 provides a discussion and summary of our findings and outlines the future prospects of this work.

1.4 References

1. Barbulovic-Nad, I. Lucente, M., Sun, Y., Zhang, M., Wheeler, A.R. & Bussmann, M. Bio-microarray fabrication techniques - A review. *Critical Reviews in Biotechnology* **26**, 237-259 (2006).
2. Choudhuri, S. Microarrays in biology and medicine. *Journal of Biochemical and Molecular Toxicology* **18**, 171-179 (2004).
3. Schena, M., Shalon, D., Davis, R.W. & Brown, P.O. Quantitative Monitoring of gene-expression patterns with a complementary-DNA microarray. *Science* **270**, 467-470 (1995).
4. Kost, G.J. (ed.) Principles and Practice of Point-of-Care Testing, first edition. (Lippincott Williams & Wilkins, 2002).
5. World Health Organization: WHO, http://www.who.int/, Retrieved (2013).
6. Mabey, D., Peeling, R.W., Ustianowski, A. & Perkins, M.D. Diagnostics for the developing world. *Nature Reviews Microbiology* **2**, 231-240 (2004).
7. Kong, F., Zheng, Y.F. & Chen, W. Automatic liquid handling for life sciences – a critical review of the current state-of-the-art, *IEEE International Conference on Robotics and Biomimetic*s, **1**, 480-486 (2009).

Chapter 2: Background Knowledge

2.1 Microfluidics

Microfluidics refers to the science and technology of manipulating fluids with length scales of less than a millimeter and greater than one micron.[1] To depict the relative size of microchannels in comparison to other chemical and biological substances, Fig. 2.1 illustrates the size of various molecules and simple microorganisms with one millimeter as a scale unit.[2] Due to the small length scale of microchannels, microfluidic devices have led to the significant changes in countless applications, including chemical and particulate separation and analysis, biological characterization and biosensors.[3] Miniaturization of fluidic devices is useful because it allows us to work with smaller reagent volumes, thus reducing the cost of analysis, enabling parallel operations, and decreasing reaction times by increasing the surface-to-volume ratio and accelerating mass transfer limited reactions.[4]
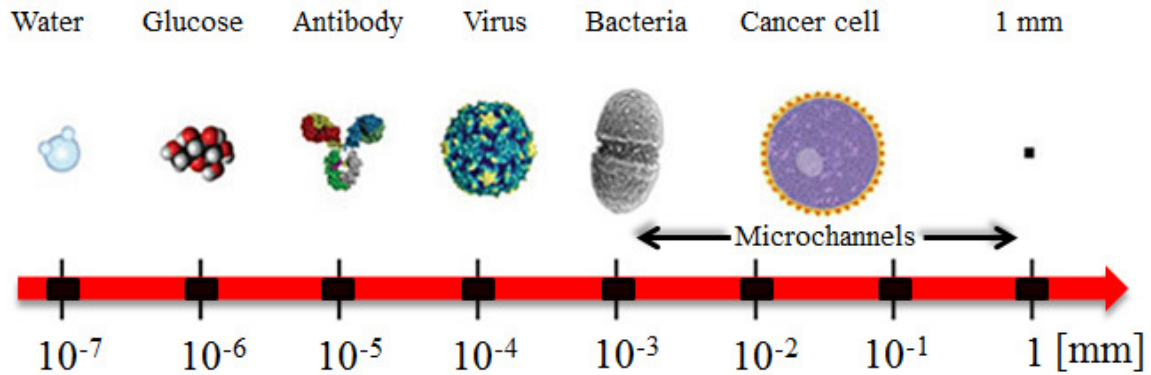
Fig. 2.1: Length scale of some chemical/biological substances, ranging from a few angstroms (e.g. water) to tens of micrometers (e.g. large cells). The comparative length scale of the microchannels (i.e. 10^{-3} mm to 1 mm) enables us to efficiently work with these chemicals. Reproduced from the website of US National Cancer Institute.[2]

In order to take advantage of the opportunities brought about by shrinking the length scales of microfluidic devices, it is important to know the physical phenomena that occur at these microscales. Some of these phenomena include laminar flow, capillarity, and wetting, which are explained in the sections below.

2.1.1 Laminar Flow

In general, the flow of a fluid can be investigated based on the ratio of the inertial to viscous forces. This ratio can be expressed as a non-dimensional number

called Reynolds number (*Re*), and, as for the flow in a conduit, it can be formulated as:[5]

$$\mathrm{Re} = \frac{\rho U \, D_h}{\mu}$$

(2.1)

where ρ and μ are the density and viscosity of the fluid, respectively, U is the velocity magnitude of the flow, and D_h is the characteristic length of the flow. For a microchannel, D_h is equal to the hydraulic diameter, which is defined as:

$$D_h = \frac{4A}{P}$$

(2.2)

where A and P are the area and the premier of the conduit cross section, respectively. When the inertial forces are small enough relative to the viscous forces, the fluid flows in parallel layers, and the condition is called laminar flow. In contrast, when the inertial forces outweigh the viscous forces, then the fluid undergoes stochastic fluctuations, which is called turbulent flow.[6] Fig. 2.2 illustrates streamlines in both laminar and turbulent flows.
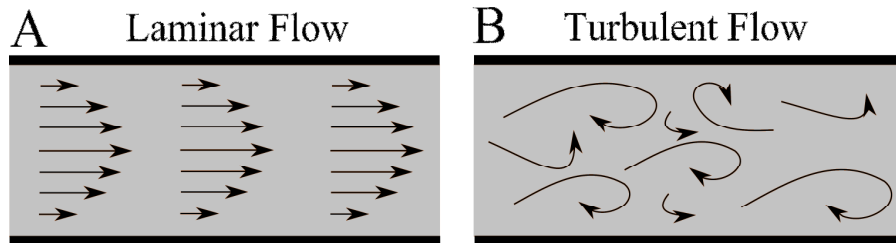
Fig. 2.2: Comparison of streamlines in both laminar and turbulent flow.

The onset transition threshold for the *Re* number to switch from laminar to turbulent flow is highly dependent on geometry, surface roughness, and the

length scale of the flow.[5] For example, for flow through a smooth channel, $Re < 2200$ is generally considered as laminar flow,[7] whereas a cylindrical liquid jet at $Re \sim 20$ is considered completely turbulent.[8]

Due to the small size of microchannels, flow inside these conduits is laminar. If we consider the fluid to be a Newtonian liquid, the continuity and momentum equations of flow can be written as:[5]

$$\nabla^2 \vec{U} = 0 \tag{2.3}$$

$$\rho \left(\frac{\partial \vec{U}}{t} + \nabla.\nabla \vec{U} \right) = -\nabla P + \rho \vec{g} + \mu \nabla^2 \vec{U} \tag{2.4}$$

where $\vec{U}$ is the velocity vector of the flow, t is time, P is pressure, and $\vec{g}$ is the gravitational vector.

As for flow through a conduit, under specific conditions, where only a pressure gradient is applied to drive the liquid, the flow is fully developed ($\nabla.\nabla \vec{U} = 0$), steady state ($\frac{\partial \vec{U}}{t} = 0$), with no effect from gravitational forces ($\rho \vec{g} = 0$), the flow is called a Poiseuille flow, and the Navier-Stokes equation (Eq. (2.4)) can be simplified and thus solved analytically to calculate the hydrodynamics of the flow. For example, for a Poiseuille flow in a circular straight conduit, the flow rate becomes:

13

$$Q = \frac{\Delta P}{8\mu L} \times \pi \times r^4 \qquad (2.5)$$

where r and L are the radius and the length of the conduit, respectively, ΔP is

the pressure drop across the conduit, and Q is the volumetric flow rate.
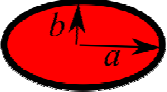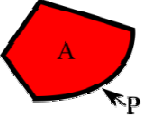
2.1.2 Flow Resistance

In Poiseuille flows, the pressure drop across the conduit (ΔP) and the flow rate

(Q) can be correlated with a constant parameter, which is a function of the

conduit geometry and the viscosity of the fluid. This parameter is called flow

resistance, and can simplify the hydrodynamic solution for the flow as:

$$Q = \frac{\Delta P}{R} \qquad (2.6)$$

The flow in fluidic networks can be calculated using the same approach as that

used to analyze electrical circuits (i.e. Kirchhoff's circuit laws).[9] In this case, Eq.

(2.6) can correspond to Ohm's law ($I = \frac{\Delta V}{R}$) in electrical circuits,[9] where the flow

rate (Q) is analogous to electrical current (I), and ΔP is equivalent to ΔV. The

flow resistances for various conduits with different geometries have previously

been calculated.[10] Table 2.1 lists the flow resistances of some of these conduits.

Table 2.1: A list of flow resistances of straight conduits with different cross sections[10]

Shape		R
Circle		$\dfrac{8 \times \mu \times L}{\pi \times r^4}$
Ellipse		$\dfrac{4 \times \mu \times L \times \left(1 + \left(\dfrac{b}{a}\right)^2\right)}{\pi \times \left(\dfrac{b}{a}\right)^3 \times a^4}$
Triangle		$\dfrac{320 \times \mu \times L}{\sqrt{3} \times a^4}$
Rectangle		$\left[\left(\dfrac{w \times h^3}{12 \times \mu \times L}\right) \times \left(1 - \dfrac{192 \times h}{\pi^5 \times w} \tanh\left(\dfrac{\pi \times w}{2 \times h}\right)\right)\right]^{-1}$
Arbitrary		$\approx \dfrac{2 \times \mu \times L \times P}{A^3}$

2.1.3 Capillarity

Unlike a gas, a liquid cannot expand freely, and thus, always forms an interface with another liquid, gas, or solid; capillarity is caused by the interaction between these interfaces.[11] Molecules in a liquid are attracted to each other by cohesive forces. If we consider a molecule in the bulk of a liquid, it is attracted by all its neighbors and thus finds itself in an optimum energy state. However, when the molecule is on the surface of the liquid, it loses half of its cohesive interactions, putting it in an unfavorable energy state. Assuming the cohesive energy of a molecule deep within a liquid is "X", a molecule segregated on the surface has

an energy shortage of " $\dfrac{X}{2}$ ". This shortage of energy per unit of surface area is

defined as the surface tension.[12] For example, if a molecule has a diameter of

"d", and the surface area in the order of "$\cong d^2$", the surface tension, γ_{LG}, is in the

order of $\gamma_{LG} = \dfrac{X}{2 \times d^2}$.

In general, molecules with Van der Waals cohesive forces have small surface

tensions. For example, at 25°C most oils have a surface tension of

around $\cong 2 \times 10^{-2}$ N.m^{-1}. In contrast water, which contains hydrogen bonding, has

a fairly large surface tension (i.e. $\cong 7 \times 10^{-2}$ N.m^{-1}). Similarly, mercury contains

strong metallic bonds that significantly increase its surface tension

(i.e. $\cong 5 \times 10^{-1}$ N.m^{-1}).[12]

2.1.4 Wetting and Static Contact Angle

Wetting is the capability of a liquid to adhere to a solid or other liquid substrate.[12]

Various studies have been performed to investigate the collision of a liquid

droplet on a solid surface,[13] a thin liquid film,[14] or the bulk of a liquid.[15] When a

small droplet is deposited on a flat solid substrate, two scenarios may occur, as

shown in Fig. 2.3. Spreading parameter, *S,* which defines the difference between

the energy states of the system before and after deposition of the droplet (per

unit of surface area), is used to distinguish between two scenarios, and can be

expressed as:[12]

$$S = G_{dry\ substrate} - G_{wet\ substrate}$$ (2.7)

or alternatively,

$$S = \gamma_{SG} - (\gamma_{SL} + \gamma_{LG})$$ (2.8)

where γ_{SG}, γ_{SL} and γ_{LG} are the surface tensions of the solid/gas, solid/liquid and

liquid/gas interfaces, respectively.

In the scenario where $S>0$, the liquid wets the entire surface so as to lower its

energy state and ideally, where there is no evaporation, a thin film of liquid with

nanometer thickness is formed on the substrate. In this scenario, the static

contact angle between the liquid and the solid surface is zero ($\Theta_E=0°$) and it is

called total wetting.

In the scenario where $S<0$, the droplet forms a spherical cap deposited on the

surface, and the phenomenon is called partial wetting. In the case of using water

as the liquid, two conditions are possible: (i) if $\Theta_E<90°$, the substrate is called

hydrophilic or (ii) if $\Theta_E>90°$, the surface is called hydrophobic.
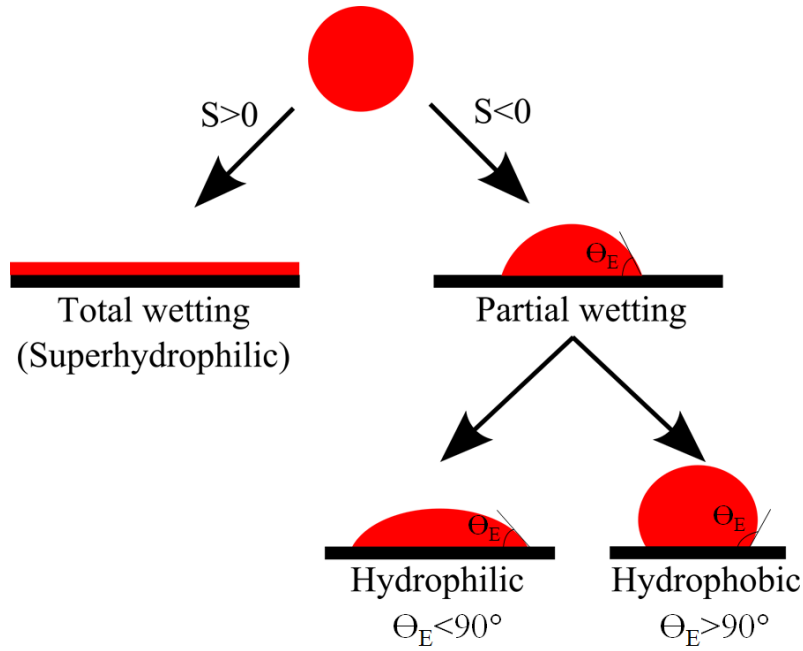
Fig. 2.3: Possible wetting scenarios following the deposition of a droplet on a solid surface; two conditions are possible: if S>0, the droplet completely wets the surface and is called total wetting (θ_E=0°), whereas if S<0, a minimal energy state is produced where the droplet only partially wets the substrate and is called partial wetting. In this condition two scenarios are possible: in the case where θ_E<90°, the substrate is called hydrophilic, whereas in the case where θ_E>90°, the substrate is called hydrophobic.

When a droplet is deposited on a flat substrate, Young's equation can be used to correlate the surface tensions of three phases with the static contact angle as:[16]

$$\gamma_{LG} \times \cos\theta_E = \gamma_{SG} - \gamma_{SL} \tag{2.9}$$

In general, high energy substrates, such as those composed of materials with metallic, and ionic bonds have a tendency to make more wettable surfaces compared to lower energy substrates with covalent bonds such as polymers.[17]

2.1.5 Advancing and Receding Contact Angles

The static contact angle, Θ_E defined in Young's equation is valid only when the substrate is planar without any surface contamination.[12] However, when we inflate a small droplet, the contact angle starts increasing without any motion of the liquid/solid contact line. If we keep inflating the droplet after it reaches the threshold value for the contact angle, the contact line of the droplet also begins to move; this threshold value of the contact angle is called advancing contact angle, Θ_a, as shown in Fig. 2.4A.

Similarly, when we deflate a droplet, the static contact angle decreases to a threshold value, after which the contact line begins to move; this value of the contact angle is called receding contact angle, Θ_r, as shown in Fig. 2.4B. The difference between the advancing and receding contact angles is called contact angle hysteresis.[12]
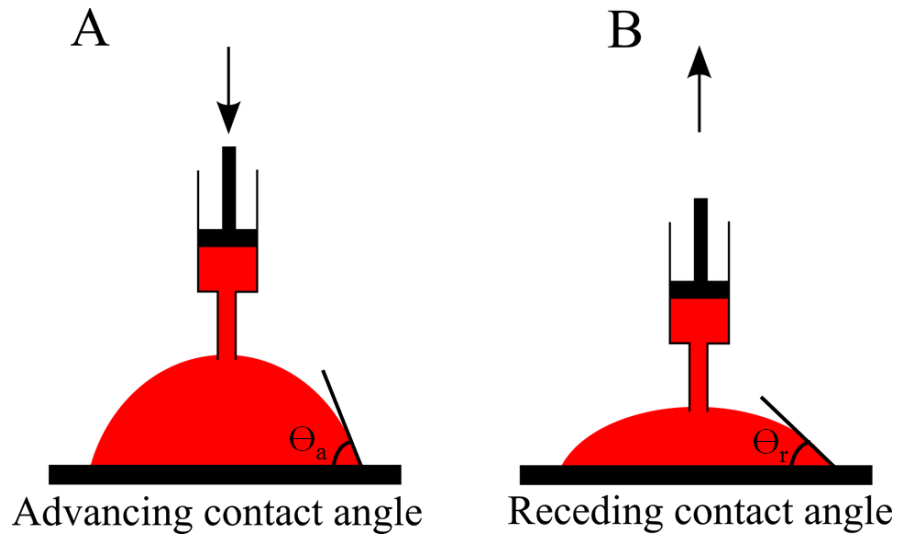
Fig. 2.4: Advancing and receding contact angles of a droplet. (A) The threshold contact angle when the liquid/solid contact line starts moving during droplet inflation is called advancing contact angle. (B) Similarly, a receding contact angle is defined as the contact angle after which the contact line begins to move while the droplet is deflated.

Various studies have been conducted to model the contact angle hysteresis and the variations in contact angles when the liquid/solid contact line moves. A comprehensive review on the topic can be found in the work by Eral *et al.*.[18]

2.1.6 Capillary Pressure in Microchannels

When a liquid is deposited at the inlet of a microchannel, in order for the liquid to spontaneously fill the conduit by capillarity, the interfacial energy of the system needs to be larger when it is in a dry state than when it is in a wet state , or:

$$\Delta G = \gamma_{SG} \times \Delta A_{SG} + \gamma_{SL} \times \Delta A_{SL} + \gamma_{LG} \times \Delta A_{LG} < 0 \qquad (2.10)$$

where ΔG is the respective changes in the interfacial energy in the two states and ΔA_{ij} are the changes in the interfacial areas in the solid, liquid, and gas phases. Eq. (2.10) is valid assuming that we can neglect the effects of gravitational forces. The variation in the interfacial energy of the system creates a pressure difference across the interface between the liquid and its neighboring media. This pressure difference is called capillary pressure, which can be correlated with the energy difference as: [19]

$$\Delta P = \frac{\Delta G}{V_L} \qquad (2.11)$$

where ΔP is the capillary pressure, and V_L is the volume of the liquid transferred in to the system. The capillary pressure provides a negative pressure and pulls the liquid inside the conduit. Using Eqs. (2.9), (2.10) and (2.11), the capillary pressure of straight microchannels with various geometries can be calculated. For example, the capillary pressure generated in a circular capillary with the radius of r can be written as:[20]

$$\Delta P = -\frac{2 \times \gamma_{LG} \times \cos\theta}{r} \qquad (2.12)$$

Similarly, a capillary pressure of a rectangular microchannel can be expressed as: [20]

$$\Delta P = -\gamma_{LG} \left(\frac{\cos\theta_b + \cos\theta_t}{w} + \frac{\cos\theta_l + \cos\theta_r}{h} \right) \qquad (2.13)$$

21

where w and h are the width and the height of the microchannel respectively, and the $\theta_{i=b,t,l,r}$ are the contact angles between the liquid and the bottom, top, left, and right walls of the microchannel.

It is worth mentioning that in some examples of capillary driven flows, such as when the conduit is not straight or some of the walls are hydrophobic, there are other effects such as corner flows, which play an important role in defining the capillary pressure, complicating the calculation.[21]

2.2 Birth and Evolution of Microfluidics

Although the fluid dynamics in microscale dimensions have been investigated since the 18th century [22, 23] in the context of viscous flow,[24, 25] liquid jet breakup,[26] colloidal sciences,[27] and plant biology,[28, 29] the development of methods and technologies to precisely dispense and regulate fluids in microscales only dates back to the 1950s, with the invention of inkjet printing.

In 1951, Elmqvist of Siemens was the first to patent an inkjet printing mechanism,[30] which can be recognized as the first microfluidic device. The invention was later developed and became the first commercial inkjet printer used for recording analog signals.[31] Following Elmqvist's design, major

companies such as IBM, Canon, and Hewlett-Packard developed various inkjet technologies for use in computer printers.[31] For example, in the 1970s, IBM introduced electrostatic inkjet printing technology, which was used for word processing hardcopy-output.[32] Similarly, Canon independently developed the bubble jet printer, where a small heater near the nozzle orifice generated the growth and collapse of a water vapor bubble that pushed the ink out of the nozzle. Subsequently, they used the technology for making low-cost inkjet printers.[33]

Although printing technologies continued to advance, microfluidic dispenser technology was not applied to the life sciences until the 1990s, when an interest in arraying a library of multiple targets, such as cellular genes, DNA, and protein, lead to the development of technologies such as the dot blot, and later, microarrays,[34-36] which allowed biochemical experiments to be performed in parallel.[37, 38] Due to the high throughput nature of these technologies, miniaturization and automation were necessary. As a result, in the last twenty years, various microfluidic spotters, including inkjet printers (1996),[39] pins (1997)[40] and TopSpot® printers(2000)[41, 42] were developed and adopted to generate microarrays. An interesting article reviewing various mechanisms of microfluidic spotters can be found in a work by Haeberle *et al.* [3]

The technology of making microfluidic devices, in which the fluid flows inside microchannels, dates back in the late 1970s. In 1979, Stephen Terry *et al.*[43] used the fabrication techniques for making micro-electromechanical systems (MEMS), and presented the first miniaturized gas chromatography device, which was the first MEMS-based microfluidic device. However, it was not until 1990 that microfluidic systems started to gradually gain attention. Anderias Manz *et al.*[44] were the first to introduce the concept of miniaturized total analysis systems (μTAS) and described the unique advantages of miniaturization, which lead to the development of various glass- and silicon-based microfluidic systems for the life sciences, including a capillary electrophoresis microfluidic chip.[45] After the development of glass- and silicon-based μTAS, another turning point in microfluidic technology was soft lithography, which was presented by Dr. Whitesides' lab in 1996.[46-48] The technique significantly decreased the capital investment required for the manufacturing of microfluidic devices, thus allowing the field to flourish and making it an attractive application for use in the life sciences. From 1998 onward, the field of microfluidics experienced rapid growth and brought about the introduction of various novel technologies to address complex biochemical and health-related problems; such technologies include multilayer soft lithography (2000)[49], autonomous capillary systems (2002),[50] and

paper-based microfluidics (2007)[51]. These techniques had various applications, such as high throughput analysis of biomarkers,[52] low-cost point-of-care diagnostics,[53, 54] and synthesis of microparticles,[55, 56] thus solidifying the role of microfluidics as a powerful tool in the life sciences. It is believed that the application of microfluidic devices will continue to grow and will be used to solve more complex health-related problems, such as diagnosis of complex diseases like cancer,[57] or personalized therapeutic techniques like gene therapy, by encoding DNAs to produce therapeutic protein drugs, or injecting the engineered DNAs for replacing the mutated genes in patients cells.[58] Fig. 2.5 illustrates the birth and evolution of microfluidic devices.
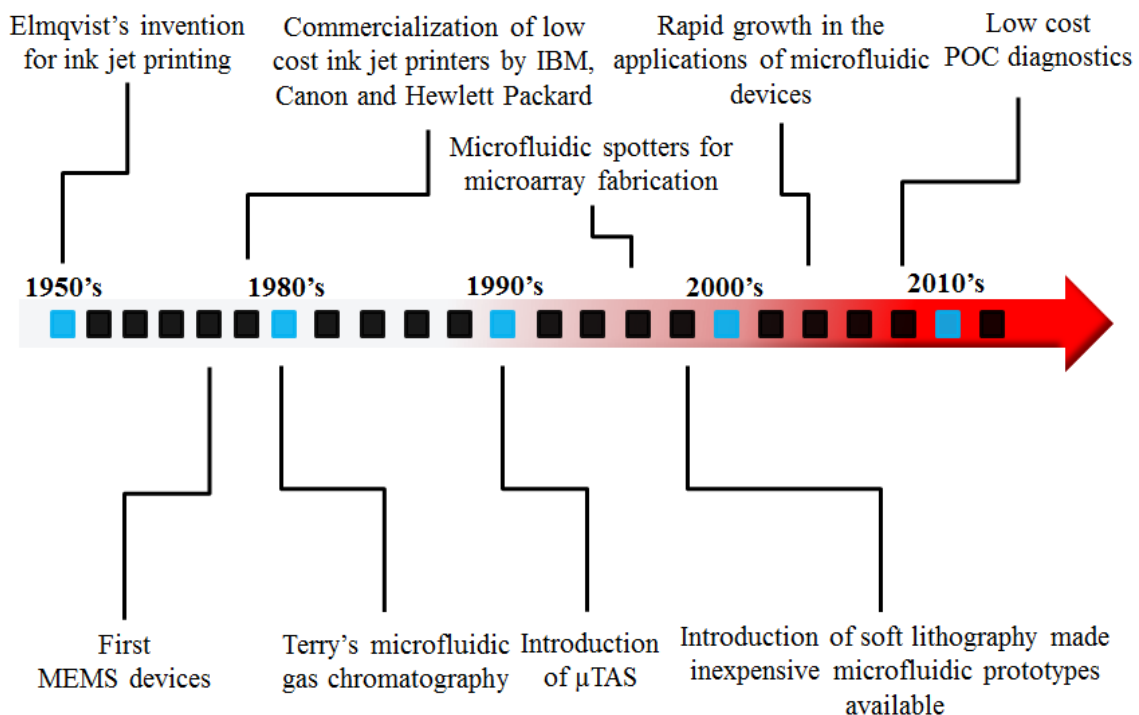
Fig. 2.5: Birth and Evolution of microfluidics. Modified from a graph by Gervais *et al.*[59]

2.3 Liquid Handling Mechanisms

To drive the liquids into the microchannels, various forces can be used to generate a pressure gradient in the conduits. Some of these forces include electric fields that generate electro-osmotic flow,[60] sound waves that generate acoustic streaming (acoustofluidics),[61] and mechanical forces that generate hydrodynamic pressure (i.e. using syringe pumps). However, most of these liquid-handling strategies require significant macro accessories, such as external pumps and complex power supplies,[62, 63] making them bulky and expensive to fabricate.

During the past decade, a number of microfluidic platforms have been proposed in which the liquid handling can be performed in a self-powered and self-contained format, making these devices portable. These systems include centrifuge-based microfluidics (Lab on a CD),[64] structurally programmable microfluidic systems (sPROMs),[65] chemically-powered microfluidic chips,[66, 67] electrophoretic-based microfluidic immunoassays,[68, 69] electro-wetting based digital microfluidics, [70] and microfluidic capillary systems.[50, 71] These devices are discussed below.

Lab on a CD devices use centrifugal forces to drive and control liquid flow. These systems are advantageous for many applications, particularly those where a high flow-range is needed. Consequently, these devices have been commercially successful for use in point-of-care diagnostics.[72] Nevertheless, they need external rotational instruments to drive and control the liquid flow rates.[64, 73]

sPROM[65] and chemically-powered[66] devices use a chamber with either pressurized air or H_2O_2, integrated into the chip as their pumping system. The chamber is either electrically activated[65] or manually triggered.[66] In addition, these systems include passive microfluidic manipulation systems, which allow preprogrammed sets of microfluidic operations. Some disadvantages of these systems are that the liquid flow rate is not fully controllable (the pumping systems are not programmable) and they provide a limited range of flow rates.[65, 66, 74]

Electrophoretic-based systems rely on the electrophoretic transport of ionic molecules, and are used to separate molecules based on their hydrodynamic radius and their charges. These devices can perform complex liquid operations, including the separation of the desired molecules (i.e. using molecular weight cut-off methods). However, having gels inside their systems makes them complicated to preserve and expensive to operate.[68, 69]

As an interest for this thesis is to develop capillary-driven fluidic devices, the following section will illustrate a few examples of capillary driven microfluidic systems.

2.4 Capillary Microfluidics

In Capillary Microfluidics (CM), the capillary pressure generated between the liquid and its surrounding interface drives and controls the flow. As a result, these devices do not need any peripheral equipment, such as external pumps, which makes them portable and inexpensive to fabricate. During the past decade, various capillary-driven microfluidic platforms have been developed, among which, fibrous CM,[51, 75] positive pressure CM [76, 77] and autonomous CM[50, 78] are worth mentioning. These platforms are briefly explained in the sections below.

2.4.1 Fibrous Capillary Microfluidic Systems

Fibrous CM systems employ fibrous materials, such as paper or thread, to transport liquids using capillary forces. Various attempts have been made to pattern microchannels and reservoirs in paper. For example, Whitesides and colleagues used photolithography and wax printing to pattern microchannels and

reservoirs in paper.[51, 79-81] Similarly, other groups created microchannels in paper by cutting it using a computer controlled knife[82] or a laser cutter.[83]

Efforts have also been made to enhance the functionality of fibrous CM by integrating various capillary-driven valves into these systems. For example, Noh *et al.*[84] regulated the flow rate in paper-based microfluidics by printing various concentrations of paraffin wax in paper, and Toley *et al.*[85] integrated a sodium polyacrylate gel as a swellable polymer actuator, and showed that the actuator can be used to either stop or start the liquid flow after a certain amount of time.

2.4.2 Positive Pressure Capillary Microfluidics

A hemispheric droplet with a radius of *r* has a capillary pressure that can be calculated as:[86]

$$\Delta P = \frac{2 \times \gamma_{SG}}{r} \tag{2.14}$$

In positive pressure CM, two hemispheric droplets with different radii are deposited at the extremity of a microchannel. The difference between the capillary pressures generated by these two droplets drives the liquid from the smaller drop to the larger one. The principle of these devices is illustrated in Fig. 2.6. Due to their simplicity, these systems have been used in various

applications, including gradient generators[87] and high throughput analysis of cells.[88]
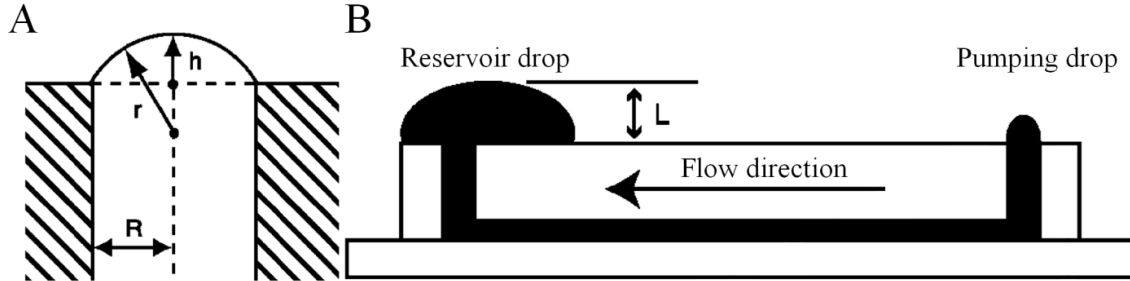
Fig. 2.6: Schematic illustrating the capillary-driven pumping method used in positive pressure CM. (A) A side-view of a hemispheric droplet with the radius of curvature, r, which generates a capillary pressure $\Delta P = \dfrac{2 \times \gamma_{SG}}{r}$. (B) The difference between the capillary pressures generated by the two droplets drives the flow from the small drop (pumping drop) to the larger one (reservoir drop). Adapted from Walker *et al.*.[76]

2.4.3 Autonomous Microfluidic Capillary Systems (AMCS)

In AMCS, the capillary pressure in a microfluidic circuit is preprogramed by engineering the geometry of the microconduits. Delamarche and colleagues were the first group who introduced the concept of AMCS.[50] Their very first device consisted of five parts: (i) a service port, (ii) an access channel, (iii) a capillary retention valve (CRV), (iv) a reaction chamber, and (v) a capillary pump (CP), as shown in Fig 2.7A. Their CP consisted of parallel microchannels, which defined

the capillary pressure and provided sufficient volume to pump the solutions. The

CRV was a localized narrow microchannel with high capillary pressure (higher

than that of the CP), which prevented the access channel from being drained.

The reaction chamber was fabricated with a shallow depth so that it dominated

the flow resistance of the circuit, and thus the flow rate of the circuit stayed

constant as the liquid progressed in the CP. One of the main advantages of their

platform was that upon depletion of the liquid from the service port, the liquid

stops at the CRV, and thus prevents the bubble-trapping or cross-contamination,

allowing them to add another liquid and perform multistage reactions, as shown

in Fig 2.7B. Using this process, they showed that they can perform a 16-step

sandwich immunoassay to detect a cardiac marker (CRP).[50]
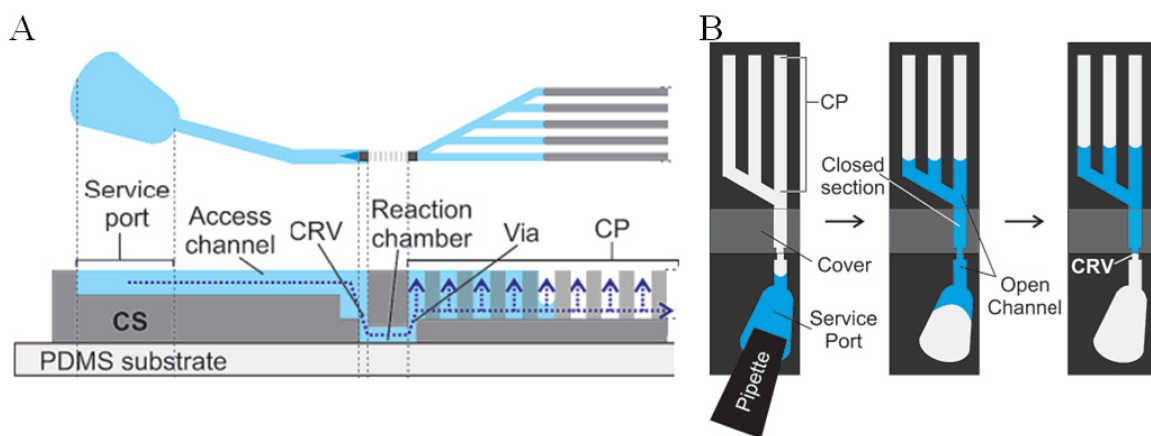
Fig. 2.7: Schematic of autonomous microfluidic capillary systems. (A) Top and

front views of the very first AMCS, illustrating its five functional parts: service

port, access channel, capillary retention valve (CRV), reaction chamber, and

capillary pump (CP). (B) Operation of the AMCS. A solution is introduced into the service port that spontaneously fills the conduits and moves to the CP. As all the liquid drains from the service port, the liquid stops at the CRV, allowing a second liquid to be introduced into the system without trapping any bubbles or any cross-contamination. Adapted from of Juncker *et al.*. [50]

Later, to enhance the functionality of the AMCS, the group introduced and integrated various capillary pumps and valves into their systems.[89, 90] For example, it's theoretically proven that abrupt changes in the dimension of the capillary will change the curvature of the meniscus at the filling front, and this can be used to stop the flow or regulate it, as shown in Fig. 2.8A.[91] Zimmerman *et al.*[90] implemented this principle and designed a variety of stop and trigger valves. Their stop valves consisted of a PDMS sealing layer, which was hydrophobic, and the chip, which was hydrophilic. They found that although the PDMS prevented the failure of the valve at the top wall, their valves fail after a few seconds by leaking through the bottom wall, which is hydrophilic. To resolve the issue, they minimized the area of the bottom wall by fabricating high aspect ratio valves (i.e. depth/width>10). They then showed that they can stop the liquid for up to 5 minutes with a success rate of 85%, enabling them to design a trigger valve by combining two stop valves, in which two liquids must meet in

the valve to trigger flow through the main channel. The micrograph and operation

of one of their trigger valves are demonstrated in Fig. 2.8B&C.
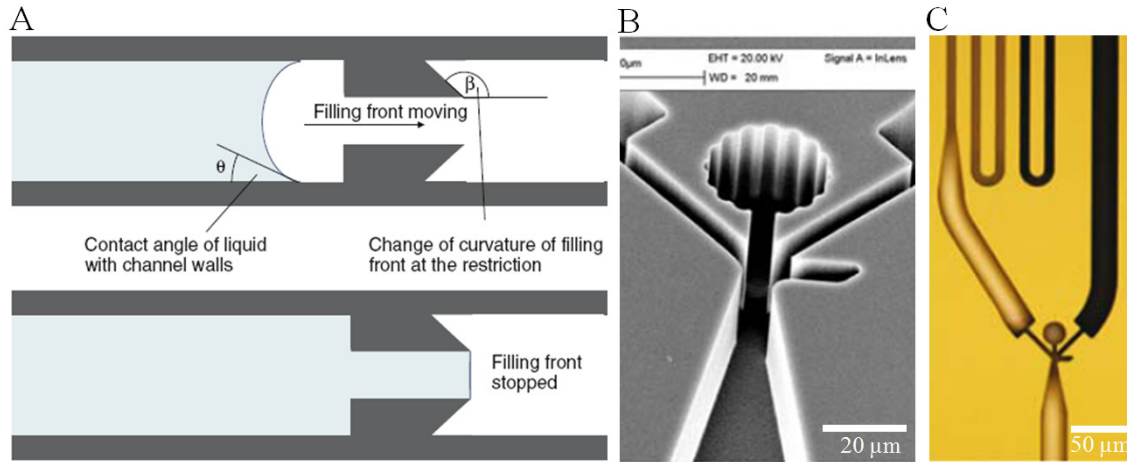
Fig. 2.8: Principle and operation of the capillary trigger valves. (A) It has been

shown that in a two dimensional microchannel, if the abrupt enlargement of the

conduit curvature is set in a way that $\beta>(90°-\Theta_c)$, the liquid would stop at the

restriction.[91] (B) SEM micrograph of a trigger valve made with the an aspect ratio

of ~10. (C) Operation of a trigger valve to prevent the liquid from entering the

main channel. Once the liquid fills the second conduit, the valve is triggered, and

the flow starts in the main channel. Adapted from Zimmerman *et al.* [90]

Other than designing different valves for the AMCS, the group investigated the

possibilities of preprogramming the capillary pressure in the CPs using three

strategies; (i) microposts with various densities, (ii) parallel tree line

micochannels, and (iii) posts with different shapes (i.e. hexagons, balled lines,

etc.), as shown in Fig. 2.9A. Additionally, since the progression of the liquid filling front was not well controlled, bubbles could potentially get trapped in their CPs, introducing inaccuracies in the volume of the liquid metered by the CP. To resolve this issue, they proposed arch-shaped hierarchical bridges with decreasing capillary pressure, which acted as a delay valve; thus avoiding trapping any bubble, as shown in Fig. 2.9B. Finally, using this strategy, they showed that they can connect various CPs with different capillary pressures in series, as shown in Fig. 2.9C.[89]
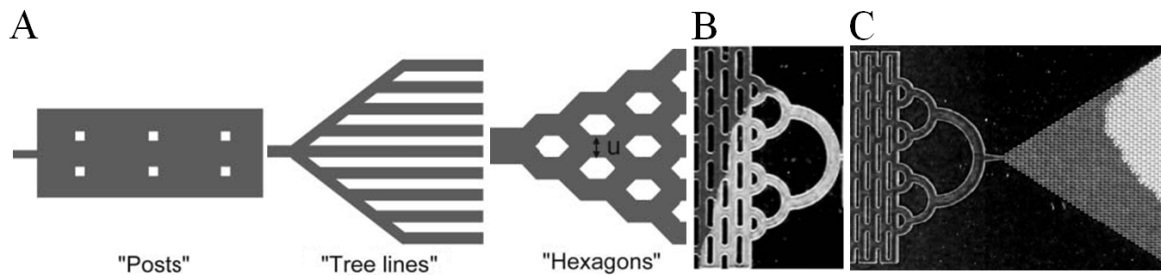
Fig. 2.9: Pre-programmable CPs. (A) Possibilities of engineering the capillary pressure in the CPs using posts with various densities, tree line microchannels, and posts with different geometries (e.g. hexagons). (B) Arch-shaped hierarchical bridges at the end of a CP that avoid trapping bubbles. (C) Hierarchical bridges allow for the serial connection of different CPs with different capillary pressures. Adapted from Zimmerman *et al.*[89]

Attempts have also been made to combine some of these CPs and valves to make capillary circuits and perform bioassays.[66, 92, 93] For example, Gervais *et al.*[92] dehydrated various reagents in different parts of a capillary circuit, and, by engineering the flow resistance of the circuit, limited the crosstalk between reagents, thus showing that the circuit can perform a one-step immunoassay with multiplexing capability, Fig. 2.10.
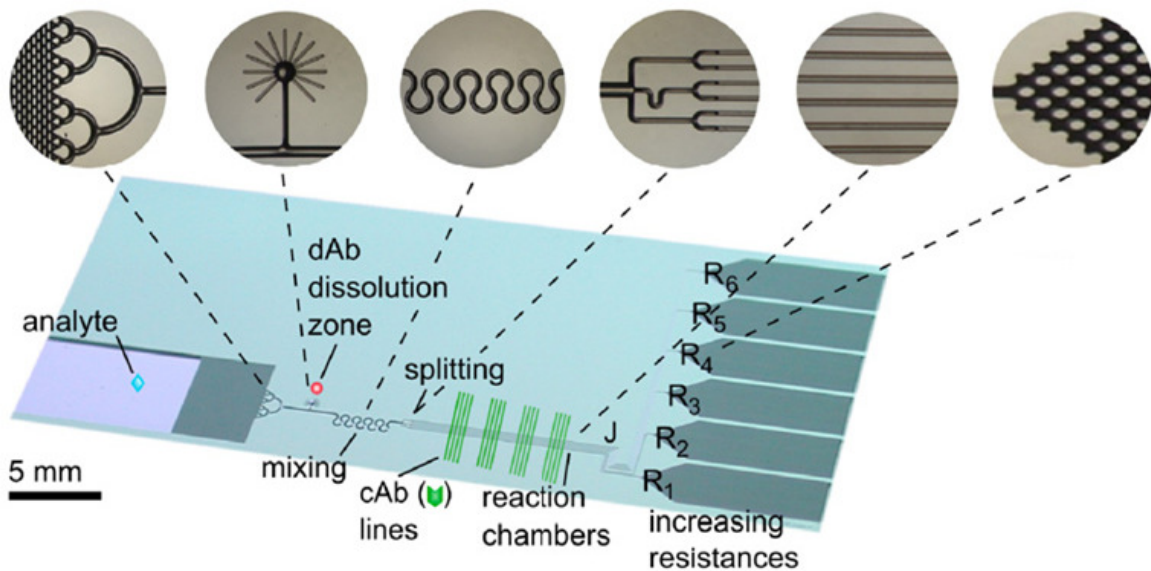
Fig. 2.10: AMCS used to perform multiplex one-step immunoassay. The inset micrographs illustrate various capillary elements designed for the circuit, including: (i) a reservoir to dehydrate and then rehydrate the detection antibody (dAb), (ii) a mixer using a serpentine microchannel for releasing dAb, (iii) a flow splitter that allows for multiplexing ability, (iv) flow resistors (R_1-R_6) to control the flow rate in each microchannel, and (v) CPs. Adapted from Gervais *et al.*[92]

In Chapters 5 and 6, we further expand the functionality of these systems by introducing new CPs, valves, and capillary circuits.

2.5 Immunoassays

The body's immune system produces specific proteins known as antibodies or immunoglobulins to recognize extrinsic molecules or pathogens in the body.[94] Each individual antibody binds to a specific molecule named an antigen (i.e. an antibody generating molecule). In immunoassays, the strong and specific binding between an antibody and its corresponding antigen is used to identify a protein of interest in a sample.[95]

Over the past 50 years, various immunoassay formats have been developed. However, the most common approach used in point-of-care diagnostics is called *sandwich heterogeneous immunoassay*. The general protocol for carrying out the assay is illustrated in Fig. 2.11A. First, a protein, normally an antibody, is immobilized on a surface using physical absorptions or chemical bindings.[96] This protein is called a capture antibody. Second, the sample is delivered over the capture antibody and the protein of interest binds specifically to the capture molecules. Finally, a detection antibody conjugated with a label is introduced and binds to the captured sample, forming a sandwich. Having a label conjugated

with the detection antibody is used to identify whether or not the protein of interest is present in the sample. Additionally, the concentration of the label at the capture surface is used to quantify the concentration of the protein.

The human body can produce around 10^8 different antibodies.[97] These antibodies can be categorized as either immunoglobulin A (IgA), IgG, IgM, IgE, or IgD, depending on the type of heavy chain that they possess.[94] IgGs are the most common type of antibody used in immunoassays. The structure of these antibodies is shown in Fig. 2.11B. It consists of four polypeptide chains, two γ heavy chains (shown in red) and two similar light chains (shown in blue). The heavy and light chains are connected to each other via disulfide bonds, causing the antibody to form a Y-like conformation. Also each IgG has two F_{AB} fragments, which specifically bind to the antigens and an F_C region, which holds the antibody together.[94, 98]
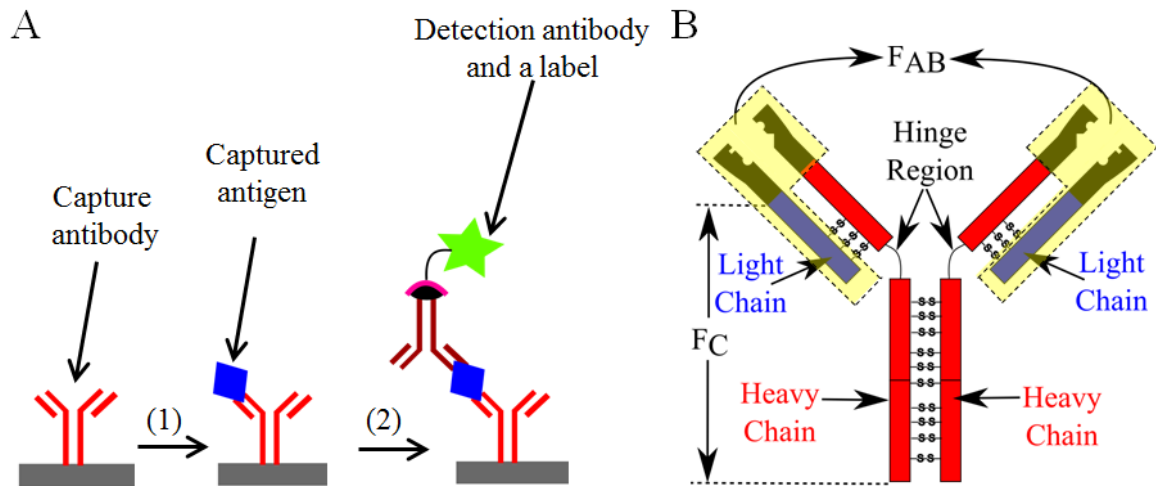
Fig. 2.11: Sandwich immunoassays (A) Schematic illustrating the steps required to perform a heterogeneous sandwich immunoassay. First, a capture antibody is immobilized on the surface. The sample then flows over the capture surface resulting in the binding of specific antigen of interest to the capture antibody. Finally, a detection antibody conjugated with a label passes over the captured antigen. (B) The structure of an IgG antibody. Due to the disulfide bonds between the γ heavy chains and the light chains, the antibody forms a Y-like conformation. The F_{AB} fragments are the regions where the antibody binds specifically to its antigen of interest, while the F_C fragments hold the antibody together. Modified from Purves *et al.*[98]

Antibodies are generally categorized as either polyclonal[99] or monoclonal.[100] Polyclonal antibodies are a combination of different antibodies specific to the

antigen of interest; thus, they can bind to different epitopes of an antigen. These antibodies are popularly used as capture antibodies in immunoassays.[99]

In contrast, monoclonal antibodies are specific for a single epitope of an antigen. These antibodies are more specific than that of the polyclonal ones and are mainly used as a detection antibody in an immunoassay.[100]

2.6 Dynamics of the Mass Transfer in Heterogeneous Immunoassays

In order to produce a quick assay with high sensitivity and minimal sample requirement, it is essential to optimize the assay conditions (such as flow rate, concentration of patterned capture molecules, and the geometry of the reaction chamber).

In general, the mass transfer dynamics in microfluidic immunoassays can be classified into three major physico-chemical processes: *convection, diffusion,* and *surface binding*.[101, 102] The convection along the microchannel is the dominant mass transfer along the axis of the microchannel; diffusion is the principle process for transporting an analyte from the bulk layer to the mass transfer boundary layer; and the surface binding brings about the reaction of an analyte from the boundary layer to the solid surface, which is functionalized over the capture zone. Fig. 2.12 illustrates the three processes.
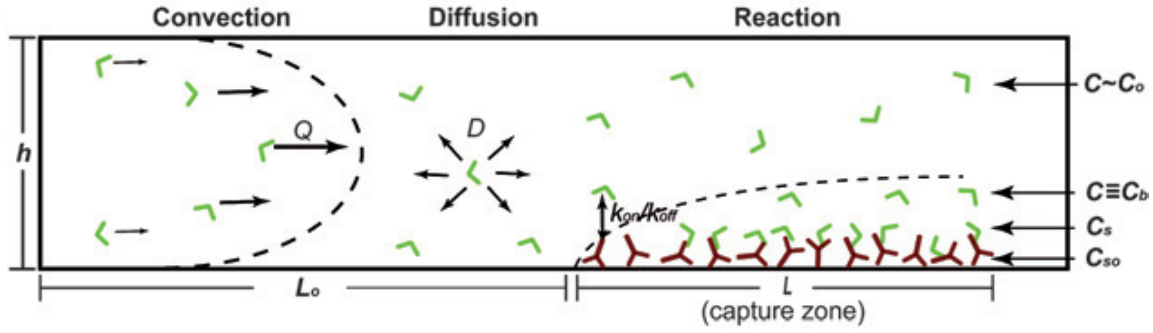
Fig. 2.12: Schematic diagram illustrating the three physico-chemical processes (convection, diffusion, and surface binding), and key parameters in this study. The parameters h, and L_0 define the microfluidic geometry. Adapted from *Parsa et al.*.[101]

In the condition where the microchannel can be assumed as a two-dimensional conduit, i.e. $\dfrac{h}{w} \ll 1$, where h and w are the height and width of the microchannel, respectively, three timescales can be defined: (i) a convection timescale (t_c), (ii) a diffusion timescale (t_d) and (iii) a reaction timescale (t_r).

The convection timescale can be calculated as: [101]

$$t_c = \frac{L}{U} \tag{2.15}$$

where U is the average flow velocity, and L is the length of the reaction chamber.

The diffusion timescale can be quantified by:

$$t_d = \frac{h^2}{D}$$ (2.16)

where D is the diffusion coefficient, and can be calculated from the Stokes-Einstein-relation as:[102]

$$D = \frac{k \times T}{6 \times \pi \times \mu \times R_h}$$ (2.17)

μ is the dynamic viscosity of the sample, R_h is the hydrodynamic radius of the molecules, k is the Boltzman constant, and T is the absolute temperature.

The reaction timescale can be expressed as:[101]

$$t_r = \frac{h}{k_{on} \times C_{SO}}$$ (2.18)

K_{on} (m³/mol.s) is the association rate constant, the rate at which smaller molecules bind to form more complex compounds, and C_{so} is the concentration of surface-bound capture antibody.[102]

Based on these timescales, non-dimensional numbers have been defined to perceive the dominance of each mass transfer phenomenon with respect to one another. For example, $Da = \frac{k_{on} \times C_{SO} \times h}{D}$ (*Damköhler number*) is the ratio of the diffusion time scale and the reaction time scale,[102, 103] and explains the

dominance of diffusion over reaction in the process. For $Da \gg 1$ the assay is diffusion limited, whereas for $Da \ll 1$ the system is confined by the reaction limited regime. Alternatively, $\xi = \dfrac{L \times D}{U \times h^2}$ (*Graetz number*) is the ratio of the convection timescale over diffusion timescale, and demonstrates the significance of axial convection over lateral diffusion.[101, 103]

Using these non-dimensional parameters, it is possible to determine and optimize various parameters including (i) what operating regime the assay would fall into. The operating regime can be either reaction limited or the diffusion limited, (ii) what is the critical flow rate at which the sample needs to pass over the reaction zone. The critical flow rate is the flow rate below which running the assay would take longer time, without gaining any signal, and (iii) how much reagent needs to be used in order to detect a maximum signal.

2.7 Detection Systems Used in Microfluidic Immunodiagnostic Devices

Different methods have been developed to detect the binding events of immunodiagnostic assays, which can be mainly classified into electrochemical and optical methods.[104, 105]

Electrochemical detection methods are based on the measurements of voltage, solution resistance, current, and current-voltage profile. These methods include

amperometric (measuring the currents as the output), conductometric (measuring the conductive properties of the electrodes), and potentiometric (measuring the charge accumulation).[106] The Electrochemical systens can successfully quantify the concentrations of certain small molecules such as glucose, urea, and electrolytes. However, since they are very sensitive to the variations of physico-chemical factors in the sample, such as pH, ionic concentrations, and temperature, they are not ideal for all assays, including those require low detection limits such as cancer biomarkers.[104]

Optical detection methods have also been used in the Lab-on-a-chip applications, which can be mainly categorized into Surface Plasmon Resonance (SPR), colorimetric/absorbance, fluorescence, chemiluminescence, nanoparticles and nanowires, and spectroscopic methds.[104] A comprehensive review on the topic can be found in Myer *et al.* .[104] SPR detections are based on the change in refractive index at a metal surface, which has been functionalized with the capture molecules. The techniques are sensitive, and can be integrated into microfluidic systems. As a result, SPR-based, disposable biosensors are available commercially.[107, 108] Despite these advantages, SPR-based techniques are sensitive to temperature variations, and require a metal deposition process

on the chip, which makes the fabrication process of the biosensor costly. Also they are less sensitive than fluorescence based methods in practice.[104]

Fluorescence detection is another commonly used method in biosensor applications. The technique has excellent sensitivity and popularly used in commercially available biosensors.[104] There are different protocols available for selectively labeling molecules.[104] However, auto-fluorescence is a problem with many materials, including polymers, papers, and some biomolecules present in the sample. In addition, although there have been various attempts to integrate fluorescence detection systems on-chip,[109] the detection systems require expensive hardware (i.e. fluorescence microscopes), which is difficult to miniaturize.

Chemiluminescence detection methods, where a chemical reaction causes photochemical emission, are also very sensitive. [110] As a result, a number of point-of-care diagnostics have been developed using chemiluminescence detection methods.[111, 112] The main advantage of these systems is that they do not require any excitation instrument, and consequently, the problems associated with the background noise are eliminated. Similarly in electrochemiluminescence (ECL) methods the a luminescent reaction happens only when an appropriate

voltage exists in the solution containing the luminescent compounds.[113,114] Nevertheless, these systems require highly sensitive detectors, which make them quite expensive.[104]

Nanoparticles have also recently improved both optical and electrochemical detection methods by enhancing their sensitivity, increasing their shelf-life, and improving their controllability.[104] As for the optical methods, different types of nanoparticles have been introduced and commercialized for point-of-care diagnostic devices.[104] For example, gold nanoparticles are commonly used to label secondary antibodies in the lateral flow assays. These nanoparticles enhance the detection sensitivity through catalytic silver deposition, allowing for imaging. Alternatively, ceramic phosphorous nanoparticles have also recently been introduced, which can absorb multiple photons of infrared light and emit photons in the visible spectrum.[104]

Overall the variety of the detection techniques described above can measure the analyte binding at a surface. However, the choice of the detection method depends on the required sensitivity, type of the analyte, which needs to be measured, and the ultimate price of the disposable biosensor and its available interfaces.

2.8 Summary

In this chapter we briefly presented the background knowledge required to understand the remainder of the dissertation. First we explained the dominant fluid phenomena in microchannels, including laminar flow, surface tension, wetting, and capillary pressure. We then provided a historical review of liquid handling mechanisms developed over the last 70 years with a main focus on capillary microfluidic systems. Afterwards, we discussed immunoassays and showed how they can be optimized and integrated into microchannels to identify proteins of interests. Finally, we presented a few examples of available detection methods which can be integrated into microfluidic devices and used to measure the binding of an analyte on a surface.

2.9 References

1. Whitesides, G.M. The origins and the future of microfluidics. *Nature* **442**, 368-373 (2006).
2. Website of U.S National Institue of Health, http://nano.cancer.gov/media_backgrounder.asp, retrieved 2013/04/23.
3. Haeberle, S. & Zengerle, R. Microfluidic platforms for lab-on-a-chip applications. *Lab on a Chip* **7**, 1094-1110 (2007).
4. Stone, H.A. & Kim, S. Microfluidics: Basic issues, applications, and challenges. *AICHE Journal* **47**, 1250-1254 (2001).
5. White, F.M. Fluid Mechanics, third edition (McGraw-Hill Inc, 1994).

6. Beebe, D.J., Mensing, G.A. & Walker, G.M. Physics and applications of microfluidics in biology. *Annual Review of Biomedical Engineering* **4**, 261-286 (2002).

7. Soumerai, H. & Soumerai-Bourke, B.E. Analytical method of predicting turbulence transition in pipe flow. *Scientific Reports* **2** (2012).

8. Tang, L. & Masutani, S.M. Laminar to turbulent flow liquid-liquid jet instability and breakup. *Proceedings of The Thirteenth International Offshore and Polar Engineering Conference*, Honolulu, Hawaii, USA 317-324 (2003).

9. Alexander, C.K. & Sadiku, M.N.O. Fundamentals of electric circuits. (McGraw-Hill Higher Education, 2007).

10. Bruus, H. Theoretical Microfluidics, Chapter 4, Page 75. (OUP Oxford, 2008).

11. Adamson, A.W. & Gast, A.P. Physical chemistry of surfaces. (Wiley, 1997).

12. Gennes, P.G.d., Brochard-Wyart, F. & Quéré, D. Capillarity and Wetting Phenomena: Drops, Bubbles, Pearls, Waves. (Springer, 2004).

13. Yarin, A. Drop impact dynamics: splashing, spreading, receding, and bouncing. *Annual Review of Fluid Mechanics* **38**, 159-192 (2006).

14. Thoroddsen, S., Etoh, T.G. & Takehara, K. Crown breakup by Marangoni instability. *Journal of Fluid Mechanics* **557**, 63-72 (2006).

15. Prosperetti, A. & Oguz, H.N. The impact of drops on liquid surfaces and the underwater noise of rain. *Annual Review of Fluid Mechanics* **25**, 577-602 (1993).

16. Young, T. An essay on the cohesion of fluids. *Philosophical Transactions of the Royal Society of London* **95**, 65-87 (1805).

17. Fowkes, F.M., Zisman, W.A. Contact angle, wettability and adhesion: the Kendall award symposium honoring William A. Zisman, Los Angeles, California, April 2-3, 1963. (American Chemical Society, 1964).

18. Eral, H. & Oh, J. Contact angle hysteresis: a review of fundamentals and applications. *Colloid and Polymer Science* **291**, 247-260 (2013).

19. Leverett, M. Capillary behavior in porous solids. *Transactions of the American Institute of Physics* (1940).

20. Middleman, S. An Introduction to Fluid Dynamics: Principles of Analysis and Design. (Wiley, 1998).

21. Weislogel, M.M. & Lichter, S. Capillary flow in an interior corner. *Journal of Fluid Mechanics* **373**, 349-378 (1998).

22. Navier, C. Mémoire sur les lois du mouvement des fluides. *Mémoires de l'Académie Royale des Sciences de l'Institut de France* **6**, 389-440 (1823).

23. Cannone, M. & Friedlander, S. Navier: Blow-up and collapse. *Notices of the American Mathematical Society* **50**, 7-13 (2003).

24. Batchelor, G.K. in Theoretical and applied mechanics; Proceedings of the Fourteenth International Congress 33-55 (North-Holland Publishing Co., 1977).

25. Reynolds, O. On the theory of lubrication and its application. *Philosophical Transactions of the Royal Society of London*, 157-234 (1886).

26. Rayleigh, L. On the instability of jets. *Proceedings of the London Mathematical Society* **1**, 4 (1878).

27. Hauser, E.A. The history of colloid science: In memory of Wolfgang Ostwald. *Journal of Chemical Education* **32**, 2 (1955).

28. Hales, S. Statical Essays: Vegetable Staticks, page 28. (Innys, 1738).

29. Canny, M.J. Flow and transport in plants. *Annual Review of Fluid Mechanics* **9**, 275-296 (1977).

30. Elmqvist, R. Measuring instrument of the recording type, **US Patent 2,566,443** (1951).

31. Le, H.P. Progress and trends in ink-jet printing technology. *Journal of Imaging Science and Technology* **42**, 49-62 (1998).

32. Buehner, W.L., Hill, J.D., Williams, T.H. & Woods, J.W. Application of ink jet technology to a word processing output printer. *IBM Journal of Research and Development* **21**, 2-9 (1977).

33. Endo, I., Sato, Y., Saito, S., Nakagiri, T. & Canon, S.O. Liquid jet recording process and apparatus there for **Great Britain Patent 2007162** (1979).

34. Southern, E.M. DNA microarrays. History and overview. *Methods in molecular biology (Clifton, N.J.)* **170**, 1-15 (2001).

35. Heller, M.J. DNA microarray technology: Devices, systems, and applications. *Annual Review of Biomedical Engineering* **4**, 129-153 (2002).

36. Schena, M., Heller, R.A., Theriault, T.P., Konrad, K., Lachenmeier E. & Davis, R.W. Microarrays: biotechnology's discovery platform for functional genomics. *Trends in Biotechnology* **16**, 301-306 (1998).

37. Kafatos, F.C., Jones, C.W. & Efstratiadis, A. Determination of nucleic-acid sequence homologies and relative concentrations by a dot hybridization procedure. *Nucleic Acids Research* **7**, 1541-1552 (1979).

38. Hoheisel, J.D., Ross, M.T., Zehetner, G. & Lehrach, H. Relational genome analysis using reference libraries and hybridization fingerprinting. *Journal of Biotechnology* **35**, 121-134 (1994).

39. Blanchard, A.P., Kaiser, R.J. & Hood, L.E. High-density oligonucleotide arrays. *Biosensors & Bioelectronics* **11**, 687-690 (1996).

40. Barbulovic-Nad, I. Lucente, M., Sun, Y., Zhang, M., Wheeler, A.R. & Bussmann, M. Bio-microarray fabrication techniques - A review. *Critical Reviews in Biotechnology* **26**, 237-259 (2006).

41. Ducre´e, J., Gruhler, H., Hey, N., Muller, M., Bekesi, S., Freygang, M., Sandmaiser, H. & Zengerle, R. A new method for the fabrication of microarrays, MEMS 2000. The Thirteenth Annual International Conference on Micro Electro Mechanical Systems317-322 (IEEE, 2000).

42. Gutmann, O., Kuehlewein R., Reinbold S., Niekrawietz R., Steinert C.P., Heij B.D, Zengerle, R. & Daub, M. Fast and reliable protein microarray

production by a new drop-in-drop technique. *Lab on a Chip* **5**, 675-681 (2005).

43. Terry, S.C., Jerman, J.H. & Angell, J.B. Gas-chromatographic air analyzer fabricated on a silicon-wafer. *IEEE Transactions on Electron Devices* **26**, 1880-1886 (1979).

44. Manz, A., Graber, N. & Widmer, H.M. Miniaturized total chemical-analysis systems - a novel concept for chemical sensing. *Sensors and Actuators B-Chemical* **1**, 244-248 (1990).

45. Harrison, D.J., Fluri, K., Seiler, K., Fan, Z., Effenhauser, C.S. & Manz, A. Micromachining a miniaturized capillary electrophoresis-based chemical analysis system on a chip. *Science* **261**, 895-897 (1993).

46. Xia, Y.N. & Whitesides, G.M. Soft lithography. *Angewandte Chemie-International Edition* **37**, 551-575 (1998).

47. Whitesides, G.M., Ostuni, E., Takayama, S., Jiang, X.Y. & Ingber, D.E. Soft lithography in biology and biochemistry. *Annual Review of Biomedical Engineering* **3**, 335-373 (2001).

48. Zhao, X.M., Xia, Y. & Whitesides, G.M. Soft lithographic methods for nano-fabrication. *Journal of Materials Chemistry* **7**, 1069-1074 (1997).

49. Unger, M.A., Chou, H.P., Thorsen, T., Scherer, A. & Quake, S.R. Monolithic microfabricated valves and pumps by multilayer soft lithography. *Science* **288**, 113-116 (2000).

50. Juncker, D., Schmid, H., Drechsler, U., Wolf, H., Wolf, M., Michel, B., de Rooij, N. & Delamarche, E. Autonomous microfluidic capillary system. *Analytical Chemistry* **74**, 6139-6144 (2002).

51. Martinez, A.W., Phillips, S.T., Butte, M.J. & Whitesides, G.M. Patterned paper as a platform for inexpensive, low-volume, portable bioassays. *Angewandte Chemie-International Edition* **46**, 1318-1320 (2007).

52. Bernard, A., Michel, B. & Delamarche, E. Micromosaic immunoassays. *Analytical Chemistry* **73**, 8-12 (2001).

53. Yager, P., Edwards, T., Fu, E., Helton, K., Nelson, K. Tam, M.R. & Weigl, B.H. Microfluidic diagnostic technologies for global public health. *Nature* **442**, 412-418 (2006).

54. Yager, P., Domingo, G.J. & Gerdes, J. Point-of-care diagnostics for global health, *Annual Review of Biomedical Engineering* **10**, 107-144 (2008).

55. Choi, C.H., Lee, J., Yoon, K., Tripathi, A., Stone, H.A., Weitz, D.A. & Lee, C.S. Surface-Tension-Induced Synthesis of Complex Particles Using Confined Polymeric Fluids. *Angewandte Chemie-International Edition* **49**, 7748-7752 (2010).

56. Duncanson, W.J., Lin, T., Abate, A.A., Seiffert, S., Shah, R.K. & Weitz, D.A. Microfluidic synthesis of advanced microparticles for encapsulation and controlled release. *Lab on a Chip* **12**, 2135-2145 (2012).

57. Swami, M. Proteomics: A discovery strategy for novel cancer biomarkers. *Nature Reviews Cancer* **10**, 597-597 (2010).

58. Misra, S. Human Gene Therapy: A Brief Overview of the Genetic Revolution. *Journal of the Association of Physicians of India* **61**, 127 (2013).

59. Gervais, L., de Rooij, N. & Delamarche, E. Microfluidic Chips for Point-of-Care Immunodiagnostics. *Advanced Materials* **23**, H151-H176 (2011).

60. Wu, Z., Liu, A.Q. & Hjort, K. Microfluidic continuous particle/cell separation via electroosmotic-flow-tuned hydrodynamic spreading. *Journal of Micromechanics and Microengineering* **17**, 1992 (2007).

61. Wiklund, M., Green, R. & Ohlin, M. Acoustofluidics 14: Applications of acoustic streaming in microfluidic devices. *Lab on a Chip* **12**, 2438-2451 (2012).

62. Dittrich, P.S., Tachikawa, K. & Manz, A. Micro total analysis systems. Latest advancements and trends. *Analytical Chemistry* **78**, 3887-3907 (2006).

63. Laser, D. & Santiago, J. A review of micropumps. *Journal of micromechanics and microengineering* **14**, R35 (2004).

64. Madou, M., Zoval, J., Jia, G., Kido, H., Kim, J. & Kim, N. Lab on a CD. *Annual Review of Biomedical Engineering* **8**, 601-628 (2006).

65. Ahn, C.H. Choi, J.W, Beaucage, G., Nevin, J., Lee, J.B., Puntambekar, A. & Lee, J.Y. Disposable Smart Lab on a Chip for Point-of-Care Clinical Diagnostics. *Proceedings of IEEE Special Issue on Biomedical Applications for MEMS and Microfluidics* **92**,154-173 (2004).

66. Qin, L.D., Vermesh, O., Shi, Q.H. & Heath, J.R. Self-powered microfluidic chips for multiplexed protein assays from whole blood. *Lab on a Chip* **9**, 2016-2020 (2009).

67. Esquivel, J. P., Castellarnau, M., Senn, T., Lochel, B., Samitier, J. & Sabate, N. Fuel cell-powered microfluidic platform for lab-on-a-chip applications. *Lab on a Chip* **12**, 74–79 (2012)

68. Herr, A.E., Hatch, A.V., Throckmorton, D.J., Tran, H.M., Brennan, J.S., Giannobile, W.V. & Singh, A.K. Microfluidic immunoassays as rapid saliva-based clinical diagnostics. *Proceedings of the National Academy of Sciences of the United States of America* **104**, 5268-5273 (2007).

69. Meagher, R.J., Hatch, A.V., Renzi, R.F. & Singh, A.K. An integrated microfluidic platform for sensitive and rapid detection of biological toxins. *Lab on a Chip* **8**, 2046-2053 (2008).

70. Sista, R., Hua, Z., Thwar, P., Sudarsan, A., Srinivasan, V., Eckhardt, A., Pollack, M. & Pamula, V. Development of a digital microfluidic platform for point of care testing. *Lab on a Chip* **8**, 2091-2104 (2008).

71. Yetisen, A.K., Akram, M.S. & Lowe, C.R. Paper-based microfluidic point-of-care diagnostic devices. *Lab on a Chip* (2013).

72. Chin, C.D., Linder, V. & Sia, S.K. Commercialization of microfluidic point-of-care diagnostic devices. *Lab on a Chip* **12**, 2118-2134 (2012).

73. Zimmermann, M., Hunziker, P. & Delamarche, E. Autonomous capillary system for one-step immunoassays. *Biomedical Microdevices* **11**, 1-8 (2009).

74. Do, J., Lee, S., Han, J., Kai, J., Hong, C.C., Gao, C., Nevin, J.H., Beaucage, G. & Ahn, C.H. Development of functional lab-on-a-chip on polymer for point-of-care testing of metabolic parameters. *Lab on a Chip* **8**, 2113-2120 (2008).

75. Li, X., Ballerini, D.R. & Shen, W. A perspective on paper-based microfluidics: Current status and future trends. *Biomicrofluidics* **6**, 011301 (2012).

76. Walker, G.M. & Beebe, D.J. A passive pumping method for microfluidic devices. *Lab on a Chip* **2**, 131-134 (2002).

77. Ju, J., Kim, K.C., Kim, H., Berthier, E., Beebe, D.J. & Lee, S.H. Backward flow in a surface tension driven micropump. *Journal of Micromechanics and Microengineering* **18**, 087002 (2008).

78. Juncker, D., Schmid, H., Bernard, A., Caelen, I., Michel, B., de Rooij, N. & Delamarche, E. Soft and rigid two-level microfluidic networks for patterning surfaces. *Journal of Micromechanics and Microengineering* **11**, 532-541 (2001).

79. Carrilho, E., Phillips, S.T., Vella, S.J., Martinez, A.W. & Whitesides, G.M. Paper Microzone Plates. *Analytical Chemistry* **81**, 5990-5998 (2009).

80. Carrilho, E., Martinez, A.W. & Whitesides, G.M. Understanding Wax Printing: A Simple Micropatterning Process for Paper-Based Microfluidics. *Analytical Chemistry* **81**, 7091-7095 (2009).

81. Martinez, A.W., Phillips, S.T. & Whitesides, G.M. Three-dimensional microfluidic devices fabricated in layered paper and tape. *Proceedings of the National Academy of Sciences of the United States of America* **105**, 19606-19611 (2008).

82. Fenton, E.M., Mascarenas, M.R., López, G.P. & Sibbett, S.S. Multiplex lateral-flow test strips fabricated by two-dimensional shaping. *ACS Applied Materials & Interfaces* **1**, 124-129 (2008).

83. Fu, E., Lutz, B., Kauffman, P. & Yager, P. Controlled reagent transport in disposable 2D paper networks. *Lab on a Chip* **10**, 918-920 (2010).

84. Noh, H. & Phillips, S.T. Fluidic Timers for Time-Dependent, Point-of-Care Assays on Paper. *Analytical Chemistry* **82**, 8071-8078 (2010).

85. Toley, B.J., Fu, E. & Yager, P. A powerless valving system for fluid flow in paper networks. *Sixteenth International Conference on Miniaturized Systems for Chemistry and Life Sciences, Okinawa, Japan*, 305-307 (October 28 - November 1, 2012).

86. Berthier, E. & Beebe, D.J. Flow rate analysis of a surface tension driven passive micropump. *Lab on a Chip* **7**, 1475-1478 (2007).

87. He, J., Du, Y., Villa-Uribe, J.L., Hwang, C., Li, D. & Khademhosseini, A. Rapid Generation of Biologically Relevant Hydrogels Containing Long-Range Chemical Gradients. *Advanced Functional Materials* **20**, 131-137 (2010).

88. Khnouf, R., Beebe, D.J. & Fan, Z.H. Cell-free protein expression in a microchannel array with passive pumping. *Lab on a Chip* **9**, 56-61 (2009).

89. Zimmermann, M., Schmid, H., Hunziker, P. & Delamarche, E. Capillary pumps for autonomous capillary systems. *Lab on a Chip* **7**, 119-125 (2007).

90. Zimmermann, M., Hunziker, P. & Delamarche, E. Valves for autonomous capillary systems. *Microfluiduidics and Nanofluidics* **5**, 395-402 (2008).

91. Man, P.F., Mastrangelo, C.H., Burns, M.A. & Burke, D.T. Microfabricated capillarity-driven stop valve and sample injector, *Proceedings MEMS 98. IEEE. Eleventh Annual International Workshop on Micro Electro Mechanical Systems,* 45-50 (1998).

92. Gervais, L., Hitzbleck, M. & Delamarche, E. Capillary-driven multiparametric microfluidic chips for one-step immunoassays. *Biosensors & Bioelectronics* **27**, 64-70 (2011).

93. Hitzbleck, M., Gervais, L. & Delamarche, E. Controlled release of reagents in capillary-driven microfluidics using reagent integrators. *Lab on a Chip* **11**, 2680-2685 (2011).

94.   Alberts, B. Molecular Biology of the Cell: Reference Edition. (Garland Science, 2008).

95.   Lin, C.C., Wang, J.H., Wu, H.W. & Lee, G.B. Microfluidic immunoassays. *Journal of the Association for Laboratory Automation* **15**, 253-274 (2010).

96.   Williams, R. & Blanch, H. Covalent immobilization of protein monolayers for biosensor applications. *Biosensors and Bioelectronics* **9**, 159-167 (1994).

97.   Nelson, D.L., Lehninger, A.L. & Cox, M.M. Lehninger Principles of Biochemistry. (W. H. Freeman, 2008).

98.   Purves, W.K, Sadava, D., Orians, G.H. & Heller, H.C. Life: The Science of Biology. (Palgrave Macmillan, 2004).

99.   Hanly, W.C., Artwohl, J.E. & Bennett, B.T. Review of polyclonal antibody production procedures in mammals and poultry. *ILAR Journal* **37**, 93-118 (1995).

100.   Wang, S. Advances in the production of human monoclonal antibodies. *Antibody Technology Journal* **1**, 1-4 (2011).

101.   Parsa, H. et al. Effect of volume- and time-based constraints on capture of analytes in microfluidic heterogeneous immunoassays. *Lab on a Chip* **8**, 2062-2070 (2008).

102.   Squires, T.M., Messinger, R.J. & Manalis, S.R. Making it stick: convection, reaction and diffusion in surface-based biosensors. *Nature Biotechnology* **26**, 417-426 (2008).

103.   Gervais, T. & Jensen, K.F. Mass transport and surface reactions in microfluidic systems. *Chemical Engineering Science* **61**, 1102-1121 (2006).

104.   Myers, F.B. & Lee, L.P. Innovations in optical microfluidic technologies for point-of-care diagnostics. *Lab on a Chip* **8**, 2015-2031 (2008).

105.   Javanmard, M. et al. Electrical detection of protein biomarkers using bioactivated microfluidic channels. Lab on a Chip 9, 1429-1434 (2009).

106. Li, P.C.H. Microfluidic Lab-on-a-Chip for Chemical and Biological Analysis and Discovery, Vol. 94. (2006).

107. Waswa, J., Irudayaraj, J. & DebRoy, C. Direct detection of E-Coli O157 : H7 in selected food systems by a surface plasmon resonance biosensor. *Lwt-Food Science and Technology* **40**, 187-192 (2007).

108. Chinowsky, T.M., Quinn, J.G., Bartholomew, D.U., Kaiser, R. & Elkind, J.L. Performance of the Spreeta 2000 integrated surface plasmon resonance affinity sensor. *Sensors and Actuators B-Chemical* **91**, 266-274 (2003).

109. Balslev, S., Jorgensen, A.M., Bilenberg, B., Mogensen, K.B., Snakenborg, D., Geschke, O., Kutter, J.P. & Kristensen, A. Lab-on-a-chip with integrated optical transducers. *Lab on a Chip* **6**, 213-217 (2006).

110. Bhattacharyya, A. & Klapperich, C.M. Design and testing of a disposable microfluidic chemiluminescent immunoassay for disease biomarkers in human serum samples. *Biomedical Microdevices* **9**, 245-251 (2007).

111. Yacoub-George, E., Hell, W., Meixner, L., Wenninger, F., Bock, K., Lindner, P., Wolf, H., Kloth, T. & Feller, K.A.. Automated 10-channel capillary chip immunodetector for biological agents detection. *Biosensors & Bioelectronics* **22**, 1368-1375 (2007).

112. Marchand, G., Broyer, P., Lanet, V., Delattre, C., Foucault, F., Menou, L., Calvas, B., Roller, D., Ginot, F., Campagnolo, R. & Mallard, F. Opto-electronic DNA chip-based integrated card for clinical diagnostics. *Biomedical Microdevices* **10**, 35-45 (2008).113. Forster, J. R., Bertoncello, P. & Keyes, T. E. Electrogenerated Chemiluminescence, *Annual Review of Analitical Chemistry* **2** 359-385, (2009)

114. Han, K. N., Li, C. A. & Seong, G. H. Microfluidic Chips for immunoassays,

Annual Review of Analitical Chemistry **6** 119-141, (2013)

Chapter 3: SU-8 pins for microarray spotting

3.1 Preface

Pin spotting has been widely used for printing microarrays over the last decade. These array of pins operate by first dipping them in a 96 or 384 microtiter well plate containing spotting solutions, retracting it along with a small droplet of solution captured by capillary effects and then printing the pin array onto a surface, thus affecting the transfer of the solution from the pin to the surface.

Currently, these pins are fabricated out of metals, ceramics, or silicon, and thus they are either expensive to fabricate, or very brittle and break easily upon contacting to the surface of the substrates.

Our work presents a post processing annealing protocol, which allows making of 30 mm long and straight free standing structures out of SU-8, and then uses this fabrication process to make SU-8 pins for microarray spotting.

The main novelty of this work is 1) the fabrication process for making fully flat free standing structures out of SU-8, and 2) the design of the pins, which have a novel stop valve to transfer a very accurate amount of liquids.

This work resulted in the following publication:

Safavieh, R., Roca, M.P., Qasaimeh, M.A., Mirzaei, M. & Juncker, D. *Straight SU-8 pins*. Journal of Micromechanics and Microengineering, 20, (2010).

3.2 Abstract

SU-8 can be patterned with high resolution, is flexible and tough. These characteristics qualify SU-8 as a material for making spotting pins for printing DNA and protein microarrays, and potentially replace the commonly used silicon and steel pins that are expensive, brittle in the case of silicon, and can damage the substrate during the printing process. SU-8 however accumulates large internal stress during fabrication and as a consequence, thin and long SU-8 structures bend and coil up, which precludes using it for long, free-standing structures such as pins. Here we introduce (i) a novel fabrication process that allows making 30 mm long, straight spotting pins that feature (ii) a new design and surface chemistry treatments for better flow control and more homogeneous spotting. A key innovation for the fabrication is a post-processing annealing step with slow temperature ramping *and* mechanical clamping between two identical substrates to minimize stress buildup and render it symmetric, respectively, which together yield a straight SU-8 structure. SU-8 pins fabricated using this process are compliant and resilient and can buckle without damage during printing. The pins comprise a novel flow stop valve for accurate metering of fluids, and their surface was chemically patterned to render the outside of the pin hydrophobic while the inside of the slit is hydrophilic, and the slit thus spontaneously fills when dipped into a solution while preventing droplet

attachment on the outside. A single SU-8 pin was used to print 1392 protein spots in one run. SU-8 pins are inexpensive, straightforward to fabricate, robust, and may be used as disposable pins for microarray fabrication. These pins serve as an illustration of the potential application of ultralow stress SU-8 for making freestanding microfabricated polymer microstructures.

KEYWORDS: SU-8, microarray printing, pins, protein, capillary flow

3.3 Introduction

The negative tone epoxy photoresist EPON SU-8 can readily be patterned with aspect ratios as high as 20, and with thickness varying from nanometers to one millimeter.[1] SU-8 has been used for making a wide variety of devices, including cantilever based biosensors,[2, 3] low cost point-of-care diagnostics[4, 5] and microvalves.[6] One of the major drawbacks of SU-8 is its high residual stress, which leads to bending of the microstructures[7, 8] caused by the mismatch between the thermal expansion coefficients of SU-8 and the substrate.

Many approaches have already been developed to reduce the residual stress in SU-8. One efficient way is to use an adaptive layer made of polymers such as polyethylene terephtalate (PET)[8] or polystyrene[9] that have an expansion coefficient similar to SU-8. These adaptive layers also act as release layers,

which can be dissolved and allows detaching the SU-8 structures without resorting to mechanical forces.[9, 10] Similarly, SU-8 itself can be used as an adaptive layer by evaporating a protective layer of metal (i.e. gold or chromium) on top. The sacrificial SU-8 layer is shielded from UV light and from being cross-linked by the metal, and can thus be dissolved at the end of the process leaving free-standing structures.[11] Another approach is to modify the baking parameters[8-10, 12, 13] and specifically reduce the temperature of the pre-bake. A Lower pre-bake temperature results in a higher residual solvent content, which leads to increased mobility of monomers that in turn allow lowering the post-bake temperature and thus reduces the overall stress.[13] A drawback of this method is a high residual solvent content which tends to evaporate subsequently and lead to stress buildup, which is what we observed as part of our experiments and describe in the results section. Whereas these strategies help reduce the residual stress and bending by orders of magnitude, the distortion still remains significant. Due to these issues, SU-8 has not yet been used for making thin, long freestanding and straight structures, such as pins for microarray spotting, to the best of our knowledge.

Pin spotting (or printing) is the original method developed for patterning biomolecules such as DNA and proteins as microarrays and is still widely used due to its ease of operation.[14] The idea of robotized pin spotting was introduced

as early as 1996 for making DNA microarrays.[15] In protein microarrays antibodies or purified proteins are microarrayed instead of DNA. Antibody microarrays are used analogously to DNA microarrays to measure the concentration of tens or hundreds of proteins at once from minute amounts of (crude) sample by measuring the fluorescent intensity on each spot.[16] Pin spotting operates by first dipping an array of pins in a 96 or 384 microtiter well plate containing spotting solutions, retracting it along with a small droplet of solution captured by capillary effects on each pin, or inside the slit if there is one, and then printing the pin array onto a surface thus effecting the transfer of the solution from the pin to the surface. The transfer of liquid is a result of the balance between the capillary retention of the pin, and the capillary effects resulting from the dynamic contact between pin and substrate; a microscopic gap is formed immediately before and after contact between pin and substrate and draws liquid onto the surface. Scaling is easy for contact printing and print heads with 96 pins are common, and heads with up to 192 pins have been produced,[17] which is much larger than for bioinkjet printers that are limited to 16 or 32 heads. The scalability stems from the fact that loading and spotting operate using capillary effects so that a single functional pin can be cloned and used as part of an array of pins with identical properties for each one.

Many different pin designs have been developed ranging from simple needles with a blunt tip useful for a few spotting cycles only to pins with slit and reservoirs that can be used to print hundreds of spots following a single dip-loading.[14] Pins are traditionally made out of stainless steel, tungsten and titanium, and are manufactured serially using techniques such as sawing, grinding, electric discharge machining (EDM), and laser machining.[14, 15] Ceramic pins and microcapillaries[18] have also been made and shown to be more durable and less susceptible to tapping forces, while improving the spot morphology and consistency.[19] However, both for metal and ceramic pins the fabrication remains time consuming and cost intensive.

More recently, Si pins have been introduced. These pins can be fabricated by batch processing using micromachining techniques such as deep reactive ion etching. When using Si, much higher resolution can be achieved, much smaller pins can be made, and they can be arrayed at a much higher density, up to one pin every 2.25 mm (which is the same spacing as a 1536 microtiter well plate).[17] However, the Si pins remain expensive, because costly deep reactive ion etchers are needed, and they need to be etched through a wafer, further entailing long fabrication time. Another drawback of Si is that it is a brittle material, and consequently the pins break easily during manipulation and the tips rapidly

deteriorate and lose their functionality. Si pins therefore need to be replaced regularly. In addition, another important issue of these pins is droplets sticking on the outside of the pins, which is more pronounced with rectangular silicon pins compared to the rounded steel pins.[20]

One of the major issues with the usage of pins is that the contact between the pin and the substrate can lead to inhomogeneous spreading of the sample. Spot homogeneity still remains a challenge despite many years of work on pins and is difficult to control, as it depends not only on the geometry of the pin itself, but also on its surface chemistry, on capillary effects, and can vary as a function of the number of printing cycles. In particular the first spots tend to be larger than the later ones as the solution is being used up.

Polymer materials have not been used for fabricating pins despite the fact that they are inexpensive, tough and therefore likely to sustain many printing cycles. An important reason is that polymers are difficult to structure at the microscale with the high aspect ratios needed for making spotting pins, with the notable exception of SU-8, but which suffers from high internal stress.

In this paper, we present a novel fabrication process with an annealing step for making long, thin freestanding SU-8 structures that are straight over a length of thirty millimeters without measurable bending as assessed by optical microscopy. This process is used to make SU-8 pins with an improved design, including a novel capillary stop valve that allows precise metering of the sample. We also introduce surface patterning of pins by microcontact printing of hydropbobic and hydrophilic thiols on the rectangularly shaped pins. We illustrate the resilience of SU-8 pins by reversible buckling them, and assess their spotting performance by testing the number of spots that can be produced and measuring the homogeneity of a microarray of spots.

3.4 Design of the pins

The pins need to be inserted into a commercial pin holder (see Fig. SI. 1 in APPENDIX I) with collimators that serve to align the pins and made for pins that are 200 µm thick and 1 mm wide, and which impose the width and thickness of the pins.[17] The length of the pins was chosen to be 30 mm, which is needed to reach the bottom of the wells of microtiter plates for loading liquids. The design is shown in Fig. 3.1.
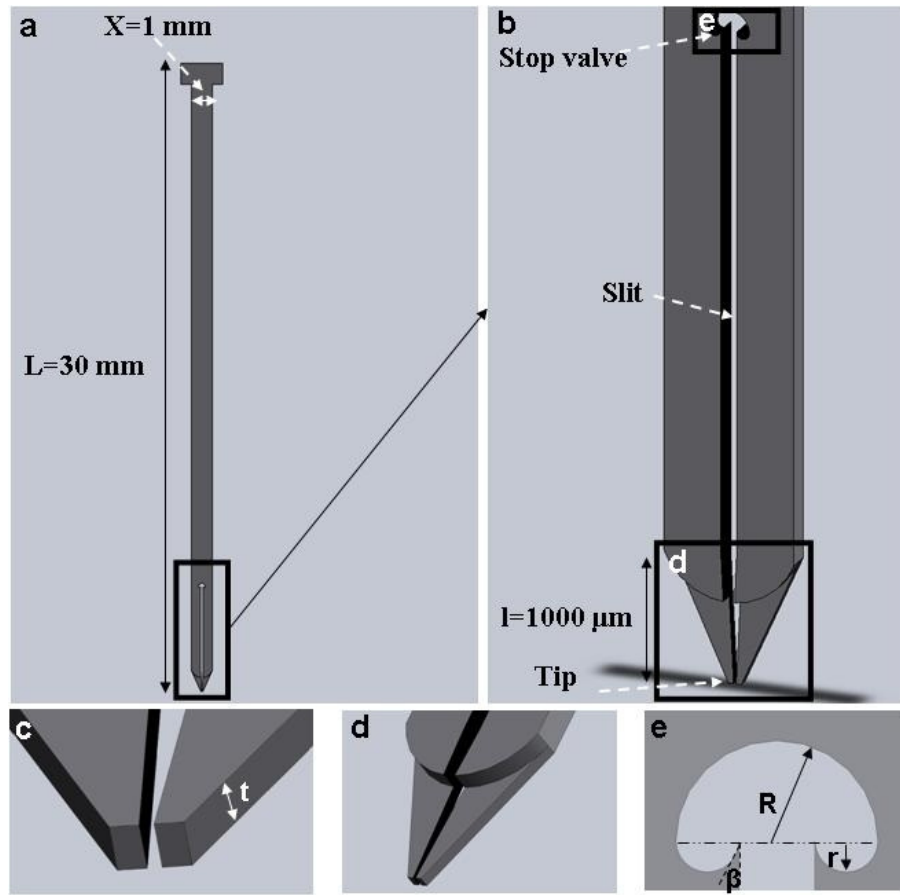
Fig. 3.13 Design features and dimensions of the pin. (a) Overview of the pin and (b) view of the tip, slit and the stop valve. (c) Enlarged view of the tip of the pin and (d) featuring the [two] layers of the pins. (e) Bubble with a capillary stop valve, the capillary stop valve was designed to stop the liquid at the end of the microchannel; R = 200 μm is the radius of curvature in the top part of the stop valve, r = 50 μm is the radius of curvature in the bottom part of the stop valve, and β is the angle at the interface between channel and bubble, which makes the liquid stop at the end of the channel.

The pins can be divided into three functional parts. The first one is the tip, which comes in contact with the substrate and controls the size of the spots; the second one is the slit, which acts as a microfluidic reservoir and a capillary pump; and the third part is a "bubble" with a stop valve, which is used to precisely control the amount of liquid loaded into the pin. The basis for our design were the pins commercially distributed by Parallel Synthesis,[17] The main changes are the bubble & slit geometries, surface chemistry and material used, all of which contribute to added functionality.

3.4.1 Tip

The size of the tip is determined by the thickness of the tip and its width, which in turn controls the size of the spot deposited on the surface. The pin consists of one or two layers (Fig. 3.1d), where the first layer controls the "height" of the spots, t, and the two layers together make up 200 µm in thickness, which is imposed by the size of the collimator. When making 200 µm spots, a single layer is suitable; however, for spot sizes less than 200 µm two layer pins are needed. A tip with a square cross-section of 100×100 µm^2 leads to a spot with a rounded square shape with a diameter of 140 µm.

3.4.2 Slit

For spontaneous filling of the microfluidic channel there needs to be a free energy gain. The increase of solid-liquid interface during filling (energy gained) needs to compensate for the increase in liquid-air interface (energy lost) in the slit. Expressed differently, the capillary pressure at the filling front in the slit needs to be negative. For pins with a slit (capillary gap) of width w and a depth t, and an advancing contact angle between solid-liquid interface in the microchannel, θ_a, the governing equation for the total pressure of the liquid in the pin's slit can be written as follow :[21]

$$P = +\frac{2\gamma}{t} - \frac{2\gamma Cos\theta_a}{w} + \rho g h < 0$$

(3.1)

For a capillary slit with a maximal length of 7 mm, as is the case here, the hydrodynamic pressure difference due to the gravity is ΔP = 70 Pa and can be neglected, when compared to the capillary pressure. The pressure in the liquid depends on the width of the slit and on the aspect ratio, t/w. By decreasing the aspect ratio, the capillary pressure decreases and when the ratio of the thickness, t, to the width, w, approaches one, filling becomes conditional on having contact angles very close to zero degrees, and turns into energetically unfavorable under all circumstances for $t \geq w$. Using a design according to the one proposed here, the thickness of the slit is t = 200 μm, water was assumed as a working media with γ = 70 mN.m⁻¹, and θ_a = 45°.[22] Under these conditions

$\mathit{\Delta P}\mathit{<}\mathit{0}$ for w < 141 µm, and the liquid will fill the slit spontaneously. Fig. 3.2. shows the capillary pressure of the liquid as a function of the width w of the slit. In order to ensure robust filling of the pins and provide a sufficient volume, w was set to 100 µm. Close to the tip, where the thickness and width of the pin are reduced, w narrows down as well, but since the tip is the last to be drained, it does not affect the capillary pressure during spotting.
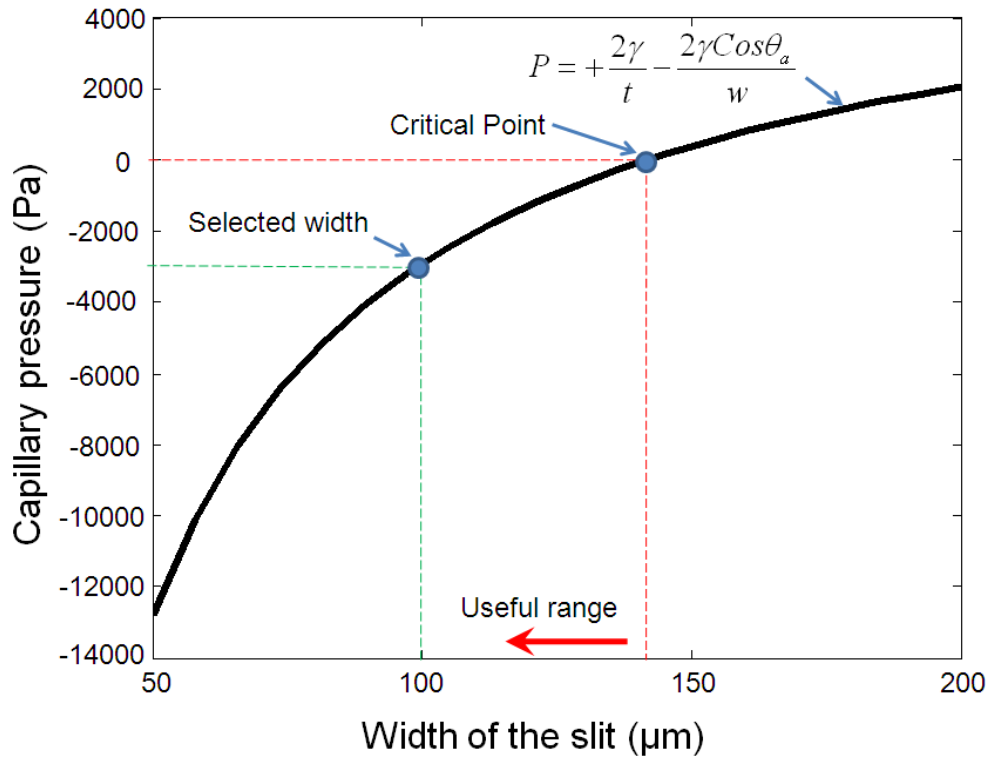
Fig. 3.214: Capillary pressure of the liquid as a function of the width w of the slit

for a constant thickness t = 200 µm and a liquid-solid contact angle θa = 45°. The

capillary pressure is negative for w < 141 µm, and consequently the liquid will fill

the microchannel. A width of 100 µm (corresponding to an aspect ratio of 2:1)

was selected for the slit to provide both a high capillary pressure and sufficient volume.

In addition, we estimated the elastic deformation of the tip of the pins due to the capillary pressure, which after filling may lead to bending of the tips, if the pins are too soft. For SU-8, which has an elastic modulus of 5.25–6.21 GPa.,[23] the tip deflection is only about 1 µm for a pin that has 7 mm long prongs (see Fig. SI. 2 in APPENDIX I). This value is negligible in practice for the slit sizes of 100 µm and will not influence the capillary transfer from the pin to the substrate.

3.4.3 Stop valve

To minimize the variation of spot size and volume during spotting, it is important that the capillary pressure is constant during the entire printing process. A pin with a straight conduit that stops at once (*i.e.* a dead-end channel) would satisfy the capillary pressure condition; however, because the conduit is open, dewetting of the liquid at the "dead-end" is energetically unfavorable and the liquid column would dewet somewhere along the path and liquid remain trapped in the pin at the dead-end. It is therefore important to include a stop valve in the flow path that stops the liquid from reaching the end of the slit, and design the valve so that it constitutes the location offering the least resistance to the draining of the liquid. Existing pins typically use graded enlargement of the channel width at the end of

the capillary, which gradually increases the width to depth aspect ratio until filling becomes unfavorable. Because of the graded change, there is not a definite stop, which in turn can lead to initial variability when starting to spot.[17] Stop valves can be formed by a sudden enlargement of a microfluidic conduit. When operating in a closed microchannel, it is difficult to make an efficient stop valve, because although the width can easily be enlarged, it is challenging to enlarge the depth simultaneously.[24] In the case of a pin however, there are no bottom and top walls, and very robust valves can be produced that reliably stop a solution, even for highly wetting liquids.[24-27]

3.5 Materials and methods

3.5.1 Microfabrication of the pins

We fabricated one and two layer SU-8 pins using standard microfabrication procedures, Fig. 3.3. (for one-layer pins, step (d) and (e) were skipped). First we crushed a polystyrene Petri dish (Fisher Scientific, Canada) and dissolved 10 g of polystyrene chips in 100 ml of toluene (Fisher Scientific, Canada) by stirring the solution at 80 ºC for 5 hrs. We then poured 5 ml of the solution on a 4´´ Si wafer and spin coated the substrate at the rate of 3000 rpm for 30 seconds to form a 3-4 µm thick polystyrene layer. Subsequently we placed the silicon wafer on a hotplate at 80 ºC for 5 minutes to remove the solvent. The thin layer of

polystyrene fulfills two functions. Firstly, it helps minimize the residual stress in the SU-8, and secondly, it serves as a sacrificial layer that facilitates the release of the pins from the substrate [9]. We patterned two layers of SU-8 using standard photolithography process atop the polystyrene layer. The parameters of the baking steps used to make the SU-8 pins are summarized in Table 3.1. We then developed the microstructures of both layers at once by immersing the wafer in the SU-8 developer (Propylene glycol methyl ether acetate, Microchem, USA), which was followed by the release of the SU-8 by dissolving the polystyrene layer with toluene. The pins were characterized by both optical (LV150 industrial microscope, Nikon, Japan) and scanning electron microscopy (S-3000N Variable Pressure-SEM, Hitachi, Japan).
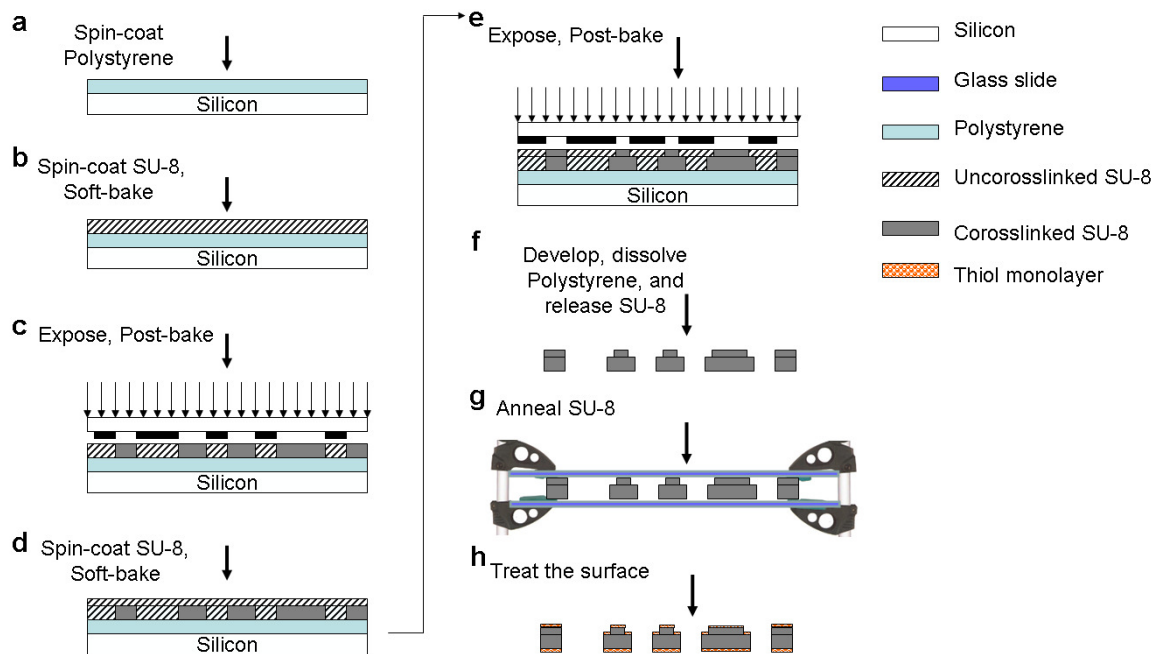
Fig. 3.15: Schematic illustration of the fabrication process of SU-8 pins. (a) A solution of polystyrene dissolved in toluene is spin-coated on the substrate (3-4 μm thick) to serve as an adaptive release layer. (b) A layer of SU-8 is spin coated and soft-baked. (c) The SU-8 is exposed to UV through a photomask and post-baked. (d&e) A second layer of SU-8 is spin-coated over the first layer and processed identically to the first one. (f) The SU-8 is developed and the polystyrene dissolved using toluene to release the patterned SU-8 pins. (g) The pins are then clamped between two glass slides and annealed at 150°C for 24 hours to fully cross-link the SU-8, while minimizing internal stress. (h) Finally, the pin is coated with Au and the surface patterned with hydrophobic (outside) and hydrophilic (inside) thiols.

Table 3.1: SU-8 processing parameters

	Obtained Thickness (μm)	Soft bake	Exposure Energy (mJ/cm^2)	Post exposure bake (heating)	Post exposure bake (cooling)
1st Layer	75	5 min @ 65°C and 25 min @90 °C	200	From 20°C to 70 @ 0.5 °C/min keep @70 °C for 30 min	From 70°C to 20 @ 0.5 °C/min
2nd Layer	100	5 min @ 50°C and 45 min @70 °C	230	From 20°C to 70 @ 0.5 °C/min keep @70 for 30 min	From 70°C to 20 @ 0.5 °C/min

3.5.2 Annealing of SU-8 to eliminate the residual stress

We developed an annealing process to remove the residual stress in SU-8. The freestanding pins were clamped between two rigid glass slides ($75 \times 25 \times 1$ mm^3 microscope slides, Fisher Scientific, Canada) by using paper clips (fold back clips, Staples, Canada; see Fig. 3.3., g). Using a programmable oven (Lindberg Blue M, Fisher scientific, Canada), we subjected the setup to a heat cycle, which consisted of first a temperature ramp from room temperature to 150 ºC in 15 hours, then keeping it constant at 150 ºC for 15 hours, and finally cooling it down to room temperature in 24 hours.

3.5.3 Surface treatment of the pins

We coated the pins by sputtering 10 nm Ti followed by 50 nm of Au. Then we used a flat stamp of poly(dimethylsiloxane) (PDMS; Sylgard 184, Dow Corning, USA) inked with a solution of 1% n-decanethiol (Fluka, Canada) in ethanol to print on the top- and back-side surface of the pin to coat the outer surfaces with a hydrophobic n-decanethiol.[22] The slit of the pins was then selectively coated with hydrophilic tihols by immersing them for 1 h in a 1 mM solution of PEG-thiol (Rapp Polymere, Germany) in water. Fig. SI. 3 in APPENDIX I illustrates the entire patterning process.

3.5.4 Spotting and imaging of proteins

We first placed the pins in a commercial pin-holder (Parallel Synthesis, USA) with two micromachined collimators (see Fig. S4 in APPENDIX I for more details), and spotted the microarray using a customized spotting robot (nano-plotter 2.0, Gesim, Germany). Chicken antigoat IgG, labeled with fluorescein was diluted at a concentration of 200 μg mL^{-1} in a solution of carbonate buffer at pH 9 containing 10% glycerol. The solution was spotted with a single pin on an epoxy coated glass slide (Nexterion, Schott, USA). The slide with the array of droplets forming the protein array was scanned with a laser scanner (LS400, Tecan, NC, USA) using 532 nm laser and a resolution of 10 μm. The images were analyzed using Image J (http://rsb.info.nih.gov/ij/).

3.6 Results and discussions

3.6.1 Fabrication

Two variants of the pins were fabricated using either one or two layers of SU-8, but always with a total thickness of 200 μm so as to fit into the collimator (see Fig. SI. 4). Fig. 3.4 shows micrographs of both types of pins. The single layer SU-8 pins made using only one lithographic exposure had a slit with a width of 50 μm and a total width of 75 μm at the tip. Two layer pins were fabricated using

two-step lithography process with a tip size of 50×75 µm^2 and therefore lead to much smaller spots.
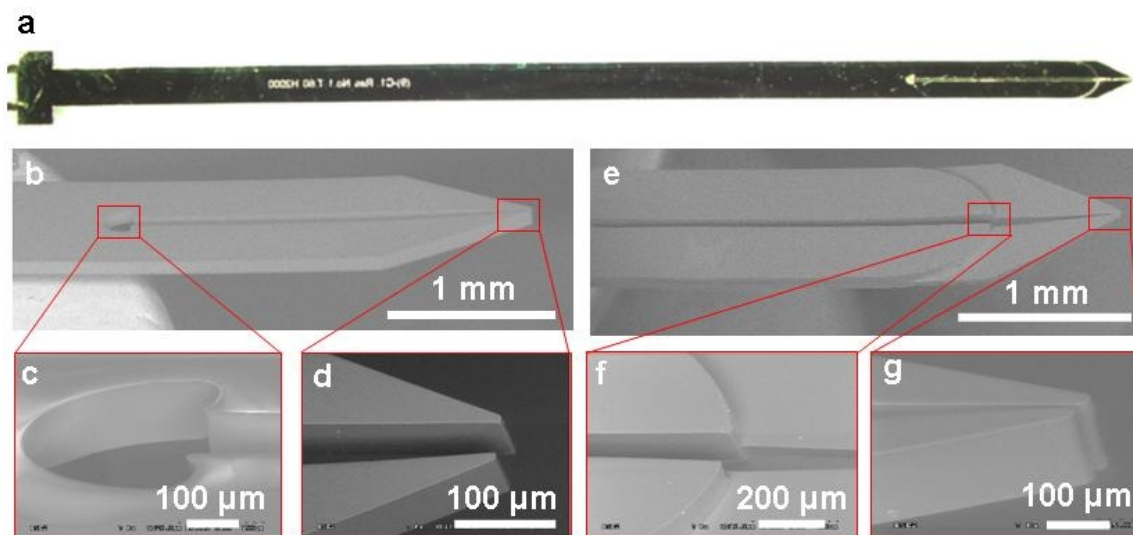
Fig. 3.16: Micrographs of microfabricated SU-8 pins. (a) Overview of a pin coated with Au. The pattern in the middle of the pin is a label that was structured into each pin. The 7 mm long, 100 µm wide slit is visible at the right. (b) SEM image showing the entire slit and tip of a single-layer, 200 µm thick tip along with close-up views of (c) the stop valve (d) and the tip. (e) SEM of a double layer pin, (f) the interface of the two layers and (g) the 75 µm thick tip.

The volumetric capacity of the pins was adjusted by making channels with different lengths, and by making pins with two channels; (see Fig. SI. 5 in APPENDIX I for additional details). The pins presented here have a transfer capacity of 100-300 nL.

3.6.2 Annealing process

A critical parameter for pin spotting is the alignment and straightness of the pins. Indeed, high density arrays have a pitch of only 250 µm, which implies that the pins need to be perfectly straight as even a deviation of a few hundred micrometers (for a length of 30 mm) can lead to overlap of adjacent spots. Bending of the SU-8 structures is caused by the internal stress, arisen as a consequence of the thermal mismatch and the asymmetric configuration of the SU-8 atop of the Si wafer during the post-baking process. So the requirements for thin, slender and straight pins represent a major challenge for SU-8 pins.[13]

To quantify the deflection of the pins due to the residual stress, we introduce a deflection variable $\partial\zeta$, which is defined as the deflection of the pin, once it is placed between the two anchor points in the pin collimators used for spotting. Fig. 3.5a shows the deflection of an SU-8 pin that was spin-coated directly on a sacrificial layer of polystyrene and processed according to recipes of the manufacturer.[12] As can be seen, the pin is strongly bent and deflects $\partial\zeta \approx 6$ mm. With optimized baking parameters and using an adaptive polystyrene layer, (as described in table 3.1.), the deflection could be decreased to $\partial\zeta = 500 \pm 200$ µm, (See Fig. 3.5b). The ± 200 µm corresponds to the maximal variability observed among different pins. The residual stress of the pin can be approximated as:[28]

$$\sigma_{max} = -\frac{Et}{2\rho}$$

(3.2)

Where ρ is the radius of the curvature, σ_{max} is the maximum residual stress, E is the elastic young modulus of SU-8 and t is the thickness of the pin.

$\partial\zeta \approx 500 \pm 200$ µm corresponds to $\rho = 172 \pm 68$ mm (see Fig. SI. 6 in APPENDIX I for more details). Substituting in to equation (3.2), the maximum residual stress in the pin after optimizing the baking parameters is found to be $\sigma_{max} = 33.4 \pm 13.4$ MPa, which is within the range of stress values reported in the literature.[11, 12]

SU-8 shrinks 6-10% during the cross-linking and post-baking processes,[11, 29] which is a great source of stress, and makes it difficult to find a substrate that follows the same expansion cycles during post-bake and subsequent thermal cooling of the SU-8. However, we reasoned that by having a symmetric setup – achieved by clamping the SU-8 structure between two identical substrates – the asymmetric stress buildup arising when a single substrate is used could be reduced. An additional annealing step was therefore introduced at a temperature of 150 ºC using two glass slides to clamp the pins (see Fig. 3.3g). Since the SU-8 glass transition temperature is around 175 ºC,[30] we found that when annealing with 175 ºC or more, the tips of the pins were stuck to one another

after processing. By reducing the annealing temperature to 150 ºC, the tips remained separate, while still minimizing the stress. We also found that slow ramping, and in particular slow cooling further helped reducing the residual bending. When using the set of optimized parameters presented in section 3.5.1, the residual bending of SU-8 was reduced within the accuracy of the optical measurements used, $\partial\zeta = 0 \pm 30$ µm, Fig. 3.5c. Here, the ± 30 µm corresponds to the estimated accuracy of our imaging setup. We also found that annealed pins were stable over for at least 10 months (i.e. the pins described in Fig. 3.5.c), whereas pins that were not annealed tended to bend after a few weeks up to $\partial\zeta = 2000 \pm 1400$ µm (figure is not shown) which we attribute to the evaporation of the residual solvent.
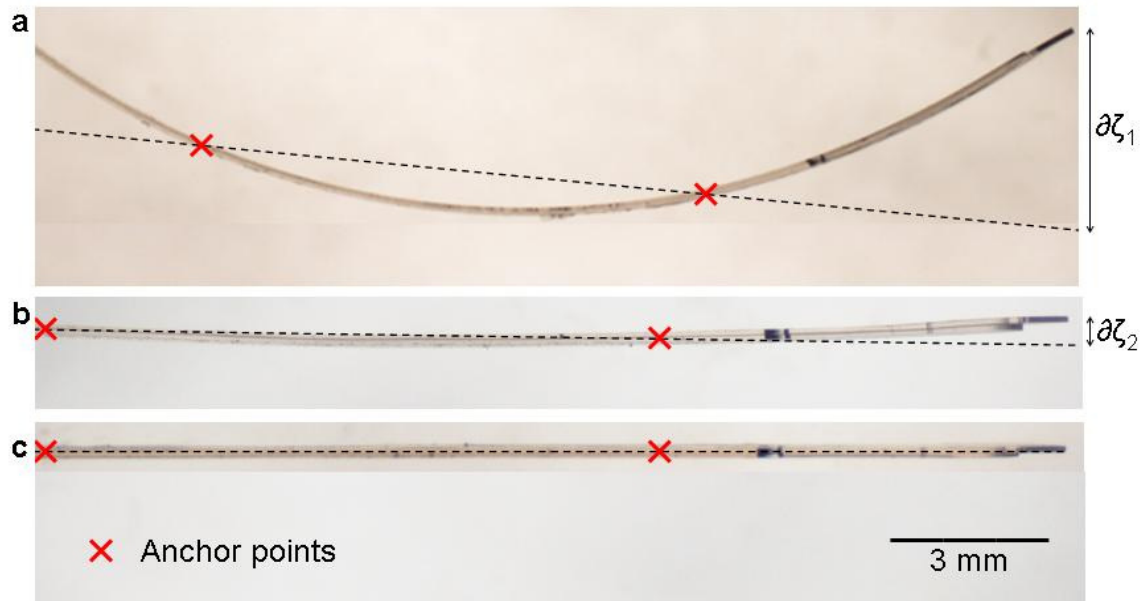
Fig. 3.17: Visualization and quantification of the deflection $\partial\zeta$ of 200 µm thick SU-8 pins seen lying on their side and that were fabricated using different processes

78

described in the text. $\partial\zeta$ is defined as the deflection of a pin at the tip when fixed by the two anchor points of a collimator marked by an X. (a) Pin fabricated according to the recipe recommended by the manufacturer, which leads to a deflection of $\partial\zeta_1 \approx$ 6mm. (b) Pin made using optimized baking parameters and an adaptive polystyrene layer, $\partial\zeta_2$ = 500 ± 200 µm. (c) Pin fabricated with the same recipe as in (b), and subjected to an annealing step, $\partial\zeta_3$ = 0 ± 30 µm

3.6.3 Toughness and Flexibility of the Polymer Pins

Polymers are tougher and more flexible than Si, which should translate into more reliable pins. Indeed, Si pins regularly break due to the brittleness of Si. To illustrate the resilience of the SU-8 pins they were subjected to a bending cycle, Fig. 3.6, showing how the pin buckles without breaking and flexes back to its original. The tip of the pin did not show any visible deterioration (data not shown). Although such high loads are not normally applied during microarray spotting, software glitches and human errors sometimes result in pins being subjected to high strain, which often lead to the destruction of metal or Si pins. In the course of a printing experiment described below, a pin was subjected to 2000 buckling cycles as shown in Fig. 3.6 without observing notable permanent deformation for the pin or the tip.
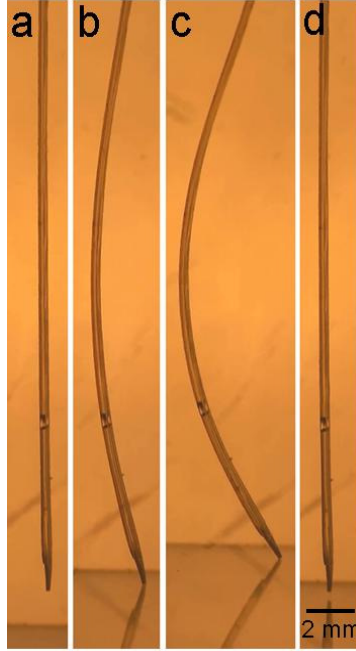
Fig. 3.18: Images extracted from a movie showing the elastic buckling of an SU-8 pin as it is being pressed against a substrate, followed by its unbending. (a) The SU-8 pin before elastic deformation; (b,c) during elastic buckling, and (d) after buckling.

3.6.4 Surface Treatment

Native SU-8 is hydrophobic with $\theta_{water\text{-}SU\text{-}8}$=90 °(see reference 31)[31] and therefore in the absence of surface treatment aqueous solutions do not spontaneously fill the slit of the pin. Fig. 7a shows a native SU-8 pin that was dipped into an aqueous solution containing fluorescent rhodamine dye. Whereas the slit was not filled, a drop attached to the tip of the pin. To ensure spontaneous filling of the slit with water, the inside of the slit was selectively made hydrophilic using a self-

assembled PEG-thiol monolayer. Following this treatment, the liquid spontaneously filled the slit and no drops attached to the outside of the pin, Fig. 3.7b-e). The surface treatment is critical to obtain functional pins and to prevent droplets from attaching to the outer surfaces of the pins.
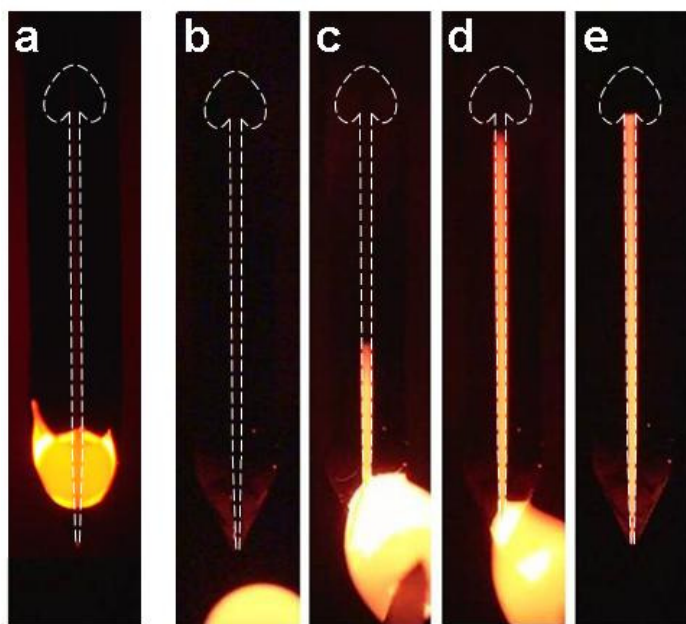
Fig. 3.19: Capillary filling of pins. (a) Fluorescence micrograph of an SU-8 pin without surface treatment that was dipped into a solution containing fluorescent rhodamine. (b) Pin coated with a hydrophobic thiol on the outside and a hydrophilic PEG-thiol on the inside. (c) Upon contacting a droplet, (d) the liquid spontaneously fills the slit. (e) The bubble with the stop-valve stops the filling and ensures precise metering of the solution within the pin.

3.6.5 Spotting of proteins

Pins were used to spot a solution with a fluorescently labeled protein as a microarray. Slides are commonly scanned after washing only, the size and homogeneity of the spot can vary due to inhomogeneity of the surface chemistry. To avoid this problem, we scanned the slides immediately after spotting with an SU-8 pin 2000 times, while the droplets were still present on the glass slide. For the protein spotting, a two layer pin with a tip size of 50×75 µm², and a 7 mm long slit with a capacity of 140 nL was used. The humidity was set at 70% and the solution contained 10 % glycerol to further reduce evaporation, which allowed printing 1392 spots in a single run, Fig. 3.8. The spots produced by this pin are 90 µm along the diagonal. The subsequent spots are barely visible indicating that the sample was used up. Neglecting evaporation, the volume of each deposited spot is 100 pL, which is comparable to the volumes of liquid deposited by conventional pins or inkjet spotting. We found that the maximum size variation falls within the ten-micrometer-resolution of the scanner for the first 1392 spots of the array. Further studies are needed to determine whether the attachment of proteins to the slide surface follows the same trends, which will be tested in future studies.
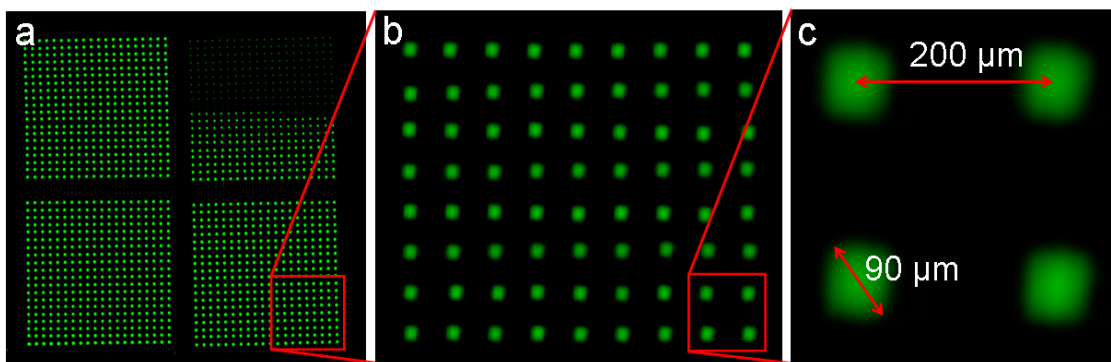
Fig. 3.20: Fluorescence images of a microarray of 1392 spots of a fluorescent protein that were spotted using an SU-8 pin in one run with a pitch 200 µm. (a) overview of the array with 4 sub-arrays of 20 × 20 spots. The last visible well printed spot is at the 12th row on the 10th line. (b) Close up view of 8×9 spots and (c) 4 spots of the microarray.

3.7 Conclusion

We have introduced SU-8 fabrication process that allows making stress free, straight structures. The key to the successful fabrication of these pins was the development of an annealing step, which allows making 200 µm thin polymer structures that are 30 mm long and straight within 30 µm. Polymer pins with a novel stop valve design and surface chemical treatment served to illustrate some of the possibilities of this process. The functionality of the pins was demonstrated by mechanically loading and buckling them, and by printing 1392 spots with a constant diameter of 90 ± 4 µm using a single filling. These pins are made by a two-step standard lithography process without need for complicated equipment

beyond a mask aligner, hot plates and an oven for annealing. The capital investment needed for microfabricating SU-8 pins is much smaller when compared to Si pins for example, which require a deep reactive ion etcher. In addition, the material costs are low as well, since no more than 10 ml of SU-8 are used for making 100 pins, which corresponds to a material cost of less than 10 cents per pin. SU-8 thus represents a robust and low cost alternative for making microarray spotting pins.

The fabrication process outlined here may be applied to any flat, freestanding patterned polymer structure made of SU-8. We foresee that it may for instance be used to fabricate neuronal probes for invasive recording in the brain, which need to be straight and flexible.[32] In addition, the strategy outlined here may also be applied to molded thermoplasts such as poly(methyl methacrylate), polystyrene, polycarbonate, and cyclic-polyolefin copolymer and so on, because residual stress also builds up as a result of thermal gradients and asymmetric shrinkage of structures.[33] The concept of symmetrical heating and cooling may be adapted to polymer features that remain (partially) attached to a substrate. By using two identical substrates to clamp the polymer, asymmetrical stress buildup following thermal cycling can be prevented by using a perfectly symmetrical setup.

84

3.8 Acknowledgement

3.9 References

1.   Liu, G., Tian, Y. & Kan, Y. Fabrication of high-aspect-ratio microstructures using SU-8 photoresist. *Journal of Microsystem Technologies* **11**, 343-346 (2005).

2.   Nordström, M., Keller, S., Lillemose, M., Johansson, A., Dohn, S., Haefliger, D., Blagoi, G., Havsteen-Jakobsen, M. & Boisen, A. SU-8 cantilevers for bio/chemical sensing; Fabrication, characterisation and development of novel read-out methods. *Sensors* **8**, 1595-1612 (2008).

3.   Backmann, N., Zahnd, C., Huber, F., Bietsch, A., Plückthun, A., Lang, H.P., Güntherodt, H.J., Hegner, M. & Gerber, C. A label-free immunosensor array using single-chain antibody fragments. *Proceedings of the National Academy of Sciences* **102**, 14587-14592 (2005).

4.   Abgrall, P., Conedera, V., Camon, H., Gue, A.M. & Nguyen, N.T. SU-8 as a structural material for labs-on-chips and microelectromechanical systems. *Electrophoresis* **28**, 4539-4551 (2007).

5.   Ruano-Lopez, J.M., Agirregabiria, M., Olabarria, G., Verdoy, D., Bang, D.D., Bu, M., Wolff A., Voigt A., Dziuban, J.A., Walczak, R. & Berganzo J. The SmartBioPhone (TM), a point of care vision under development

through two European projects: OPTOLABCARD and LABONFOIL. *Lab on a Chip* **9**, 1495-1499 (2009).

6. Ezkerra, A., Fernandez, L.J., Mayora, K. & Ruano-Lopez, J.M. Fabrication of SU-8 free-standing structures embedded in microchannels for microfluidic control. *Journal of Micromechanics and Microengineering* **17**, 2264-2271 (2007).

7. Bystrova, S., Luttge, R. & van den Berg, A. Study of crack formation in high-aspect ratio SU-8 structures on silicon. *Journal of Microelectronic Engineering* **84**, 1113-1116 (2007).

8. Abgrall, P., Charlot, S., Fulcrand, R., Paul, L., Boukabache, A. & Gué, A.M. Low-stress fabrication of 3D polymer free standing structures using lamination of photosensitive films. *Journal of Microsystem Technologies* **14**, 1205-1214 (2008).

9. Luo, C., Govindaraju, A., Garra, J., Schneider, T., White, R., Currie, J. & Paranjape, M. Releasing SU-8 structures using polystyrene as a sacrificial material. *Journal of Sensors and Actuators, A* **114**, 123-128 (2004).

10. Foulds, I.G., Johnstone, R. & Parameswaran, M. Polydimethylglutarimide (PMGI) as a sacrificial material for SU-8 surface-micromachining. *Journal of Micromechanics and Microengineering* **18** (2008).

11. Conedera, V., Salvagnac, L., Fabre, N., Zamkotsian, F. & Camon, H. Surface micromachining technology with two SU-8 structural layers and sol-gel, SU-8 or SiO2/sol-gel sacrificial layers. *Journal of Micromechanics and Microengineering* **17**, N52-N57 (2007).

12. Hammacher, J., Fuelle, A., Flaemig, J., Saupe, J., Loechel, B. & Grimm, J. Stress engineering and mechanical properties of SU-8 layers for mechanical applications. *Journal of Microsystem Technologies* **14**, 1515-1523 (2008).

13. Keller, S., Blagoi, G., Lillemose, M., Haefliger, D. & Boisen, A. Processing of thin SU-8 films. *Journal of Micromechanics and Microengineering* **18** (2008).

14. Barbulovic-Nad, I. Lucente, M., Sun, Y., Zhang, M., Wheeler, A.R. & Bussmann, M. Bio-microarray fabrication techniques - A review. *Critical Reviews in Biotechnology* **26**, 237-259 (2006).

15. Schena, M., Shalon, D., Davis, R.W. & Brown, P.O. Quantitative monitoring of gene-expression patterns with complementary-DNA microarray *Science* **270**, 467-470 (1995).

16. Kambhampati, D. (Wiley-VCH Verlag GmbH & Co. KGaA, chapter 2, 2005).

17. Parallel Synthesis Co., http://www.parallel-synthesis.com/, Retrieved 2008/12.

18. Rose, D., Tisone, Thomas C., Vol. US6551557 (Cartesian Technologies, Inc. (Irvine, CA) United States 12/10/1999).

19. George, R.A., Woolley, J.P. & Spellman, P.T. Ceramic capillaries for use in microarray fabrication. *Journal of Genome Research* **11**, 1780-1783 (2001).

20. Microarray Biochip Technology, first edition (Eaton Publishing, chapter 9, 2000).

21. Bruus, H. Theoretical Microfluidics, first edition, (Oxford University Press, chapter 7, 2008).

22. Juncker, D., Schmid, H., Drechsler, U., Wolf, H., Wolf, M., Michel, B., de Rooij, N. & Delamarche, E. Autonomous microfluidic capillary system. *Analytical Chemistry* **74**, 6139-6144 (2002).

23. Al-Halhouji, A.T., Kampen, I., Krah, T. & Buettgenbach, S. Nanoindentation testing of SU-8 photoresist mechanical properties. *Journal of Microelectronic Engineering* **85**, 942-944 (2008).

24. Zimmermann, M., Hunziker, P. & Delamarche, E. Valves for autonomous capillary systems. *Journal of Microfluidics and Nanofluidics* **5**, 395-402 (2008).

25. Melin, J., Roxhed, N., Gimenez, G., Griss, P., Wijngaart, W. & Stemme G. A liquid-triggered liquid microvalve for on-chip flow control. *Journal of Sensors and Actuators, B* **100**, 463-468 (2004).

26. Chen, J.M., Huang, P.C. & Lin, M.G. Analysis and experiment of capillary valves for microfluidics on a rotating disk. *Journal of Microfluidics and Nanofluidics* **4**, 427-437 (2008).

27. Leu, T.S. & Chang, P.Y. Pressure barrier of capillary stop valves in micro sample separators. *Journal of Sensors and Actuators, A* **115**, 508-515 (2004).

28. Beer, F.P., Johnston, J. & Dewolf, J.T. Mechanics of Materials, seventh edition (McGraw Hill, chapter 3, 2008).

29. Chung, C.K. & Hong, Y.Z. Surface modification of SU8 photoresist for shrinkage improvement in a monolithic MEMS microstructure. *Journal of Micromechanics and Microengineering* **17**, 207-212 (2007).

30. Blattler, T.M., Senn, P., Textor, M., Voros, J. & Reimhult, E. Microarray spotting of nanoparticles. *Journal of Colloids and Surfaces, A* **346**, 61-65 (2009).

31. Nordstrom, M., Marie, R., Calleja, M. & Boisen, A. Rendering SU-8 hydrophilic to facilitate use in micro channel fabrication. *Journal of Micromechanics and Microengineering* **14**, 1614-1617 (2004).

32. Hajj-Hassan, M., Chodavarapu, V.P. & Musallam, S. Microfabrication of ultra-long reinforced silicon neural electrodes. *Micro & Nano Letters* **4**, 53-58 (2009).

33. Malek, C.K., Coudevylle, J.R., Jeannot, J.C. & Duffait, R. Revisiting micro hot-embossing with moulds in non-conventional materials. *Journal of Microsystem Technologies* **13**, 475-481 (2007).

Chapter 4: Microfluidic operations and networks using knotted yarns

4.1 Preface:

Microfluidic capillary systems are normally fabricated using techniques originally used in making micro-electro-mechanical systems (MEMS). These techniques are still too expensive, particularly if we need to use them in societies with few resources. Here we introduce the use of knotted yarns for making microfluidic elements and circuits. We first present methods to control and measure the fluidic properties of the yarns and knots including the generated capillary pressure and the flow resistoce. Afterwards, we use knots for merging, mixing and branching liquid streams. Finally, we combine these fluidic elements for making a simple capillary driven microfluidic circuit.

The work resulted in the following publications:

Patent: Juncker, D. & <u>Safavieh, R</u>. *Passive preprogrammed logic systems using knotted/stretchable yarns and their use for making microfluidic platforms*. US patent App. 12/917,436, (2010).

Journal Paper: <u>Safavieh, R.</u>, Zhou, G.Z. & Juncker, D. *Microfluidics made of yarns and knots: from fundamental properties to simple networks and operations*. Lab Chip 11, 2618-2624 (2011).

4.2 Abstract

We present and characterize cotton yarn and knots as building blocks for making microfluidic circuits from the bottom up. The yarn used is made up of 200-300 fibres, each with a lumen. Liquid applied at the extremity of the yarn spontaneously wets the yarn, and the wetted length increases linearly over time in untreated yarn, but progresses according to a square root relationship as described by Washburn's equation upon plasma activation of the yarn. Knots are proposed for combining, mixing and splitting streams of fluids. Interestingly, the topology of the knot controls the mixing ratio of two inlet streams into two outlet yarns, and thus the ratio can be adjusted by choosing a specific knot. The flow resistance of a knot is shown to depend on the force used to tighten it and the flow resistance rapidly increases for single-stranded knots, but remains low for double-stranded knots. Finally, a serial dilutor is made with a web made of yarns and double-stranded overhand knots. These results suggest that yarn and knots may be used to build low cost microfluidic circuits.

4.3 Introduction

Yarn and textiles can be traced back five millennia and were used for clothing and for other practical and decorative purposes.[1] One of the primary functions of textiles is to isolate the carrier from the environment, and in particular from rain

and water, and many treatments have been developed to make hydrophobic, water repellent yarns and fabrics.[2-4] Hydrophilic textiles have also been developed, primarily as microfibre-based fabrics for fast wicking and sweat venting.[5] Natural cellulose cotton fibres can also be made hydrophilic using wet and dry (*e.g.* plasma activation) processes.[6, 7]

Natural fibres have been used for making microfluidic flow transport in the form of lateral flow devices, which rely on the wicking properties of nitrocellulose membranes (sheets) to transport liquid in predetermined ways. By optimizing the flow speed of the sample based on the biomolecular reaction rates, rapid and highly sensitive bioassays have been developed.[8-11] This lateral flow technology has been packaged into simple microfluidic devices and over-the-counter diagnostics notably in the form of rapid pregnancy tests.[9] More complex microfluidic circuits have recently been made using chromatography paper and tape.[12, 13] Microchannels were formed by defining hydrophobic barriers in the paper followed by stacking different layers so as to form three dimensional circuits. These 3D paper-based microfluidics are built based on a top-down paradigm and functional elements are patterned on a flat substrate using a sequence of processing steps as in semiconductor microfabrication.

91

We and others recently proposed yarn as a microfluidic carrier and illustrated its use for making simple microfluidic devices from the bottom up.[14-16] Li *et al.*[15] demonstrated the fabrication of three-dimensional microfluidic devices by sewing cotton yarn into polymer sheets, transporting and mixing fluids using tapes and carrying out simple colorimetric assays. Reches *et al.*[16] independently developed similar devices and studied different treatments to make the yarn hydrophilic, build simple devices by encapsulating the yarn within tapes, or by sewing it into different materials including band aids, and used it for multiplex assays of ketones, glucose, and proteins.

Here, we report our findings on the flow properties of yarn and on using knots for differential mixing and building complex microfluidic networks. We measured the flow resistance of the yarn and the knots and show that the knot topology can be used to control the mixing ratio between two inlets and two outlets. Finally, we built a serial dilutor by iterative combining of mixing and splitting of fluids using a knotted web, analyze the fluid distribution using network analysis concepts developed for electrical circuit analysis, and compare the theoretical and experimental results.

4.4 Materials and methods

4.4.1 Yarn and chemicals

The yarn used here was a white sewing thread obtained from Tehran (Iran) and from mercery stores locally (100% Cotton yarn Ne 30/1, Mahabad Riss Co, Iran).[17] They were tested for suitable wicking properties before usage. The yarns were first dried in an oven, and made hydrophilic using an air plasma (Plasmaline 415, Tegal Inc., US) for two minutes at 250 mTorr at a power of 150 mW. To obtain the cross sectional micrographs of the yarns, a 2 cm length of the yarn was soaked with blue dye and encased into Poly(dimethylsiloxane)(PDMS; Sylgard 184, Dow Corning), degassed in a desiccator for 6 h, and cured at 65 °C for 8 h in an oven (Lindberg Blue M, Fisher Scientific). A razor blade (single edged razor blade, Fisher Scientific, Canada) was used to cut thin slices.

Food dyes (McCormick & Co., MD, USA) were obtained from local stores. Experiments were performed at a relative humidity of ~ 30% and at the room temperature of 23±2 °C. Unless indicated otherwise, the yarn was positioned horizontally for all experiments and a sheet of hydrophobic polytetrafluoroethylene (PTFE) was used as substrate so as to avoid wicking of liquid in the gap between the yarn and the substrate.

4.4.2 Imaging

Images of the flow were captured using a stereomicroscope (Leica MZ8, Leica Microsystems, Switzerland) outfitted with a CCD camera (DS-Fi1, Nikon, Japan). A Scanning electron microscopy (S-3000N, Hitachi, Japan) was used for structural analysis following coating with a thin Au layer. Cross-sectional images were acquired with an inspection microscope (LV150A, Nikon).

4.4.3 Flow resistance measurement

Polyamide monofilament precision fabric (Sefar, Lumberton, NJ, USA) with pore opening of 110 μm, and thickness of 75 μm were employed as a capillary pump because they generate a constant and well defined capillary pressure. The fabric was plasma activated to make it hydrophilic before the measurements. A measurement setup was built by clamping one extremity of the yarn with the fabric between two microscope slides (Fisher Scientific, Canada), and dipping the other extremity of the yarn into a small reservoir. A known volume of solution (typically 9 μL) was added to the reservoir, and the time needed to drain the liquid from the reservoir measured. Multiple measurements were performed by repeatedly adding solutions of different colours to the reservoir.

4.4.4 Image analysis

To establish the mixing ratios of the dyes by the knots, we used the Image J software (http://rsbweb.nih.gov/ij/) to extract the hue colour intensity and compared it to a calibration curve established with known mixtures of the different dyes, see Fig. SII.1 in APPENDIX II.

4.5 Results & Discussion

4.5.1 Yarn as a flow carrier

Cotton yarn is widely available, low-cost, and like paper, the main component is cellulose.[4] The results reported in this study where obtained with regular sewing thread made of cotton, Fig. 4.1A. The yarns are 500 ± 34 μm in diameter and made up of ~200 fibres each 12-15 μm thick based as measured from SEM images, Fig. 4.1B&C. Imaging of encased cross-sections of yarn reveal that the fibers comprise a lumen, akin to wood cellulose, Fig. 4.1D&E.
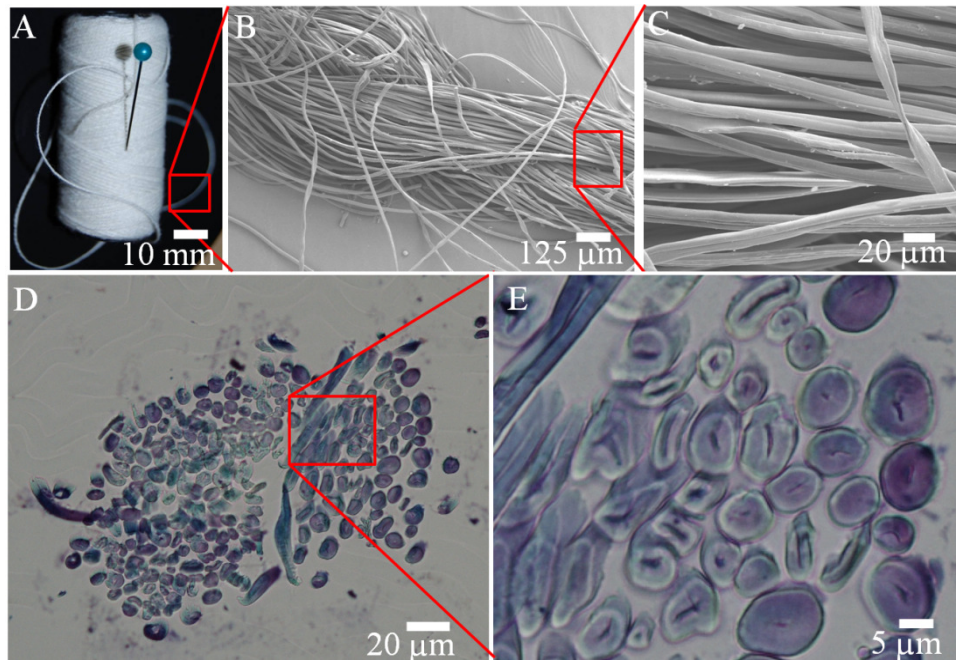
Fig. 4.21: Images of a cotton yarn at different scales and cross-sectional views of a yarn. (A) Photograph of a ball of cotton yarn; (B) SEM micrograph of the yarn illustrating the loose nature of the thread which is ~500 µm wide in diameter and contains ~200 fibres. (C) Close-up view of the fibres that are each 15-20 µm thick and that form an array of narrow gaps that can be filled with liquid. (D) Micrograph of the cross sectional view of a yarn showing the individual cotton fibres and their surface contours. (E) Enlarged view of fibres showing that they have a lumen (cavities) inside which may also contribute to the transport of liquid throughout wetting.

The wicking action of natural fibres is well known, and a red food dye solution spontaneously flowed along a cotton yarn wetting 5 mm after 40 s when using it

as received, Fig. 4.2A. The flow speed was slow, advanced stochastically, and was sensitive to the relative humidity (data not shown).Yarns are not optimized for capillary flow, and indeed for instance sewing threads are often coated with wax and other additives that improve gliding and prevent tearing of the yarn, but which render it hydrophobic.[6] When using the same yarn following activation and hydrophilization using an air plasma, the liquid advanced 32 mm during the same time, Fig. 4.2B. Capillary forces generated in the gaps between the fibres drive the flow, and the wetted length L as a function of time t is thus expected to follow Washburn's equation:[18]

$$L = \sqrt{\frac{(\gamma_{LG} \times \cos\theta) \times D \times t}{4 \times \mu}} \text{ [m]} \tag{4.1}$$

where γ is the interfacial tension, θ is the contact angle between liquid and yarn surface, D is the effective capillary diameter (yarn comprises multiple parallel, open flow paths),[19] and μ is the viscosity of the liquid. We recorded L as a function of t for both as-received and plasma activated cotton, and fitted the data with a square root function, Fig. 4.2C. The regression factors are R = 0.98 for hydrophilic yarn and for yarn used as received it is R = 0.92. However, a linear fit yields R = 0.99 for the as-received yarn indicating that filling progresses linearly over time. The linear filling may be accounted by the complex processes that underlie wetting of cellulosic fibres,[20] and indeed non-Washburn filling speeds

have also been reported in the wetting of fibrous materials notably due to

swelling of the porous medium.[21]
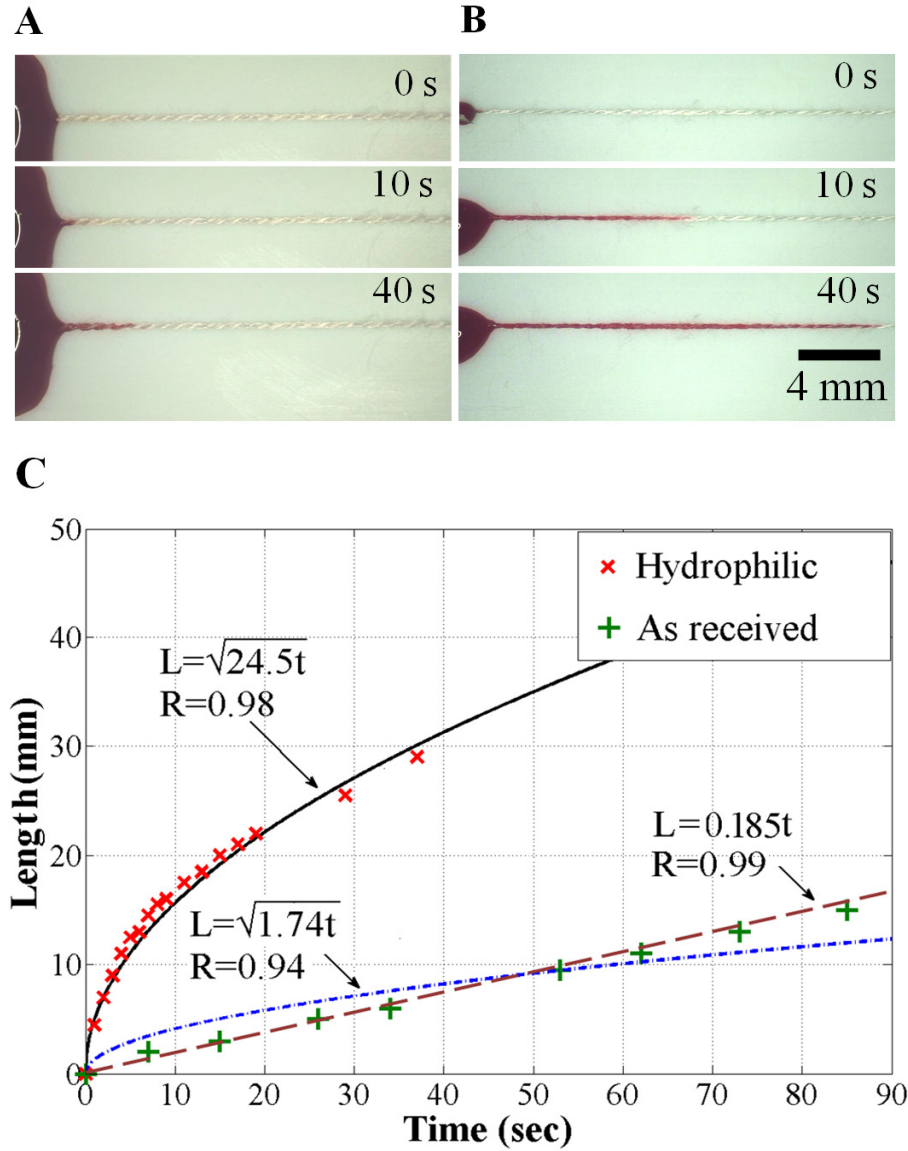
Fig. 4.22: Images extracted from a video illustrating the wicking of a red dye in

(A) as-received and (B) plasma activated, hydrophilic cotton yarn. (C) The wetted

length scales as $L \propto \sqrt{t}$ for the hydrophilic yarn and obeys a Washburn's

relation, and $L \propto t$ for the as-received yarn reflecting a constant filling speed irrespective of filled length and increasing flow resistance.

We measured that a liquid volume V of 2.5 μL wetted a yarn with a diameter of ~500 μm over a length of 43 ± 2 mm. Assuming that the geometry of the yarn is cylindrical with a diameter of 500 μm, 70% of the yarn is made of fibres and only 30% are gaps filled with liquid. Moreover, having equation 4.1, and the relationship between V and L, the flow rate of the liquid, Q, may be expressed as:

$$Q(t) = \frac{\partial V}{\partial t} = 2.9 \times 10^{-11} \times \sqrt{\frac{(\gamma_{LG} \times \cos\theta) \times D \times t}{4 \times \mu}} \quad [\text{m}^3 \cdot \text{s}^{-1}] \tag{4.2}$$

This equation is only valid for the (hydrophilic) yarns for which filling obeys Washburn's equation, and that we assume the yarn fibres do not swell during the filling process.

4.5.2 Evaporation of Water from the Surface of the Yarn

Eq. 4.2 does not consider evaporation, which is negligible initially, but becomes significant as the wetted length increases and the (capillary) flow rate diminishes. Water evaporation from a surface without air flow may be written as :[22]

$$Q_E = \frac{7.84 \times 10^{-8} \times (P_W - P_a) \times A}{\Delta H_v} \quad [\text{m}^3 \cdot \text{s}^{-1}] \tag{4.3}$$

where Q_E is the volumetric flow rate of water being evaporated from the surface, A is the surface area of water in contact with air, P_W is the saturation vapour

pressure at the water temperature, P_a is the saturation vapour pressure at the air dew point, and ΔH_a is the latent heat of water at the specific temperature [KJ·Kg^{-1}]. To calculate the mass transfer from the surface of the yarn, we used the above equation, assuming that the surface area of the yarn can be approximated by multiplying the wetted length by its circumference; however, In reality, the liquid fills both the gaps between the fibres, and wets each fibre individually, and thus likely represents a larger surface area, and the calculation using the simple circumference represents a lower limit. The values for the parameters in Eq. 4.3 were taken from the thermodynamic tables provided in reference 22,[22] for a temperature of 20°C, and a relative humidity of 30%. The evaporation rate thus becomes:[22]

$$Q_E = 8.8 \times 10^{-11} \times L \sqrt{\frac{(\gamma_{LG} \times \cos\theta) \times D \times t}{4 \times \mu}} \quad [\text{m}^3 \cdot \text{s}^{-1}] \tag{4.4}$$

For the yarn used here, the capillary flow and evaporation rate become equivalent for a wetted length of ~90 mm; this constitutes the maximal length that the yarn may be wetted with a humidity of 30%. If we arbitrarily set the maximal allowable ratio between evaporation and capillary flow to 1/3, the maximal useful length of yarn is ~30 mm. Using the results from the measurements shown in Fig. 4.2 and on the evaporation rate given by eq. 4.4, we calculated the theoretical filling speed in the absence of evaporation. (See Fig. SII.2 in APPENDIX II). Whereas in our experiment 38 s were needed to fill 30 mm,

only 34 s would be needed in the absence of evaporation, and the yarn could be wetted over much greater length.

For many biological applications, long incubation times are required, and if the flow stops in a yarn with a 500 μm diameter, it will only take 18.3 min to evaporate 50% of the liquid contained in the yarn with a relative humidity of 30% at 20 °C under the assumption that the circumference remains constant. From these results it is clear that evaporation needs to be taken into account when designing yarn based microfluidics. For bioanalytical applications, a long incubation time is often required to achieve a high sensitivity. As a result, in yarn based microfluidics the flow rate will need to be optimized to maximize sensitivity for a given volume by either keeping the flow path short while continuously resupplying liquid, or increasing the relative humidity of the environment to allow using longer yarns, or then sheathing the yarn with an impermeable coating.

4.5.3 Flow resistance of the yarn

The resistance to flow in a capillary driven conduit can be expressed in terms of the liquid flow rate and the capillary pressure difference ΔP between the inlet and the outlet of the channel as:[23]

$$R = \frac{\Delta P}{Q} \quad [\text{Pa·s·m}^{-3}] \tag{4.5}$$

where, R is the flow resistance of the yarn, and Q is the flow rate. The particularity of capillary flow is that the fluidic conduit also acts as the pump via capillary effects. As the fluid advances, the flow resistance increase as determined by the flow resistance of the conduit. For yarn, neither the flow resistance per unit length, nor the capillary pressure are known, and owing to the various scales of porosity and swelling of yarn the capillary pressure is not well defined nor constant over time.[20] Thus, to measure the flow resistance of yarn and knots, a polyamide monofilament fabric with well defined capillary pressure and with negligible flow resistance was used as a capillary pump. The capillary pressure of a plasma activated fabric was measured by clamping it between two glass slides and measuring the capillary rise, which reached a height of 133 ± 8 mm corresponding to a capillary pressure of -1303±78 Pa (three replicate experiments). The flow resistance of 25 mm of yarn was determined by repeatedly measuring the time needed to flow 9 µL of solution through the yarn using the measurement setup described in the materials and methods section, and found to be:

$$R = \frac{1303 \pm 78}{(3.05 \pm 0.05) \times 10^{-11}} = (4.3 \pm 0.28) \times 10^{13} \ [\text{Pa·s·m}^{-3}] \qquad (4.6)$$

The capillary pressure of the plasma activated yarn was calculated based on the resistance of the yarn and the flow rate as shown in Fig. SII.2 in APPENDIX II and found to be $\Delta P = 1192$ Pa.

Due to the gradual swelling of fibres inside the yarn while they are in contact with the liquid, the current technique gives more accurate and reproducible values for both the flow resistance and the capillary pressure of the yarn than those obtained from the capillary rise experiments.[24]

4.5.4 Knots as functional fluidic elements

Yarn can easily be knotted, and knots lend themselves to splitting and merging liquid streams on yarns, and may thus be used as a functional element for making microfluidic networks. A simple three-way splitter with a blue dye being distributed into outlet yarns is shown in Fig. 4.3A. Merging and mixing of two streams is illustrated with a blue and a yellow dye merging into a green one (Fig.4.3B). The flow speed at the time of the image in the outlet yarn was ~2 mm·s^{-1}. Using the cross-section of an individual yarn fibre (~15 μm) as a crude approximation of the characteristic radius of the conduit, the Reynolds number becomes Re = 0.03. Given the low Re number and hence laminar flow conditions, the relatively large diameter of the yarn and the short mixing length (the knot), the mixing of the two streams, visible by the homogenous green colour found immediately downstream of the knot, is surprisingly efficient. The entanglement of the fibres and the torsion in the yarn and knot may contribute to

enhance mixing. This was observed reproducibly over multiple experiments using hand-made knots.

We reasoned that depending on the knot topology, the mixing ratio between two outlets may be altered, and we tested this idea using the overhand and the hunter's knots. Images from the outlet yarns were recorded using a CCD camera, and the mixing ratios were determined by comparing the colour to a reference palette of yarns soaked with dyes mixed at different ratios (APPENDIX II, Fig. SII.1). We assessed the colour at the outlet of each knot by comparing the hue to a calibration curve that was established using known ratios of blue and yellow dye (see Fig. SII.1 in APPENDIX II), The overhand knot results in equal mixing ratios in both outlet yarns; however, when it is rotated 90°, using the two ends of one of the yarns as inlets, and the other yarn as outlets, the mixing is almost entirely suppressed, Fig. 4.3D-F. A thin line of green colour appears on the right yarn after a while, which reflects slightly unequal flow rates in each branch and which arise due to inhomogeneities in the yarn and variation in wicking speed.

The hunter's knot shows much less intertwining of the two yarns (Fig. 4.3G), and results in almost no mixing with a 95:5 ratio of the two fluids in each outlet,

Fig. 4.3H. Conversely, after rotating it by 90° as above, the mixing ratio was 70:30 between the two outlets, Fig. 4.3I. The results of 5 replicate experiments for different knots and orientations are shown in Fig. 4.3J, and the pictures are shown in Fig. SII.3 in APPENDIX II. These results illustrate that knot topology can be used to conveniently control mixing of different fluids, and based on the large variety of knots that exist,[25] many more mixing combinations should be feasible.
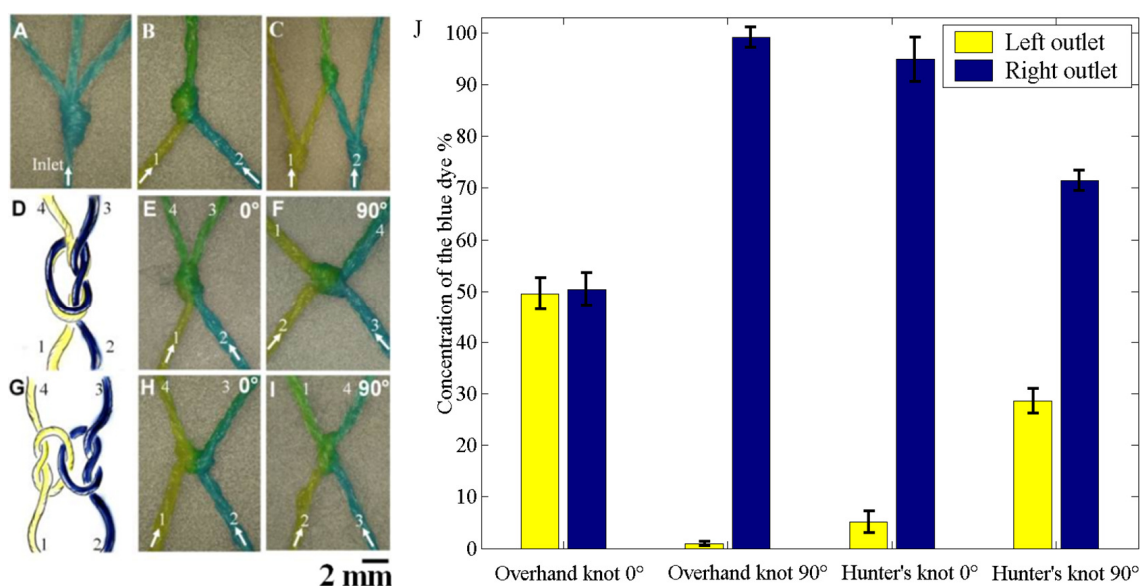
Fig. 4.23: Knots used as microfluidic splitters, mixers, and for controlling mixing ratios. (A) A microfluidic splitter used in reverse (B) becomes an efficient mixer, and (C) when combining both, splitting and mixing is observed. (D) Schematic of the overhand knot, which (E) leads to an equal distribution and mixing of yellow and blue dyes when used as depicted, and (F) to complete separation of the

dyes in each outlet when rotated by 90°. (G) Schematic of the hunter's knot, which (H) leads to complete separation when used as shown, and (I) when rotated by 90° leads to a 71:29 mixing ratio. (J) Graph of the ratio of yellow and blue dye in the left and right outlet of the various configurations E-I. Error bars are the Standard Error (SE) of five separate experiments (see Fig. SII.3 in APPENDIX II for more details).

4.5.5 The flow resistance of knots

When the knots are fastened, the fibres inside the yarn are compressed and/or twisted leading to a change of flow resistance of the yarn. The increase in volumetric flow resistance of 25 mm long yarns with a single knot of different types and tightened with different forces was measured using the setup described above, Fig. 4.4. We observed that once single stranded knots are fastened with more than 3 N tension, they added a significant resistance to the circuit; however, when the double stranded knots were fastened with the same tightening force, the resistance took much smaller values. We believe that this is due to the gap between two knotted strands, which acts as a short circuit and significantly decreases the resistance of the knot compared to that of a single stranded knot. Even with a force of 10 N, the resistance of the double stranded knots corresponded to only 3 mm length of the yarn.
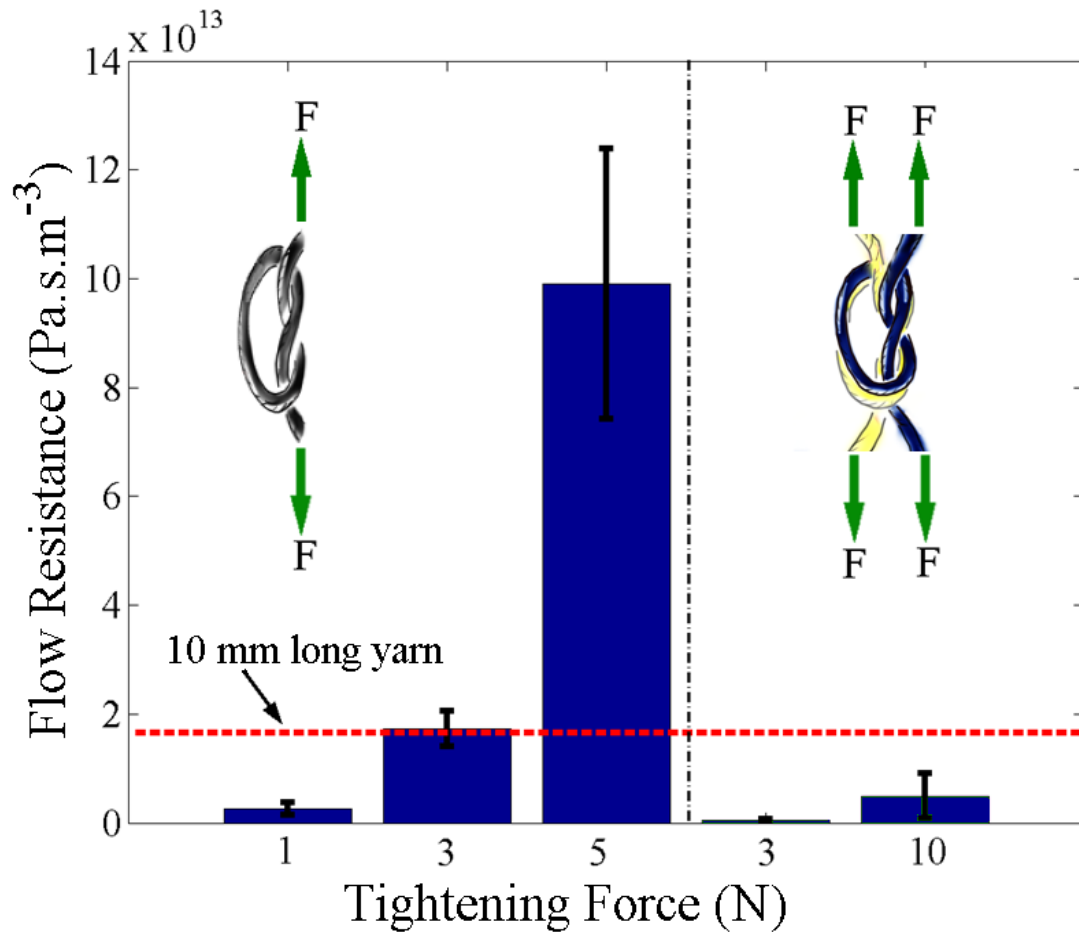
Fig. 4.24: The flow resistance of knots as a function of the force used to tighten it. On the left, the flow resistance of a single stranded overhand knot (inset) tightened with 1, 3 and 5 N is shown. The flow resistance of 10 mm of yarn is shown as a dashed line for comparison. On the right, the flow resistance of a double stranded overhand knot that was tightened with a force of either 3 N or 10 N on each strand is shown. The flow resistance of double stranded knots takes much lower values than that of the single stranded ones, presumably due to the gap formed between the two strands of the knots. Error bars are SE obtained from 3 experiments.

4.5.6 A web-based microfluidic network

Yarns may be knotted into webs to form microfluidic circuits with predictable fluidic properties. Fig. 4.5A shows a web of yarns connected with overhand knots. Based on the mixing produced by overhand knots, and on symmetry argument, it is apparent that two liquids applied to inlets 1 and 2 will be combined, mixed, and split at each node, overall reproducing the architecture of the classical microfluidic serial dilutor widely used as part of microfluidic gradient generators.[26] Is it possible to predict the exact mixing ratio of this circuit? Equation 4.5 mirrors Ohm's law for electrical current $U=R \times I$. Furthermore, based on the complete mixing achieved by overhand knots, the flow ratios in the output yarns solely depend on the flow rates of the liquids,[23, 26] and not on which yarn the liquid originates from. In addition, the results shown in Fig. 4.4 indicate that double-stranded overhand knots fastened with 3 N only generate negligible fluidic resistance, thus satisfying the characteristic of a "node", which is widely used as part of electrical circuits. Based on these similarities, a fluidic web is equivalent to an electrical circuit made of nodes and resistors, whereas each resistor represents the flow rate resistance of the branch. It should thus be possible to calculate the fluidic properties of the circuit using the electrical circuit analysis methodologies. For the sake of simplicity, the length and flow resistance of each branch of the web were assumed to be equal and to be r. The pressure

that drives the flow is generated by applying a paper wick with a pressure P_1 on each yarn. The distance from the outlet node is the same for all yarns, and is n times the length of a branch, and thus produces a resistance nr to the flow. The inlets have a resistance mr, but it has no influence on the flow distribution if the circuit is symmetric, Fig. 4.5B. The mixing ratios of inlet fluids 1 and 2 in each of the outlets can be deduced readily for outlets 3 and 8, because no mixing occurs, as well as for outlets 5 and 6 that carry 50:50 of both inlet fluids because of symmetry. The ratios in outlets 4 and 7 however are not evident and were calculated. Again, because of symmetry, it is sufficient to determine the mixing ratio in outlet 4, and outlet 7 can then be deduced as the complementary to outlet 4. The right half of the circuit used for analysis is shown in Fig. 5C. Kirchhoff's law and Nodal analysis [27], commonly used for the analysis of electrical circuits, were applied to the half circuit and used to calculate the potentials P_A and P_B defined at the two nodes (Fig. 4.5C). The flow ratio in the outlets are determined by the flow rate Q_1 and Q_2, whereas Q_1 is a 50:50 mixture of both fluids (see Fig. 4.5A and B). The detailed calculation is provided in APPENDIX II. The flow ratio $k = Q_2/Q_1$ is found to be:

$$K = \frac{Q_2}{Q_1} = \frac{3 \times n^2 + n}{5 \times n^2 + 5 \times n + 1} \qquad (4.7)$$

and the concentration C_4 for outlet 4 can be expressed as:

$$K = \frac{0.5}{K + 1} \qquad (4.8)$$

and for outlet 7, based on the rule of complementarity $C_4 + C_7 = 1$, we find:

$$C_7 = \frac{K + 0.5}{K + 1} \tag{4.9}$$

The outlet flow ratio of the two fluids thus depends on the resistance ratio n. For

$n = 0$, $C_4 = 50:50$, but rapidly increases asymptotically towards $C_4 = 68.75\%$ of

the ipsilateral fluid as n becomes larger than 1, see Fig. SII.4 in APPENDIX II.
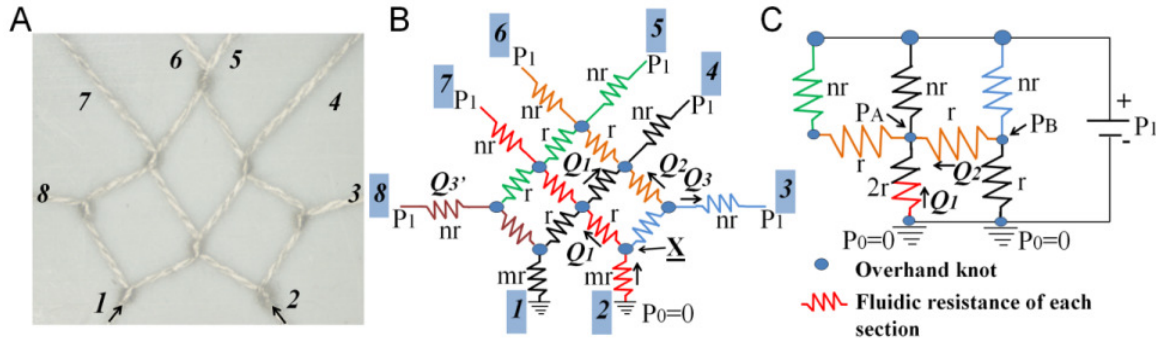
Fig. 4.25: A knotted web and the equivalent fluidic circuit. (A) Photograph of the

web made using overhand knots used for branching and mixing. Six pieces of

yarns and eight knots were employed to form this circuit, which functions as a

serial dilutor. To determine the ratio of fluid 1 and 2 in each outlet, an equivalent

electrical circuit model was derived by drawing an equivalent circuit made of

resistances and nodes whereas the colours represent different yarns (B). The

links within the web have been assigned a flow resistance r, the outlet yarns a

resistance nr, and the inlet yarns a resistance mr with n and m expressing a ratio.

P1 is the capillary pressure generated by a wick placed at a constant distance

from the outlet node on the yarn. The ratio of fluid 1 and 2 is 50:50 in outlets 5

and 6 based on the symmetry of the circuit, and 100:0 and 0:100 in outlets 8 and

3, respectively. Again, based on the symmetry of the circuit, it is sufficient to analyze the right half of the circuit in (B). Defining X as reference P0=0, the circuit can be redrawn as shown in (C). The ratio between flow rate Q1 and Q2 determines the concentration at outlet 4 (and thus 7). The flow rate ratio was calculated as described in the main text and in APPENDIX II.

The circuit was tested with a blue and a yellow dye delivered to inlet 1 and 2, respectively, Fig. 4.6. The outlet mixing ratios show a good match with the expected values of 0:100, ~69:31, 50:50, ~31:69, and 100:0, Fig. 4.6B. The discrepancies between the theoretical and the experimental values can be attributed to unequal lengths of the different branches and inhomogeneity of the yarn itself. If all outlet yarns were aligned side by side, a dilution ladder would be formed that could produce a continuous gradient upon diffusion.[26] By using knots with unequal mixing ratios or by adding more knots, intermediate mixing ratios could be produced as well. The predictability and reproducibility of such networks is not reliable when they are made by hand using natural cotton yarn, and will need to be further improved for making more complex circuits. If better defined yarns can be made, and if knitting or sewing machines could be adapted and used to fabricate such type of patterns with high accuracy, more complex fluidic circuits may be designed and built.
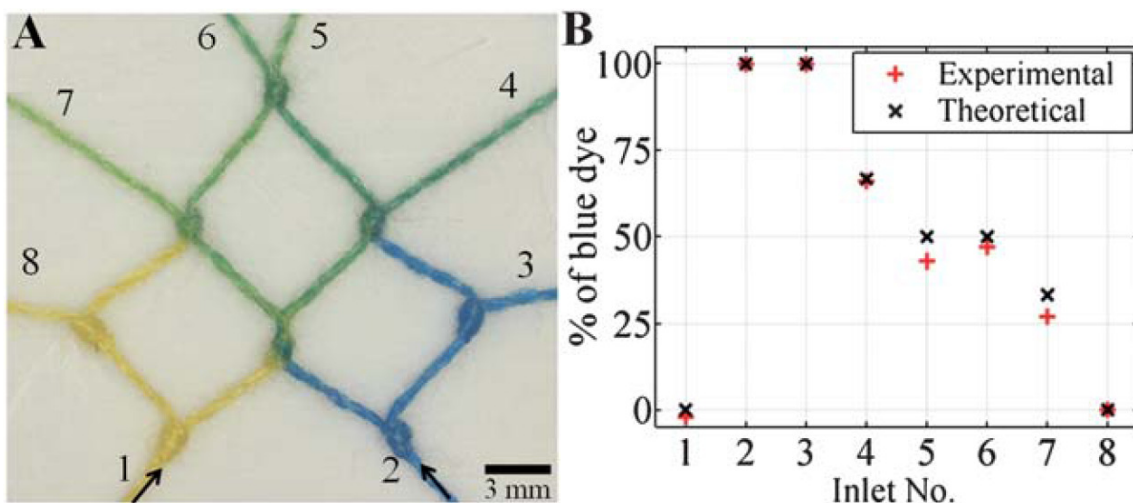
Fig. 4.26: A web made of yarns and knots operating as a serial dilutor. (A) A yellow and a blue food dye are applied at each of the two inlets 1 and 2 at the bottom of the image. The dilutor iteratively combines, mixes, and splits the two dyes which flow into the 6 outlets 3 – 8 with each a different ratio constituting to a serial dilution of one chemical vs the other (B) The mixing ratios of blue:yellow dyes calculated on the basis of the circuit model for outlets 3-8 are 0:100, ~33:67, ~50:50, ~50:50, ~67:33 and 100:0, respectively (see Fig. SII.3 in APPENDIX II), and are shown as black crosses. The experimental mixing ratios (red plus sign) show a good agreement with the calculation. This experiment illustrates that circuits with moderate complexity may be built by knotting yarns.

4.6 Conclusion

Here we showed methods to characterize and modify basic fluidic properties of the yarns, and then demonstrated examples of using cotton yarns for

constructing passive microfluidic systems. We modified the surface property of the cotton to improve its hydrophilicity, and then measured the flow resistance of the yarns. Subsequently we employed knots for both controlling the flow resistance, and making various microfluidic elements such as passive splitters, blenders and mixers out of yarns. We also quantified the mixing ratios of the proposed knotted mixers, and found that topologically different knots can make different mixing ratios. Finally, we made a web of knots (Fig. 4.6), which can be used as a serial dilutor.

In all these examples, we used yarns made of cotton, but there is a wide range of natural and synthetic yarns which may be useful for different fluidic functions.[17] This work complements recent developments in multifunctional textiles which encompass fabrics with optical, electrical and biocompatible fibres[28-30] for making wearable displays, sensors, and artificial tissues.[31, 32] We believe that the "microfluidic fibres" introduced here may be combined with some of the above mentioned approaches to further enhance the functionality of smart textiles. To fulfil the potential of yarn-based microfluidics, it will be necessary to adopt and adapt the technologies commonly used in the textile industry towards building advanced yarn-based microfluidic circuits by weaving and knitting yarns with different functions. Yarn-based microfluidics may further be enhanced by

developing tailored surface treatments of the yarn and using yarns with different diameters to increase flow rates while minimizing the effects of evaporation. We thus believe that the combination of textiles and fluidic yarns represents an exciting new paradigm that will expand the scope of both areas of research.

4.7 Acknowledgments

4.8 References

1. Harris, J. (ed.) Five thousands years of textiles. (Smithsonian, 2004).
2. Zhang, J., France, P., Radomyselskiy, A., Datta, S., Zhao, J. & van Ooij, W. Hydrophobic cotton fabric coated by a thin nanoparticulate plasma film. *Journal of Applied Polymer Science* **88**, 1473-1481 (2003).
3. Xue, C.H., Jia, S.T., Chen, H.Z. & Wang, M. Superhydrophobic cotton fabrics prepared by sol-gel coating of TiO2 and surface hydrophobization. *Science and Technology of Advanced Material* **9**, 035001 (2008).
4. Kadolph, S.J. Textiles. (Pearson Prentice Hall, 2007).
5. Kasdan, R. & Kornblum, S. Double knit fabric for athletic wear, comprises knitted synthetic yarn on back of fabric layer, and microfiber synthetic yarn on outer surface of fabric layer. (Patent US6427493-B1, 2003).

6. Karahan, H.A. & Ozdogan, E. Improvements of surface functionality of cotton fibers by atmospheric plasma treatment. *Fibers and Polymers* **9**, 21-26 (2008).

7. Gamble, G.R. Implications of surface chemistry on cotton fiber processing. *Journal of Cotton Science* **8**, 198-204 (2004).

8. Wong, R.C. & Tse, H.Y. (eds.) Forensic Science and Medicine: Drugs of Abuse: Body Fluid Testing. (Humana Press Inc, Chapter 6; 2005).

9. Yager, P., Edwards, T., Fu, E., Helton, K., Nelson, K. Tam, M.R. & Weigl, B.H. Microfluidic diagnostic technologies for global public health. *Nature* **442**, 412-418 (2006).

10. Kasahara, Y. & Ashihara, Y. Simple devices and their possible application in clinical laboratory downsizing. *Clinica Chimica Acta* **267**, 87-102 (1997).

11. Posthuma-Trumpie, G.A., Korf, J. & van Amerongen, A. Lateral flow (immuno) assay: its strengths, weaknesses, opportunities and threats. A literature survey. *Analytical and Bioanalytical Chemistry* **393**, 569-582 (2009).

12. Martinez, A.W., Phillips, S.T. & Whitesides, G.M. Three-dimensional microfluidic devices fabricated in layered paper and tape. *Proceedings of the National Academy of Sciences* **105**, 19606-19611 (2008).

13. Martinez, A.W., Phillips, S.T., Butte, M.J. & Whitesides, G.M. Patterned paper as a platform for inexpensive, low-volume, portable bioassays. *Angewandte Chemie International Edition* **46**, 1318-1320 (2007).

14. Safavieh, R., Mirzaei, M., Qasaimeh, M.A. & Juncker, D. in *Proceedings of the Thirteenth International Conference on Miniaturized Systems for Chemistry and Life Sciences,* 685-687 (Jeju, Korea; 2009).

15. Li, X., Tian, J. & Shen, W. Thread as a Versatile Material for Low-Cost Microfluidic Diagnostics. *ACS Applied Materials & Interfaces* **2**, 1-6 (2010).

16. Reches, M. et al. Thread as a Matrix for Biomedical Assays. *ACS Applied Materials & Interfaces* **2**, 1722-1728 (2010).

17. Mahabad Riss Co., http://www.mahabadriss.com/cotton-yarn-manufacturers-pr.html, Retrieved 21/12/2010.

18. Washburn, E.W. The dynamics of capillary flow. *Physical Review Letters* **17**, 273-283 (1921).

19. Safavieh, R., Roca, M.P., Qasaimeh, M.A., Mirzaei, M. & Juncker, D. Straight SU-8 pins. *Journal of Micromechanics and Microengineering* **20**, 055001 (2010).

20. Karppinen, T., Kassamakov, I., Haeggstrom, E. & Stor-Pellinen, J. Measuring paper wetting processes with laser transmission. *Measurement Science & Technology* **15**, 1223-1229 (2004).

21. Masoodi, R. & Pillai, K.M. Darcy's Law-Based Model for Wicking in Paper-Like Swelling Porous Media. *AIChE Journal* **56**, 2257-2267 (2010).

22. Parson, B. (ed.) Ashrae Handbook: Heating, Ventilating, and Air-Conditioning Applications (American Society of Heating, Refrigerating and Air-Conditioning Engineers, 1991).

23. Juncker, D., Schmid, H., Drechsler, U., Wolf, H., Wolf, M., Michel, B., de Rooij, N. & Delamarche, E. Autonomous microfluidic capillary system. *Analytical Chemistry* **74**, 6139-6144 (2002).

24. Masoodi, R., Pillai, K.M. & Varanasi, P.P. Effect of Externally Applied Liquid Pressure on Wicking in Paper Wipes. *Journal of Engineered Fibers and Fabrics* **5**, 17 (2010).

25. Pawson, D. Handbook of knots. (DK publishing Inc.1998).

26. Jeon, N.L., Dertinger, S.K.W, Chiu, D.T., Stroock, A.D. & Whitesides, G.M. Generation of solution and surface gradients using microfluidic systems. *Langmuir* **16**, 8311-8316 (2000).

27. Dorf, R.C. & Svoboda, J.A. Introduction to Electric Circuits, eighth edition, (2010).

28. Graham-Rowe, D. Photonic fabrics take shape. *Nature Photonics* **1**, 6-7 (2007).

29. Hamedi, M., Forchheimer, R. & Inganas, O. Towards woven logic from organic electronic fibres. *Nature Materials* **6**, 357-362 (2007).

30. Shim, B.S., Chen, W., Doty, C., Xu, C.L. & Kotov, N.A. Smart Electronic Yarns and Wearable Fabrics for Human Biomonitoring made by Carbon Nanotube Coating with Polyelectrolytes. *Nano Letters* **8**, 4151-4157 (2008).

31. Abouraddy, A.F., Bayindir, M., Benoit, G., Hart, S.D., Kuriki, K., Orf, N., Shapira, O., Sorin, F., Temelkuran, B. & Fink, Y. Towards multimaterial multifunctional fibres that see, hear, sense and communicate. *Nature Materials* **6**, 336-347 (2007).

32. Moutos, F.T., Freed, L.E. & Guilak, F. A biomimetic three-dimensional woven composite scaffold for functional tissue engineering of cartilage. *Nature Materials* **6**, 162-167 (2007).

Chapter 5: Capillary pumps for microfluidic capillary systems

5.1 Preface

Microfluidic capillary systems require capillary pumps to deliver accurate volumes of liquids with precise flow rates. Here, to control the liquid filling front and avoid trapping bubbles in the pumps, we introduce two novel designs of capillary pumps using different spacing between rows and columns and guidance structures at the edges. One architecture induces serpentine filling of the front using separation walls at the edges and is called serpentine pump. The other guides the liquid preferentially along one edge, called the leading edge. In both pumps, the filling front and bulk flow follow different paths. As a consequence, in the serpentine pumps the flow resistance rapidly raise as the first row is filled, following by a rapid decrease as subsequent rows are filled as well, and then a slow increase as the pump is being filled. We also develop and solve a nodal model of the flow resistance that matches the experimental data. Finally, we design pumps with variable gap-sizes between posts and show that we can modulate the flow rate as the pump is being filled.

This work resulted in the following publication:

Journal paper: <u>Safavieh, R</u>., Tamayol, A. and Juncker, D. *Serpentine and leading edge capillary pumps for microfluidic capillary systems*, Submitted.

5.2 Abstract

Microfluidic capillary systems operate using capillary forces only, and require capillary pumps (CPs) to transport, regulate and meter the flow of small amounts of liquids. Common CP architectures include arrays of posts or tri-like branched conduits that offer many parallel flow paths. However, due to uncontrolled advancement of the filling front, bubbles often get trapped in CPs, which introduce large variability in the volume metered by the CP. Here, we present novel CP architectures that prevent the entrapment of bubbles by controlling the propagation of the filling front along rows formed by large gaps between posts. One variant, named serpentine pump, guides the filling front following a serpentine path, and the other one, called leading edge pump, directs the liquid along a predetermined edge of the CP from where it fills rows of gaps between posts. Using these CPs, it is possible to vary the average angle of rows guiding the filling font from 0º to 45º. As the CP is being filled, the flow resistance changes, and because the filling front and the bulk flow follow different paths, the flow resistance increases sharply initially, then decreases, and eventually increases steadily until the CP is filled. We calculated the flow resistance of a CP as it is being filled using pore network modelling approach, and validated our calculations experimentally. Finally, a CP with a capillary pressure gradient was

made by continuously increasing the width of the rows guiding the filling front so as to continuously decrease the pumping pressure and the volumetric flow rate.

5.3 Introduction

Capillary systems are widely used for manipulating liquids in heat pipes,[1] for regulating fluid-flow in low-gravity environment in space,[2] for patterning biomolecules on surfaces,[3-5] for immunoassays,[6] and for diagnostic applications.[7-9] Capillary systems are self-powered and self-regulated by capillary effects, and are thus self-contained as there is no need for external pumps and tubes. Capillary pumps (CPs) are essential components of many capillary systems and provide a negative (suction) pressure for manipulating liquids in the capillary system. CPs are notably used in assays to flow large volumes of sample over the assay surface to reach a high sensitivity.[10] The volume of the CP serves as a metering device – the pump's capacity sets the volume of the liquid drawn in – and as a waste reservoir for reagents.[9] Indeed, since capillary systems operate by applying a negative pressure, CPs are placed at the end of the flow path, and thus hold the liquid after it passes through the reaction zones. For immunoassays, it is often desirable to keep the flow rate constant during the incubation step. Achieving this goal requires CPs that generate a constant capillary pressure and that do not significantly increase the overall flow

resistance as they are being filled. Successful designs include CPs with parallel microchannels arranged in an arborescent pattern[9] or arrays of posts,[10] or meshes[11]. Post arrays and meshes are more robust than branching channels, because they are less prone to clogging or flow stopping as the liquid can progress along many parallel, connected paths. In practice, pumps are often covered to avoid evaporation and contamination of the sample. As a consequence, bubbles can easily get trapped, if the filling front of the liquid progresses faster along one side of the CP and reaches the outlet prior to filling the CP entirely. Trapped bubbles reduce the liquid drawn into the CP, and thus result in unreliable metering and inaccurate incubation time during immunoassays. The issue of bubble trapping becomes even more pronounced when multiple pumps are connected in series.[12]

A strategy to avoid bubble trapping in microfluidic systems is to control the progression of the filling front. This has been widely implemented in hydrophobic systems where external pumps, pressure, vacuum or centrifugal forces are used to drive liquids, and where the progression is controlled and pre-programmed by adding hydrophobic obstacles to the flow path.[13, 14] The control of the liquid front is more difficult in self-filling, hydrophilic capillary systems because of the constraints of maintaining self-filling. Zimmerman *et al.*[12, 15] designed CPs with (i)

indented sidewalls that slow down the progression along the edges and (ii) outlets made by a series of arch-shaped, hierarchical "bridges" with increasing size that fill in predetermined order. Whereas this system was shown to minimize bubble trapping, one limitation is that the capillary pressure is reduced as the diameter of the bridging channels increases, thus making the system susceptible to contaminations and flow stopping. Moreover, this structure was supplemented with another structure in the form of a small serpentine side-channel, which acted as a delay valve.[15] This channel however comes at a cost of reduced metering accuracy, and ultimately each new external element added to the CP affects the functionality of the circuit and may itself become a source of failure.

Here, we introduce CPs that are both autonomous and guide the progression of the filling front with all control elements integrated into the CP. These CPs comprise arrays of microposts that are spaced differently along the X (parallel to the bulk flow) and Y (perpendicular to the bulk flow) axes so as to form rows along the Y axis. The liquid entering the pump flows into the first row, and immediately fills the narrow gaps between the posts, which act as a temporary stop valve; they are effective here because the liquid is kept at negative pressure by the filling.[12] The liquid front is thus guided to fill the row entirely, and only at the edge of the CP does it progress into the next row. Two CP designs and

strategies were developed to control the advancement of the filling front: firstly, a serpentine CP where the front is guided in an alternate direction in each row in a serpentine pattern, and secondly a leading edge CP where the liquid is guided to fill one of the edges of the CP preferentially, and then fills each row starting from this "leading edge". The filling front advances perpendicularly to the bulk flow along each row, and as a result both follow different paths. Whereas in the typical CPs the average capillary pressure in each row is constant as the liquid fills the pump, the flow resistance changes. To calculate the flow resistance in the CPs, a lumped model and nodal analysis were used. The flow resistance of the CPs does not increase monotonically, and in fact decreases after the first row is filled, which was corroborated experimentally. Finally, advanced CPs with graded capillary pressure were designed and characterized.

5.4 Materials and methods

5.4.1 Chemicals and materials

polydimethylsiloxane (PDMS) was purchased from Dow corning (Sylgard® 184, MI, USA). Curing agent and polymer base were manually mixed at a ratio of 1:10, and cured for 8 h in an oven (Lindberg Blue M, Fisher Scientific) at 60°C. A 1 mg/ml solution of Fluorescein sodium salt ($C_{20}H_{10}Na_2O_5$) (fluorescein dye, Sigma-Aldrich, USA) in water (Milli-Q purified water, Millipore, USA) was used for

characterizing the pumps. 6" Si wafers with the thickness of 650±10 µm were purchased from Silicon Quest International (San Jose, USA). Shipley-1813, a positive photoresist was purchased from Microchem Inc. (Massachusetts, USA).

5.4.2 CPs fabrication

We designed CPs using a layout editor *software (CleWin 5,* WieWeb software, Netherlands), and obtained 7"×7" chrome mask with 65,000 dots per inch resolution from Thin Metal Parts Inc. (Colorado Springs, USA). The CPs were fabricated by first coating a Si wafer with a 2.8 µm thick photoresist layer followed by photolithography and deep reactive ion etching (DRIE, Tegal SDE 110, USA). Next, diced the wafers into individual chips using a diamond scriber (Ted Pella Inc, USA). The Si chips were rendered hydrophilic by flaming them for ~45 s until they became glowing red using a microtorch (Butane fuel microtorch MT-51, Master Appliance, USA). A flat 2 mm thick PDMS was cut to size, and vents punched with a biopsy puncher (1 mm diameter, Ted Pella Inc., USA). The PDMS was sealed onto the Si chip to serve as cover.

5.4.3 Characterization of the capillary pumps

CPs were imaged using optical (LV150 industrial microscope, Nikon, Japan) and scanning electron microscopy (S-3000N variable pressure SEM, Hitachi, Japan).

The progression of the filling front in the CPs was visualized by capturing the flow of fluorescein in deionized water. For each experiment, 2.5 µl of solution were delivered to the loading port and using a stereomicroscope *(Leica MZ10f, Leica Microsystems, Germany)* a fluorescence video recorded at a rate of 30 frames per second *(infinity 3 CCD camera, USA)*. Videos were converted into images using VirtualDubMod Surround 1.6.0,(see reference 16)[16] and the velocity of the filling front established by measuring the change in position between individual frames. At least three independent experiments were performed and standard deviations were calculated. The flow resistance of the CP as a function of the position of the filling front was calculated by modelling the pump as a nodal network using an in house code programmed in Matlab (v7.13, MathWorks Inc., USA). The advancing and static contact angles between DI water and a flat Si surface, which was rendered hydrophilic, were measured using a contact angle analysis equipment (VCA optima, AST products Inc., USA).

5.5 Results and discussion

5.5.1 Design of the Capillary Pumps

The CPs we designed comprise an array of 40×80 µm^2 posts with rounded edges in a staggered arrangement. The gap between adjacent posts in two separate rows, W_1, is larger than the distance between two columns, W_2, Fig. 5.1A. By making the surface hydrophilic, the liquid spontaneously fills the CP

owing to the capillary pressure generated inside the CP, and first enters the large space forming the first row (t_0), but then immediately fills the narrow gaps between adjacent posts (t_1). However, the liquid does not flow into to the next row, because the geometry of the posts acts as a temporary capillary stop valve.[15] The liquid front thus progresses along the next post and further along the row (t_2), until it fills the next narrow gap, and so on. The filling front thus fills the entire row, and only after reaching the edge of the CP, advances to the next row. The CP is thus filled row-by-row.

Two distinct CPs were designed initially that guide the filling front in two different ways. The first is called a serpentine pump because it guides the liquid front along a serpentine path. The liquid front advances to the next row as it reaches the edge of the CP. To prevent premature leakage into the next row, guiding structures are included at the beginning of each row, Fig. 5.1B. The second CP is called leading edge pump, because the liquid front is led along one edge of the CP and starts sequentially filling each row from this edge, Fig. 5.1C. The liquid front was guided by reducing the gap between the "leading" edge and the posts compared to the other edges – hence creating a higher capillary pressure at the leading edge – and thus forcing the liquid to fill each row from that edge. In both CPs, the angle of the rows was varied and tilted between 0 º to 45 º relative to

the edge of the CP. Manipulation of the filling front along the required directions

allows filling of CPs with various geometries and thus could save the footprint of

the microfluidic circuits. Also by varying the filling front direction, the number of

posts per unit area of the CP and its capacity can be adjusted.
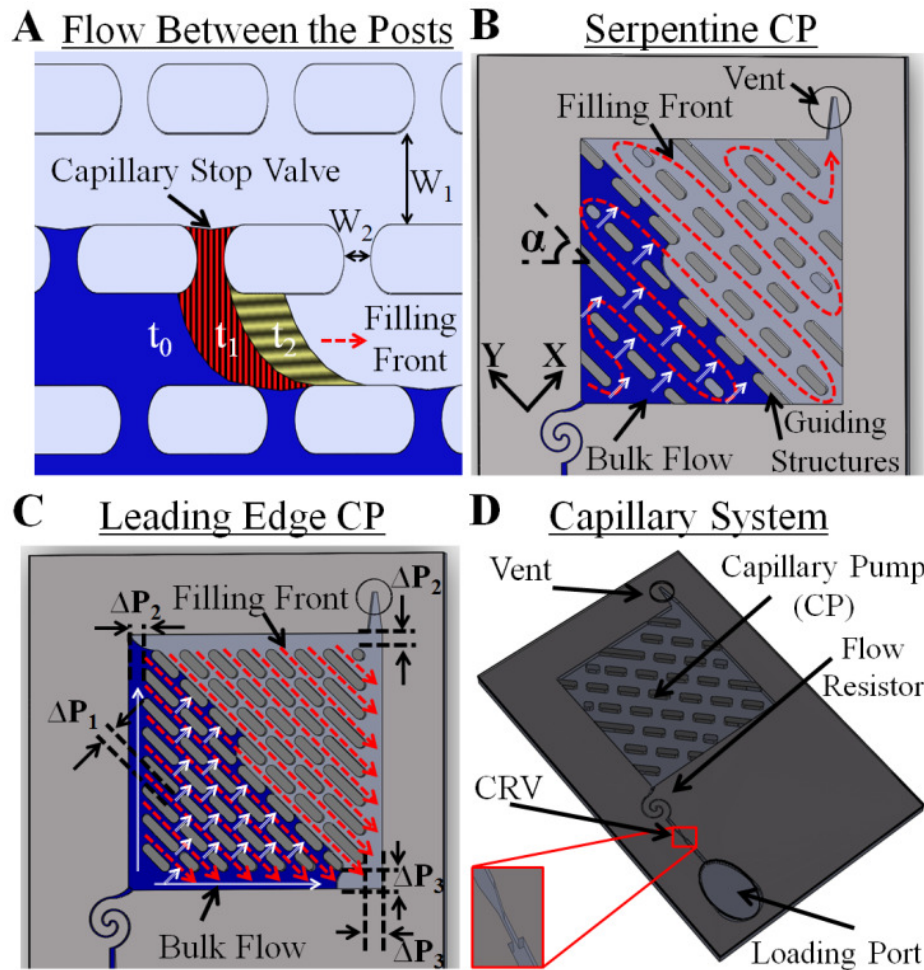

Fig. 5.1: Schematics of serpentine and leading edge capillary pumps (CPs) with

arrays of posts. (A) Schematic illustrating the progression of capillary flow

between the posts from time t_0 to t_2. The liquid fills the rows by capillary pressure,

as well as the gap between the posts, but the liquid cannot jump into the next row

as each pair of posts forms a capillary stop valve, and thus the liquid progresses along the row until it reaches the edge of the pump, and proceeds to fill the next row. (B) Serpentine CPs comprise guiding structures at the end of each alternating row to guide the liquid filling front in a serpentine pattern. (C) Leading edge CPs draw the liquid into the narrow edge with a capillary pressure, (ΔP_2), and then sequentially into each of the rows, which have the highest capillary pressure, (ΔP_1), starting with the first one. Finally, the wide gap, (ΔP_3), is filled up to the exit. The path of the filling front is indicated by the red arrows and the bulk flow by the white hashed arrows; note the difference in the paths. (D) A capillary system with a loading port, a capillary retention valve (CRV), a flow resistor and a vent is used to test the CPs.

To test the two CP designs, simple capillary systems consisting of a loading port, a capillary retention valve (CRV), an external flow resistor, and the respective CP, were built, Fig. 5.1D.[9, 17] The system was sealed with a PDMS cover that contained a loading port to fill samples, and one opening for venting.

The capillary pressure, ΔP, in the CPs was estimated using the pressure equation for rectangular cross sections:[18]

$$\Delta P = -\gamma_{LG}\left(\frac{\cos\theta_b + \cos\theta_t}{w} + \frac{\cos\theta_l + \cos\theta_r}{h}\right) \tag{5.1}$$

where γ is the surface tension of the liquid, $\theta_{i=b,t,l,r}$ are the contact angles of the liquid-air meniscus on the bottom, top, left, and right walls, respectively, and w and h are the width and height of the rows formed between the pillars. The actual pressure is expected to be lower owing to fact that the channel is not continuous, but lined by posts with narrow gaps.

The narrow gaps between the pillars were constant and equal to 15 μm for all CPs except the one with the variable capillary pressure, which was equal to 25 μm, Fig. SIII1A in APPENDIX III. The width of the rows was varied from 34 μm to 130 μm, depending on the CP. The depth of the pumps was fixed during the DRIE fabrication step and was typically ~100 μm. The spiral shaped external resistor had a width of 30 μm and an overall length of 3400 μm, Fig. SIII1C in APPENDIX III. The footprint of the CPs are from 4.2 × 4 mm^2 to 4.2 × 4.5 mm^2 with a porosity ranging from 47%-73%, and thus can accumulate between 1.02 μL-1.65 μL. For the leading edge CPs, Fig. 5.1C, we adjusted the gaps between rows that generate ΔP_1, the gap of the leading edge (left and top) that results in ΔP_2, and the gap of the trailing edge (bottom and right) that creates ΔP_3 so that the absolute value of the capillary pressures were:

$$\left|\Delta P_1\right| > \left|\Delta P_2\right| > \left|\Delta P_3\right| \tag{5.2}$$

Fig. 5.2 shows the fabricated serpentine and leading edge CPs as well as a capillary system used in the experiment, Fig. 5.2A-C.
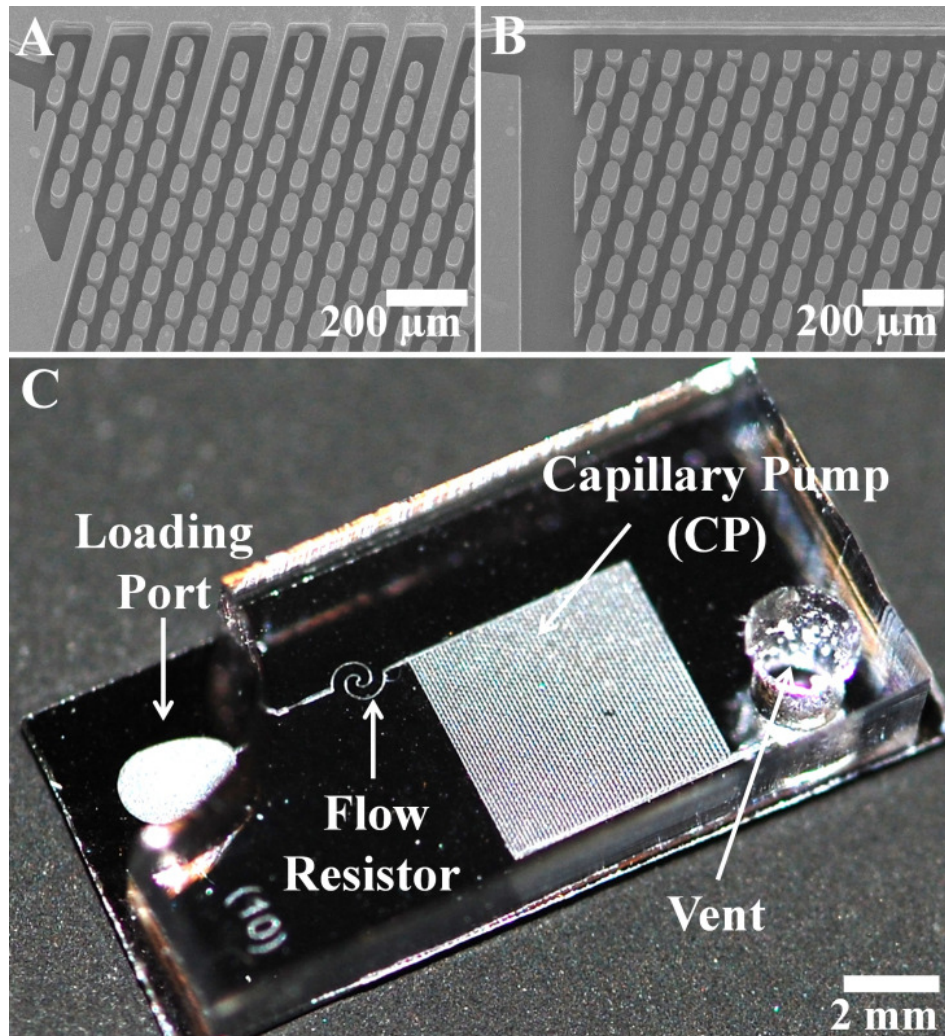

Fig. 5.27: Micrographs of CPs and the capillary system. (A) A serpentine CP with a 15 ° angle with ridges at the edge. (B)A leading edge CP with 15 ° showing the leading edge gap and the trailing edge gap. Note that the posts are cut at the edges here. (C) Overview of the capillary system used to test the CPs. The

PDMS cover with a vent was aligned to the chip manually using an

stereomicroscope.

5.5.2 Progression of the filling front in CPs

The filling of three serpentine CPs with row angles relative to the edges of α=0 °,

15 ° and 45 ° and of a leading edge CP with an angle of α=15 ° are shown in

Fig. 5.3.

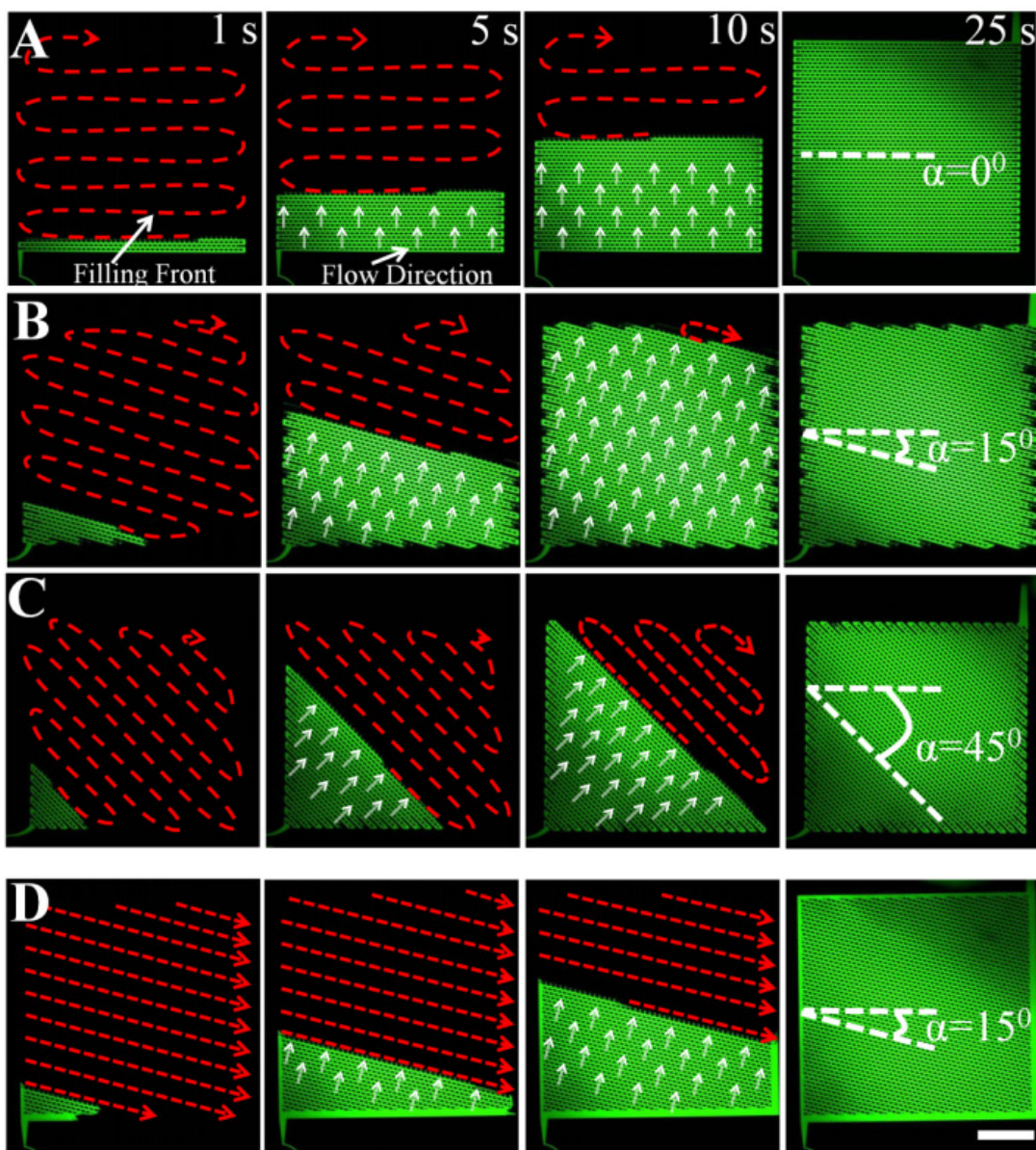Fig. 5.3: Time lapse imaging showing the progression of the filling front. Three serpentine CPs with (A) 0°, (B)15°, (C) 45° angle are shown and (D) a leading edge CP with a 15° angle. Dilute solution of fluorescein in distilled water was used to perform all the tests. The red arrows show the direction of the liquid filling front, whereas the white arrows demonstrate the direction of the flow. The scale bar is 1 mm.

5.5.3 Flow model of the CPs

The flow rates of the system used here are few tens of nanoliters per second only; thus the flow is laminar and corresponds to what is known as creeping flow. Under these conditions, the relationship between capillary pressure, *ΔP,* the flow resistance, *R,* and volumetric flow rate, *Q,* of the system becomes:[9, 19, 20]

$$R = \frac{\Delta P}{Q} \tag{5.3}$$

This is similar to the electrical relationship between voltage, resistance and current; however, in this case the flow resistance of the CP continuously changes as the filling front progresses, while flow front and bulk flow follow different paths. Both of these factors need to be considered when calculating the flow resistance and flow rate.

The flow resistance of rectangular microchannels is defined as.[19, 21]

$$R_C = \left[\left(\frac{w \times h^3}{12 \times \mu \times L} \right) \times \left(1 - \frac{192 \times h}{\pi^5 \times w} \times \tanh\left(\frac{\pi \times w}{2 \times h} \right) \right) \right]^{-1} \quad \text{[Pa s m}^{-3}\text{]} \tag{5.4}$$

where *L, w* and *h* are the length, width and height of the microchannel respectively, and μ is the viscosity of the liquid. The CP can be considered as an array of unit cells that allow for flow along the row and across the row through the small gaps, Fig. 5.4A. To simplify the calculation, the gap between the posts can be treated as a straight conduit. The resistance of each unit cell in a row can

be lumped into a single resistance R_h, and the resistance along the narrow gap between posts as R_v, Fig. 5.4.B Tamayol *et al.*[22] have shown that the suitable length scale for determining the pressure drop between adjacent cylinders is the minimum gap size. Thus, to simplify the analysis, we neglected the effects of the rounded edges in the post and assumed that the posts are completely rectangular shape with 40×80 μm^2, and that the effective gaps to calculate R_h and R_v are W_1=35 μm and W_2=15 μm respectively. The values of R_h and R_v can then be obtained using Eq. 4. More details are provided in APPENDIX III.

The regular structure of the CP lends itself to a pore network modelling approach, common in the analysis of flow through porous media, which is an equivalent to network approach as used in electronics.[23-25] In this approach, the pump can be modelled as a network of nodes interconnected by R_h and R_v resistors, Fig. SIII2 and SIII3 in APPENDIX III. For a typical serpentine CP, R_h=3.99×10^{11} Pa s m^{-3} and R_v=9.90×10^{11} Pa s m^{-3}, APPENDIX III. The staggered architecture of the CP with α=0°, Fig. 5.4B, was modelled as an in-line array of pillars so that all the four resistances connect to a single node, thus simplifying the calculations. This approximation is justified by the fact that $R_v \gg R_h$ and that the contribution of the lateral flow resistance between two rows is negligible relative to the resistance of the narrow gap.

To calculate the equivalent resistance of the network model, each node was assigned a coordinate from 1 to (j×m), where j and m are the number of rows and columns respectively, as shown in Fig. 5.4B. Using Kirchhoff's circuit laws[26] a conductance matrix of the form $C \times P = Q$ was constructed, where $C = \frac{1}{V}$ is the conductance matrix and has the dimension of (j×m)×(j×m) and once is multiplied by the matrix of nodal pressures, P, the summation of the flow rates flowing in and out of each node is obtained. with P and Q having the dimensions of (j×m). Assigning an arbitrary value for the $Q_{j,m}$, and the same negative value for $Q_{1,1}$, we calculated the associated values for $P_{j,m}$, and $P_{1,1}$ by solving the matrix. Finally the resistance between the node 1 and j×m of the pump can be calculated as:

$$R = \frac{P_{1,1} - P_{j,m}}{Q_{j,m}}$$

(5.5)

The detailed algorithm is provided in the APPENDIX III. The total flow resistance of the circuit is the summation of the resistance associated with the CP and the connecting channel.

Fig. 5.4 illustrates the resistance of the CP as the function or position of the filling front. For a serpentine CP with α = 0°, the resistance increases rapidly, as the filling front fills the first row, because here the bulk flow and filling front follow the same path, and the resistance reaches a local maximum when the liquid

reaches the edge. Indeed, as the liquid travels back along the second row, the two rows become connected by an increasing number of narrow gaps, which all serve as parallel flow paths, and hence the flow resistance diminishes as the liquid front advances. In fact, the flow resistance of the CP shown here diminishes between the first and seventh row, from R=6.98×10^{12} to R=1.87×10^{12} Pa s m^{-3}, but then starts to increase continuously until it is filled entirely as the vertical resistance of the narrow gaps dominate the overall flow resistance. Between the 7th and 55th row, it then increases roughly linearly up to R=7.53×10^{12} Pa s m^{-3}, Fig. 5.4C.

 The normalized calculated flow rates of the CP obtained from the computed flow resistance match with those of the experimental values, and they are correlated with the capillary pressure of 1210 Pa, Fig. 5.4D.

The average capillary pressure for each unit cell of the typical serpentine and leading edge CPs (shown in Fig. 5.3) is constant, and can be calculated by dividing the change in the Gibbs free energy of the unit cell (before and after filling by the liquid) over the volume of the liquid, which is transported into the cell. The equation can be formulated as: [27, 28]

$$\Delta P = \frac{\gamma_{LG} \times \left(\cos\theta_t \times \Delta A_{SV_t} + \cos\theta_b \times \Delta A_{SV_b} + 2 \times \cos\theta_r \times \Delta A_{SV_r} \right)}{V^l} \tag{5.6}$$

where γ_{LG} is the surface tension of the liquid (*i.e.* water), $\theta_{i=t,b,r}$ are the contact angle of the liquid-air meniscus in the top, bottom and right surfaces, $\Delta A_{SV_i}, i = t,b,r$ are the respective changes of interfacial areas between solid, and air before and after filling of the cell for the top, bottom and right surfaces, and V^l is the volume of the liquid transferred in the unit cell (see APPENDIX III for more details). From experiments, Fig. SIII6 and SIII7 in APPENDIX III, we know that the advancing contact angle of a freshly treated flat Si (associated with the right and bottom surfaces), is *26.4°±3.3°,* and the advancing contact angle of a layer of PDMS (associated with the top surface of the CP) is *118.7°±1.7°*; thus, the average capillary pressure generated calculated from Eq. (6) equals to $\Delta P = 3375$ *Pa* (see the APPENDIX IIII for the details of the calculation). Eq.5.6 however, only constitutes an approximation as it does neither include corner flow effects nor the change in contact angles upon rapid filling.[29]

Our experiments allowed determining the relative change of the flow rate over time, and the capillary pressure was used as a free parameter to correlate flow rate with calculated flow resistance, and was ΔP=1210 Pa. This value corresponds to an equivalent of a capillary pressure generated from a glass tube with the diameter of 80 μm, which is in line with the depth of the CP ~ 100 μm and the distance of ~75 μm between the rows.
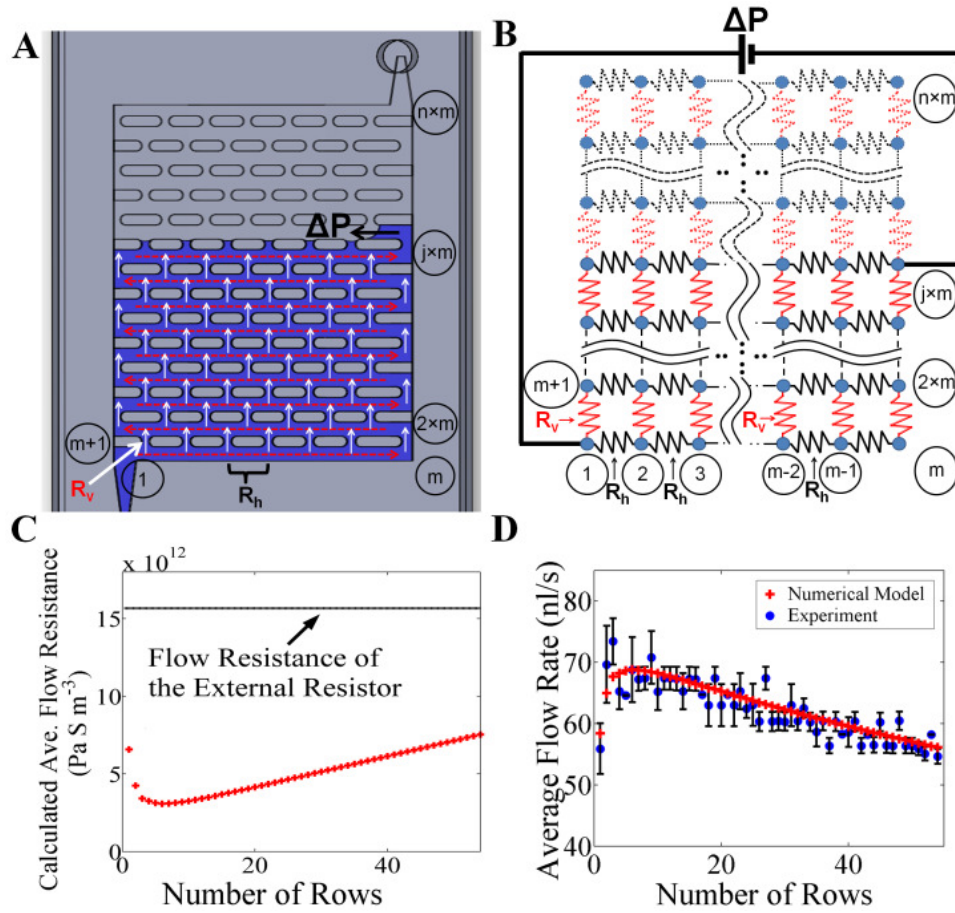
Fig. 5.4: Flow resistance of a serpentine CP. (A) Schematic showing the liquid

flow of a CP. (B) lumped resistance model of the CP. (C) Average flow resistance

for the filling front at each row based on nodal analysis of the electrical circuit

equivalent, see APPENDIX III. The calculated flow resistance decreases sharply

as the liquid passes the very first row of the CP; however, after the seventh row,

the resistance increases linearly (D) Comparison of theoretical and experimental

flow rates using the capillary pressure as a free parameter set to 1210 Pa. The

error bars in the experimental data are based on calculating the RMS values in

the variations among three independent experiments.

5.5.4 Pre-programmed serpentine CPs with varying capillary pressure

In many applications, for example microfluidic immunoassays,[30] it is desirable to adjust the flow rate for various steps of the assay. The control over the filling front enables to design CPs with variable capillary pressure. We designed CPs with a gradual decrease in the capillary pressure by increasing the width of the rows from 34 µm to 130 µm with incremental steps of 3 µm, Fig. 5.5A.

Fig. 5.5B illustrates the variation of the average flow rates from one row of the CP to the other. Although the capillary pressure decreases continuously, initially the speed of the filling front increases rapidly from 3 mm s^{-1} in the first row to 5 mm s^{-1} in the 8th row of the CP. This value corresponds to a growth from 33 nL s^{-1} to 62 nL s^{-1} in the flow rate of the CP. This increase is due to the decrease of the flow resistance, as explained in the section describing on the flow model of the CP. Subsequently, the speed of the filling front diminishes continuously to 2 mm s^{-1} in the last row, which corresponds to a flow rate 23 nL s^{-1}.

It is known that the contact angle of a liquid with a surface increases for increasing flow velocity.[29, 31, 32] Bracke *et al.* empirically established a relationship

between contact angle and capillary number $Ca = \dfrac{U \times \mu}{\gamma_{LG}}$, with U being the velocity of the filling front as: [33]

$$\frac{\cos\theta_a - \cos\theta_d}{\cos\theta_a + 1} = 2 \times Ca^{0.5} \tag{5.7}$$

With θ_a being the static advancing contact angle and θ_d the dynamic advancing contact angle. The static contact angles of Si and PDMS surfaces are θ_a=26.4° and θ_a=118.7° respectively, and thus the dynamic contact angles of these surfaces are expected to increase in the 8th and last row to 29° and 27.5° for the Si, and to 119.1° and 118.8° for PDMS, respectively, Table S1. Thus when calculating the capillary pressure at different rows, one needs not only to consider the change in geometry, the increase in flow resistance, but also the change in contact angle.

If we neglect the increasing flow resistance of the capillary pump and other dissipative energies, in theory the average ratio of the generated capillary pressure between the 34th row and the 8th row of the pump is expected to be:

$$\frac{\Delta P_8}{\Delta P_{34}} = 2.0 \tag{9}$$

where ΔP_8 and ΔP_{34} are the average capillary pressure generated in the 8th and 34th row respectively. This ratio is orderly consistent with our experimental data $\dfrac{Q_8}{Q_{34}} = 2.7$, where Q_8 and Q_{34} are the average flow rates in the 8th and 34th

rows respectively, and the difference may be in part due to the approximations that were made. The detail of the calculation for the ratio of the capillary pressures can be found in APPENDIX III.
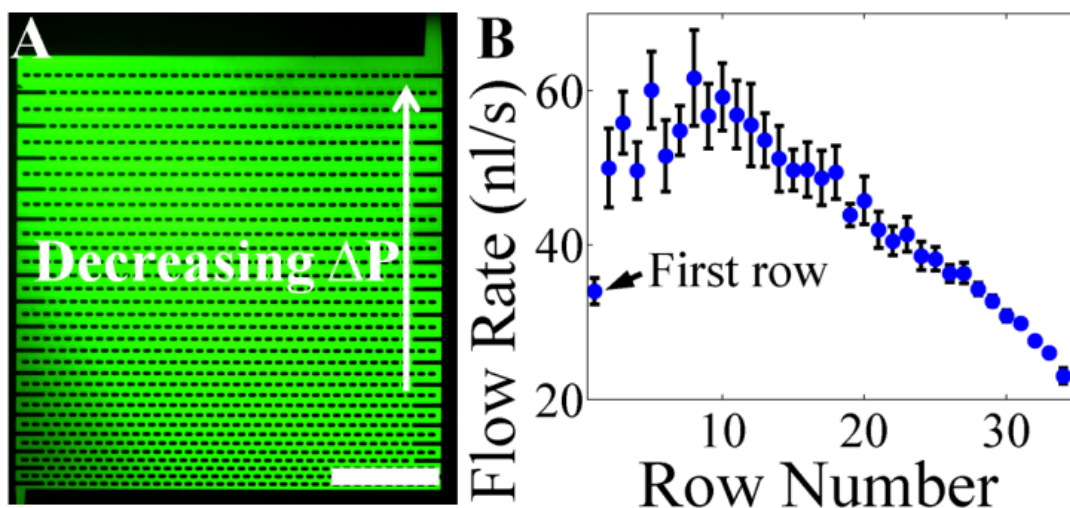

Fig. 5.28: Pre-programmed serpentine pumps with variable capillary pressure. (A) Fluorescence image of a CP filled with a green fluorescent solution revealing the increasing width of the rows that lead to a capillary pressure gradient. (B) Flow rates in each of the rows measured by video microscopy. The error bars are standard deviations of seven experiments. The scale bar is 1 mm.

5.6 Conclusions

We introduced novel architectures for CPs with guidance of the filling front along rows and at the edges to establish serpentine and leading-edge filling patterns, respectively. The flexibility and robustness of the design was highlighted using

CPs with different filling angles and gradients of pressures. A pore network analysis model was developed to calculate the flow resistance and was used to predict the pressure and flow properties of the different CPs.

Based on the examples, the functionality of capillary systems can be further expanded. For example, by tailoring the hydrodynamic properties of the CPs and the flow resistance of the circuit the filling time can be tuned from ~30 s to tens of minutes, while accurately metering the liquid. CPs with gradients of capillary pressure may allow optimizing the liquid flow rate during the incubation steps of bioassays.[30]

Using programmable CPs will expand the possibilities of passive, capillary driven microfluidics for carrying out advanced fluidic operations autonomously. This may open new opportunities for the use of capillary systems in immunoassays, point-of-care diagnostics and other areas.

5.7 Acknowledgment

5.8 References

1. Groll, M., Schneider, M., Sartre, V., Zaghdoudi, M.C. & Lallemand, M. Thermal control of electronic equipment by heat pipes. *Revue Generale De Thermique* **37**, 323-352 (1998).

2. Weislogel, M.M. Some analytical tools for fluids management in space: Isothermal capillary flows along interior corners, *Advances in Space Research,* **32** 163-170 (2003).

3. Delamarche, E., Juncker, D. & Schmid, H. Microfluidics for processing surfaces and miniaturizing biological assays. *Advanced Materials* **17**, 2911-2933 (2005).

4. Delamarche, E., Bernard, A., Schmid, H., Michel, B. & Biebuyck, H. Patterned delivery of immunoglobulins to surfaces using microfluidic networks. *Science* **276**, 779-781 (1997).

5. Lovchik, R.D., Bianco, F., Tonna, N., Ruiz, A., Matteoli, M. & Delamarche, E. Overflow Microfluidic Networks for Open and Closed Cell Cultures on Chip. *Analytical Chemistry* **82**, 3936-3942 (2010).

6. Cesaro-Tadic, S., Dernick, G., Juncker, D., Buurman, G., Kropshofer, H., Michel, B., Fattinger, C. & Delamarche, E. High-sensitivity miniaturized immunoassays for tumor necrosis factor a using microfluidic systems. *Lab on a Chip* **4**, 563-569 (2004).

7. Gervais, L. & Delamarche, E. Toward one-step point-of-care immunodiagnostics using capillary-driven microfluidics and PDMS substrates. *Lab on a Chip* **9**, 3330-3337 (2009).

8. Gervais, L., de Rooij, N. & Delamarche, E. Microfluidic Chips for Point-of-Care Immunodiagnostics. *Advanced Materials* **23**, H151-H176 (2011).

9. Juncker, D., Schmid, H., Drechsler, U., Wolf, H., Wolf, M., Michel, B., de Rooij, N. & Delamarche, E. Autonomous microfluidic capillary system. *Analytical Chemistry* **74**, 6139-6144 (2002).

10. Gervais, L., Hitzbleck, M. & Delamarche, E. Capillary-driven multiparametric microfluidic chips for one-step immunoassays. *Biosensors and Bioelectronics* **27**, 64-70 (2011).

11. Mirzaei, M., Pla-Roca, M., Safavieh, R., Nazarova, E., Safavieh, M., Li, H., Vogel, J. & Juncker, D. Microfluidic perfusion system for culturing and imaging yeast cell microarrays and rapidly exchanging media. *Lab on a Chip* **10**, 2449-2457 (2010).

12. Zimmermann, M., Schmid, H., Hunziker, P. & Delamarche, E. Capillary pumps for autonomous capillary systems. *Lab on a Chip* **7**, 119-125 (2007).

13. Vulto, P., Podszun, S., Meyer, P., Hermann, C., Manz, A., Urban, G.A. Phaseguides: a paradigm shift in microfluidic priming and emptying. *Lab on a Chip* **11**, 1596-1602 (2011).

14. McNeely, M.R., Spute, M.K., Tusneem, N.A. & Oliphant, A.R. Hydrophobic microfluidics, *Proceedings of SPIE* **3877**, 210-220 (1999)

15. Zimmermann, M., Hunziker, P. & Delamarche, E. Valves for autonomous capillary systems. *Microfluidics and Nanofluidics* **5**, 395-402 (2008).

16. Lee, A., VirtualDubMod Surround 1.6.0.0., virtualdubmod.sourceforge.net (2010).

17. Hitzbleck, M., Gervais, L. & Delamarche, E. Controlled release of reagents in capillary-driven microfluidics using reagent integrators. *Lab on a Chip* **11**, 2680-2685 (2011).

18. Delamarche, E., Bernard, A., Schmid, H., Bietsch, A., Michel, B. & Biebuyck, H. Microfluidic networks for chemical patterning of substrate:

Design and application to bioassays. *Journal of the American Chemical Society* **120**, 500-508 (1998).

19. White, F.M. in Viscous Fluid Flow, third edition, 116-125 (McGraw-Hill, 2005).

20. Safavieh, R., Zhou, G.Z. & Juncker, D. Microfluidics made of yarns and knots: from fundamental properties to simple networks and operations. *Lab on a Chip* **11**, 2618-2624 (2011).

21. Akbari, M., Sinton, D. & Bahrami, M. Pressure drop in rectangular microchannels as compared with theory based on arbitrary cross section. *Journal of Fluids Engineering* **131**, 041202-041201 (2009).

22. Tamayol, A., Yeom, J., Akbari, M. & Bahrami, M. Low Reynolds number flows across ordered arrays of micro-cylinders embedded in a rectangular micro/minichannel. *International Journal of Heat and Mass Transfer* **58**, 420-426 (2013).

23. Prat, M. Pore Network Models of Drying, Contact Angle, and Film Flows. *Chemical Engineering & Technology* **34**, 1029-1038 (2011).

24. Chapuis, O. & Prat, M. Influence of wettability conditions on slow evaporation in two-dimensional porous media. *Physical Review E* **75** (2007).

25. Ho, C., Ruehli, A. & Brennan, P. The modified nodal approach to network analysis. *IEEE Transactions on Circuits and Systems* **CAS-22**, 504-509 (1975).

26. Smith, K.C. KC's Problems and solutions for Microelectronic circuits, Chapter one **1**, fourth edition, (Oxford University Press, 1998).

27. Leverett, M.C. Capillary behavior in porous solids. *Transactions of the American Institute of Mining and Metallurgical Engineers* **142**, 152-169 (1941).

28. Hassanizadeh, S.M. & Gray, W.G. Thermodynamic basis of capillary pressure in porous media *Water Resources Research* **29**, 3389-3405 (1993).

29. Weislogel, M.M. & Lichter, S. Capillary flow in an interior corner. *Journal of Fluid Mechanics* **373**, 349-378 (1998).

30. Parsa, H., Chin, C.D., Mongkolwisetwara, P., Lee, B.W., Wang, J.J. & Sia, S.K. Effect of volume- and time-based constraints on capture of analytes in microfluidic heterogeneous immunoassays. *Lab on a Chip* **8**, 2062-2070 (2008).

31. Hoffman, R.L. A study of the advancing interface: II. Theoretical prediction of the dynamic contact angle in liquid-gas systems *Journal of Rheology* **26**, 606-606 (1982).

32. Seebergh, J.E. & Berg, J.C. Dynamic wetting in the low capillary number regime *Chemical Engineering Science* **47**, 4455-4464 (1992).

33. Bracke, M., Devoeght, F. & Joos, P. The kinetics of wetting-the dynamic contact angle *Trends in Colloid and Interface Science* **79**, 142-149 (1989).

Chapter 6: Pre-programmed, self-powered microfluidic circuits built from capillary elements

6.1 Preface

In the previous chapter, we presented two novel capillary pump architectures. Here, we first present two other microfluidic capillary elements including (i) retention burst valves and (ii) robust low aspect ratio trigger valves. Subsequently, we demonstrate that by combining these two elements with flow resistors, capillary retention valves and capillary pumps, complex capillary flow circuits that encode sequential flow of multiple liquids with distinct flow rates and flow reversal can be made. Finally, we employ the circuit to run a one-step immunoassay and measure the concentration of C-reactive protein.

This work suggests that as in electronics, complex capillary circuits may be built by combining simple capillary elements. We define the concept as "capillarics", and believe that more complex circuits will become possible by expanding the library of building elements and formulating abstract design rules.

This work resulted in the following publications:

Patent: Juncker, D. & **Safavieh, R**. *Method and system for pre-programmed self-power microfluidic circuits.* WO Patent 2,013,029,159 (2013)

Journal paper: Safavieh, R & Juncker, D. Capillarics: *Pre-Programmed, Self-Powered Microfluidic Circuits Built From Capillary Elements*, Lab Chip, **13** (2013)

6.2 Abstract

Microfluidic capillary systems employ surface effects to manipulate liquids, and are thus self-powered and self-regulated as liquid handling is structurally and chemically encoded in microscale conduits. However, capillary systems have been limited to perform simple fluidic operations. Here, we introduce complex capillary flow circuits that encode sequential flow of multiple liquids with distinct flow rates and flow reversal. We first introduce two novel microfluidic capillary elements including (i) retention burst valves and (ii) robust low aspect ratio trigger valves. These elements are combined with flow resistors, capillary retention valves and capillary pumps to build a capillary circuit that following sample addition, autonomously delivers a defined sequence of multiple chemicals according to a preprogrammed and predetermined flow rate and time. Such a circuit was used to measure the concentration of C-reactive protein. This works illustrates that as in electronics, complex capillary circuits may be built by combining simple capillary elements; we define such circuits as "capillarics", and believe that more complex circuits will become possible by expanding the library of building elements and formulating abstract design rules.

6.3 Introduction

Lab on a Chip (LOC) devices have emerged as a powerful tool for a variety of applications including bio-analysis[1, 2] and point of care diagnosis.[3] Central to microfluidic applications is the control of liquid flow within microconduits. Most microfluidic systems depend on peripheral equipment to effect and control the flow of liquid. As the complexity of these circuits increased, the similarities to electronic circuits were exploited, most notably in electrokinetic and electrophoretic microfluidics. In addition, centrifugal and hydrophobic microfluidic systems were also built where the advancement of the liquid was controlled by a combination of external control, and pre-embedded restrictions and hydrophobic patches.[4] The most complex microfluidic circuits developed to date are the ones made by multilayer soft lithography.[5] More recently, digital microfluidics that use electrical fields and capacitances to move droplets on arrays of electrodes, effectively create a connection between electronics and microfluidics, which may facilitate subsequent scaling up.[6]

6.3.1 Passive and capillary microfluidics

So-called passive microfluidic systems circumvent the need for peripheral equipment and extract the energy to move the liquids from the system, thus only requiring minimal user intervention. The flow in passive microfluidics is typically

driven by capillary effects, and they have in fact long been used in diagnostics in lateral flow tests.[7] Recently, paper-based microfluidics have attracted renewed interest from academia and microfluidic circuits with channels and reservoirs patterned in a paper or nitrocellulose substrate using photolithography, printing or laser cutting are being developed.[8] To advance the functionality of these circuits, various valves including (i) flow rate regulators by patterning dilute solutions of a water soluble wax,[9] or sugar barriers[10] in paper, and (ii) metering valves using sugar bridges[10] or expandable polymer actuators[11] combined in paper have been developed to control the timing of the fluid delivery. In addition, we and others showed that thread and yarn can be used to build fluidic circuits from the bottom up[12] and can be used for immunoassays.[13]

The heterogeneity of fibrous microfluidics however makes miniaturization difficult, implying that larger samples are required, and multiplexing will be limited. Furthermore, the limit of detection of paper and thread based microfluidics doesn't match the performance of classical ELISA and microfabricated microfluidic systems until now.

6.3.2 Autonomous capillary microfluidic systems

A landmark paper by Delamarche and colleagues highlighted the potential of self-filling microfluidics based on capillary effects.[14] Arrays of hydrophilic 2 µm-wide microfluidic channels, formed by sealing structured poly(dimethlsiloxane) (PDMS) onto silicon wafers, were used to spontaneously draw in liquids into the conduits and pattern proteins on surfaces; however, the solution could not be rinsed or exchanged. Common chemical and biochemical reactions do require addition and exchange of multiple solutions in sequence. An autonomous microfluidic capillary system (AMCS) that was self-powered and self-regulated – hence autonomous – was proposed and designed by combining a capillary pump (CP) and a capillary retention valve (CRV).[15] In AMCSs the capillary pressure is encoded in the geometry and surface properties (free surface energy of both solid surface and the liquid), which drives and controls the liquid flow on the chip. AMCS allows filling and flushing multiple solutions by simply delivering them sequentially to an inlet, without any need for removing solutions,[15] making them well adapted for conducting immunoassays that require the delivery of multiple solutions.[16]

6.3.3 One-step immunoassays

The ideal devices to conduct immunoassays and point-of-care diagnostics would only require a single manipulation, namely the addition of sample, to complete the assay, so-called one-step immunoassays.[17] Efforts to realize such systems have progressed along two directions. One is to keep fluidic functionality simple and implement the sequential delivery of chemicals by controlled dissolution or the geometry of the system. For example, Gervais *et al.*[18] pre-dried reagents in a dead-end conduit thus controlling the release, although this system required disassembling and rinsing prior to fluorescent imaging.[18, 19] Another simple approach featured three open and linked reservoirs that drain sequentially, although limited cross-talks between reagents occurred, and flow rates were not individually controlled, because of the flow resistance, the reservoirs are drained in sequence.[20] The second strategy was to expand the functionality of AMCSs to further enhance assay performance and versatility and emulate the functionality normally obtained using active systems.

6.3.4 Capillary valves

An important group of elements required for making advanced circuits are valves, but developing them is one of the challenges for building capillary systems, as on one hand they need to be self-filling and moving parts are not usable, and yet the

liquid should stop. However, to stop the liquid in capillary systems, one approach

is to design an abrupt increase in microchannel cross-section, to make it

energetically unfavourable for the liquid to flow from the narrow to the wide

channel due to the large increase in liquid-air interface at the filling front.[21] Such

geometric valves can then be triggered by flowing a sample through the wide

channel. Although the concept was proposed long ago,[22] and even multi-liquid

valving was shown,[23] an implementation that is robust and reliable for everyday

use has been difficult to achieve. The channel enlargement is often only

produced laterally within plane, and thus the liquid tends to creep along bottom

and cover of the channel. High aspect ratio valves mitigate this issue, but they

are difficult to microfabricate, even in Si, and cannot be transferred to other

materials, while still occasionally failing.[21] In a follow up study, Zimmermann *et al.*

[24] added new functionalities to their CPs and improved their performance. More

recently, valves have been made in low aspect ratio structures using less

hydrophilic surfaces, for example using a PDMS cover that can be depressed

manually for liquid activation.[25]

6.3.5 Hybrid capillary systems

Autonomous sequential delivery of samples has been demonstrated by trapping

air bubbles between liquid plugs, mirroring an approach initially implemented with

tubes and a syringe pump,[26] but using capillary effects to drive the flow.[27] However, bubbles create high flow resistance, and varying bubble sizes will affect the flow resistance and may get stuck, which will thus affect the reproducibility and reliability of such circuits.

Capillary microfluidics can also operate with positive pressures formed by hemispheric droplets dispensed atop of the inlet.[28] The simplicity of this approach makes them appealing for generating concentration gradients for example; however, the flow rate is low, and changes as the droplets are shrinking, thus only affording limited control over the flow rate. Recently, positive pressure fluidics have also been combined with capillary stop valves for more advanced fluidic operations;[29] however, the timing and triggering of liquid flow was not fully pre-programmed, and in fact required multiple timed user interventions, reminiscent of the constraints of the original AMCS.

6.3.6 Capillary elements and capillarics

Over the last few years, the functionality of capillary microfluidic systems has been expanded significantly. Here, we introduce additional capillary components, namely a robust trigger valve (TV) and a retention burst valve (RBV). Furthermore, we introduce *capillarics,* in analogy to *electronics,* denoting both the

154

complex capillary microfluidics as such, and the modularity of their architecture allowing them to be designed and assembled hierarchically by combining basic building elements selected from a library. The elemental building blocks are called capillary elements or capillaric elements depending on the context and their complexity. To illustrate this concept, a capillaric circuit was designed that upon flow a sample, reverses the flow and flushes four different chemicals in a predetermined sequence with a different flow rate. This circuit is then applied to measure the concentration of C-reactive protein.

6.4 Materials and methods

6.4.1 Chemicals and materials

Sylgard® 184 silicon elastomer kit (PDMS) was purchased from Dow corning (Midland, MI, USA). Prepolymers, i.e., curing agent and polymer base, were manually mixed at a ratio of 1:10, and cured for 8 hrs in an oven (Lindberg Blue M, Fisher Scientific) at 60°C. A 1 mg/mL solution of Fluorescein sodium salt ($C_{20}H_{10}Na_2O_5$) (fluorescein dye, Sigma-Aldrich, USA) in water (Milli-Q purified water, Millipore, USA) was used for characterizing the RBVs. Food dyes (McCormick & Co., MD, USA) were purchased from local stores and 50% diluted solutions were used to test the capillaric circuit. Experiments were performed at the room temperature of 23±2°C. Phosphate buffered saline (PBS) tablets

(Sigma-Aldrich, USA) were reconstituted in deionized (DI) water to form 1% PBS in water. Bovine serum albumin (BSA) (Jackson ImmunoResearch, PA, USA) was dissolved at a concentration of 3% in DI water. Human C-reactive protein (CRP) antigen, capture anti-CRP, and biotinylated detection anti-CRP were purchased from R&D Systems (Minneapolis, MN, USA). Streptavidin-Alexi Fluor 488 (Invitrogen, Burlington, ON, Canada) was used as a label in the immunoassay.

6.4.2 Chip design and fabrication

Circuits were designed in a layout editor software, CleWin (CleWin 5, WieWeb software, Netherland), and the designs were printed in a 7"×7" chrome mask with 65,000 dots per inch resolution (Thin metal parts, Colorado Springs, USA). A soft lithography technique was followed as described previously elsewhere.[30] Briefly, 2 level moulds were fabricated in SU-8 50 (Microchem, Massachusetts, USA), and replicated into PDMS. The elements and circuits are 100 μm deep, except the two level trigger valves, which are only 50 μm deep. The reaction chamber was designed in an oval shape with 200 μm width and 2000 μm length. A razor blade (single edged razor blade, Fisher Scientific, Canada) was used to cut the chips from the replica. The vents of the chip were fabricated using a biopsy punch (1.5 mm puncher, Ted Pella Inc., USA). The chip was rendered hydrophilic

with an air plasma (Plasmaline 415, Tegal Inc., US) for 45 s with 250-mTorr pressure and 150-mW power. A flat 2 mm thick PDMS cover was used to seal the chip.

6.4.3 Capture antibody patterning on PDMS

We used a microfluidic capillary system (CS)[31] with 16 parallel microchannels to pattern capture anti-CRP on the PDMS cover. Each microchannel was $2000 \times 100 \times 100$ μm^3 in size, and was separated from the neighboring microchannel by a 200 µm gap. The CS was activated with air plasma to render it hydrophilic, and sealed reversibly to the PDMS cover, orthogonal to the future reaction chamber that was outlined with a pen. 2 µL of anti-CRP capture antibody (250 µg/mL) were pipetted into the loading port and spontaneously filled the microchannels. The PDMS was incubated for 45 min at room temperature in a humidified closed Petri dish containing a wet tissue to prevent evaporation. The liquid was then drawn out using a clean room paper, the PDMS removed, rinsed with PBS for 15 s and blocked with a 3% BSA solution for 30 min to avoid nonspecific binding, rinsed with DI water, dried, and stored for later use.

6.4.4 One step immunoassay

For the sandwich immunoassay, we positioned a plasma activated chip on a patterned cover. The orientation of the reaction chamber was orthogonal to the capturing stripes patterned on the PDMS cover. We then preloaded 4 reagents including: (i) 1% PBS in DI water, (ii) biotinylated anti-CRP detection antibody (200 µg/mL), (iii) 1% PBS in DI water, and (iv) streptavidin-Alexa Fluor 488 (500 µg/mL) in four reservoirs in the chip by contacting the tip of a pipette to the side channel vents. Subsequently, we loaded 2.5 µL of a buffer with CRP protein, and repeated the entire experiment with a series of different concentrations of CRP. Upon the completion of the assay, we separated the cover from the chip, rinsed it with DI water for 15 s, and dried it using a nitrogen gun, followed by fluorescence imaging of the PDMS cover using a microscope.

6.4.5 Imaging Analysis and Signal Quantification

To characterize the fabricated capillaric elements and the circuits, we used both optical (LV150 industrial microscope, Nikon, Japan) and scanning electron microscopy (S-3000N variable pressure SEM, Hitachi, Japan). Images of the liquid flow in the chip were captured using a stereomicroscope (Leica MZ8, Leica Microsystems, Switzerland) outfitted with a CCD camera (DS-Fi1, Nikon, Japan). As for the immunoassay, we used a customized fluorescence confocal

microscope (C1si Nikon Inverted Confocal microscope, Nikon, Japan) connected

to a CCD camera (CoolSNAP HQ^2, Photometrics, USA) to quantify the binding of

the assay. The CRP binding curve was calculated from three independent

experiments. Average colour intensities of the fluorescence images were

extracted using Image J (NIH, Bethesda, MD), and binding curves fitted with a

four-parameter logistic curve (GraphPad Prism 5, GraphPad Software Inc., USA),

Fig. 6.7. In each experiment, we tested six chips with six different concentrations

of CRP antigen and measured the average fluorescent intensities of two stripes.

6.5 Results and discussion

6.5.1 Library of capillaric elements

To facilitate conceptualization, capillaric elements including (i) microchannels, (ii)

fluidic resistors, (iii) vents, (iv) CPs, (v) TVs, (vi) CRVs as well as novel (vii) RBVs

are schematized in Fig. 6.1.

Microchannels are transporting the liquids and while they also generate a flow

resistance, it can often be neglected, and they thus represent the equivalent of

electrical lines in electrical circuits. Fluidic resistors are typically microchannels

with reduced cross-sections. Because the flow resistance scales as R^{-4} (radius)

in channels with circular cross-section, small changes in size can have significant

effects, and a few small sections along the flow path can dominate the overall flow resistance of the circuit, as in electrical circuits. Vents are conduits that are connected to the atmosphere. It is noteworthy that the capillary pressure is proportional to R^{-1} and in practice becomes negligible when the smallest dimension in a circular or rectangular conduit is > 1 mm; thus vents should be big enough and hydrophobic to minimize surface tension.

CPs generate a constant capillary pressure similar to a voltage source in an electronic circuit. Microstructured reservoirs with posts serve as CPs and the gaps between the posts define the capillary pressure; the smaller the gap, the larger the pressure drop and the stronger the pump.[24, 32] TVs stop the flow of a first liquid at a point until it is triggered by flow of a second liquid entering through second conduit, as discussed previously.[21] RBVs are a modification of the CRVs, and both are formed by a localized reduction of the channel cross-section, which prevents the liquid from draining due to a large capillary pressure. CRVs are meant to retain the liquid permanently, while the RBVs act as release valves, once the capillary pressure exceeds a threshold value. A series of RBVs with increasing threshold can thus be used to control the sequence of liquid being delivered.
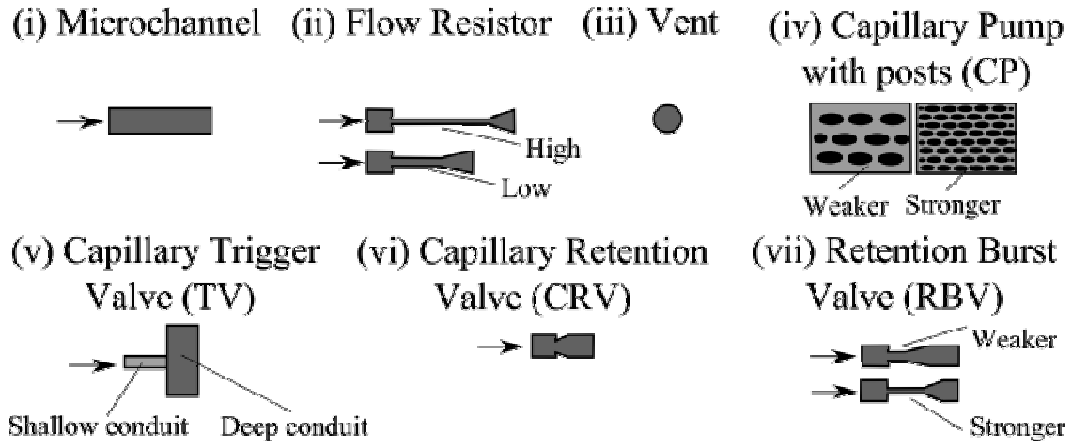
Fig. 6.1: Schematic illustrating the library of capillaric elements; the elements include, (i) microchannel, (ii) flow Resistor, (iii) vent, (iv) CP, (v) TV, (vi) CRV and (vii) RBVs.

Previously, we and other researchers have introduced some of these capillary elements, shown in Fig. 6.1, including CPs, flow resistors, and vents.[32, 33] In the following sections we explain the development of two novel capillaric elements in the library *i.e.* two-level TVs and RBVs.

6.5.2 Two-level trigger valve

Conventional capillary TVs that expand only laterally lack robustness, and are prone to spontaneous triggering.[21] A single layer TV with an aspect ratio of depth/width = 3 was made of plasma-activated, hydrophilic, PDMS and closed with native, hydrophobic, PDMS cover. This leaked in less than two seconds,

Fig. 6.2A. To overcome the lack of reliability, we propose a two-level capillary TV, which consists of a shallow conduit intersecting a deep one and a hydrophobic cover, Fig. 6.2B. The abrupt enlargement in the cross-section of the microchannel occurs laterally and vertically at the bottom, while the hydrophobic cover prevents the liquid from creeping along the top. A two level TV with the aspect ratio, depth/width =1.5, stopped the liquid for more than 20 mins, Fig. 6.2C. These valves robustly stopped liquids for over 20 min, and we did not observe a single failure in 50 experiments.
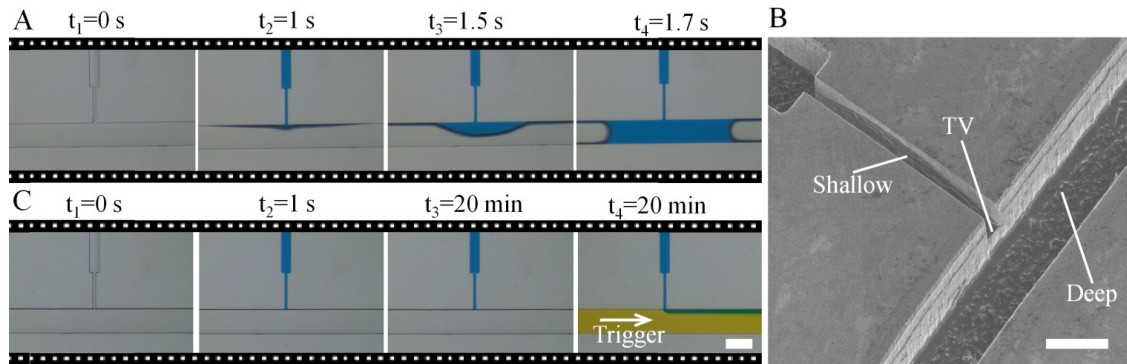
Fig. 6.2: Two-level TV used to passively stop the liquid. The microstructures are hydrophilic (plasma activated PDMS). The sealing layer is hydrophobic PDMS. (A) Time lapse images showing that the abrupt enlargement of the one-level TV fails after only 1.5 seconds; (B) SEM micrograph of the two-level TV. (C) Images showing that the abrupt enlargement of the two-level TV together with the use of a hydrophobic cover were effective to stop the liquid for periods of 20 min, and

could be triggered at any time by flowing a sample in the deep conduit. The scale bars are 200 μm.

6.5.3 Retention burst valves (RBVs)

CRVs and RBVs are formed by constrictions in the microchannel that produce high capillary pressure. The CRVs and RBVs shown here were all engineered in deep channels, while varying the width to gradually increase the capillary pressure. If the capillary pressure of a CP is weaker than the one of the constriction, a CRV is formed. If the capillary pressure of the pump is stronger than the constriction, then an RBV is formed that will retain the liquid until the pressure at that point within the circuit drops below the capacity of the valve. Thus, as long as there is flow in the circuit, the pressure may remain high, but once the flow stops, the circuit acts as a hydraulic system, and the capillary pressure of the pump is transmitted throughout. Thus, if multiple RBVs with different thresholds are included, the weakest one will burst first and the liquid stored downstream will be drained, and then the second weakest one will burst and the liquid will be drained, and so on, Fig. 6.3.

The burst pressure of the valve is related to its dimensions according to the rules of capillary pressure. However, while the advancing contact angle is present

during filling, it is the receding contact angle that arises during draining. Hysteresis between advancing and receding contact angles thus requires that the dimensions of the CP be significantly smaller than the one of the RBVs to burst it. Moreover, although not reflected in the equations, we found that the length of the RBV also contributed to the strength of the RBV. We then designed a series of RBVs with varying width and length, and integrated them in a simple circuit to illustrate sequential drainage of 6 valves, Fig. 6.3A. The RBVs are located at the extremity of each side arm. CRVs with a capillary pressure exceeding the one of the CP were included at the junction of each side arm and the main conduit, as well as on the inlet side to prevent drainage of the main conduit. Fig. 6.3B show time-lapse images of the filling and sequential drainage of the six side arms with a solution containing fluorescein. The liquid was added to the loading port (not visible) and then started filling the microchannels and the CP. A flow resistor in front of the CP ensured that all side-arms were filled despite the large capillary pressure of the CP. Next, as the liquid in the loading port is drained, it is pinned and stopped at the CRV. As all flow stops at this moment, the pressure of the CP acts throughout the entire circuit, and bursts the first RBV, followed by drainage of the first conduit until the liquid is pinned at the CRV next to the main channel. Then, the second RBV is burst, and so on until all 6 side arms are drained.
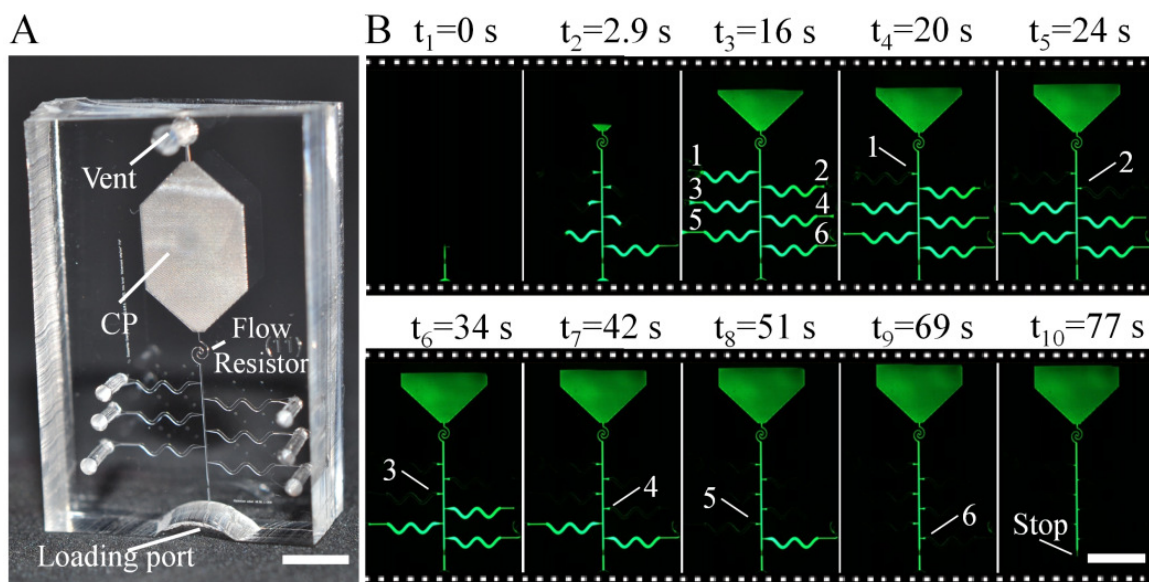
Fig. 6.29: Operation of the RBVs. (A) Micrograph of a circuit to test the RBVs. (B) Time lapse imaging showing sequential filling and draining of reservoirs using the RBVs. In each of the serpentine microchannels, we designed an RBV and a CRV. The CRVs were placed at the junctions of the side arms and the main conduit, and have a stronger capillary pressure that that of the CP. The RBVs were at the end of each side arm, and have the capillary pressures weaker than that of the CP. By adjusting the length and the width of these valves, we controlled the sequence of draining of 6 side-arms. The depth of the microchannels is 100 μm. Scale bars are 3 mm.

6.5.4 Capillaric circuit with flow reversal

To illustrate the possibility of making complex systems using a variety of capillaric elements, we designed a capillaric circuit for performing one-step immunoassays, Fig. 6.4A. The chip is sealed with a hydrophobic PDMS cover

with vents and loading ports to add the reagents and a sample. The circuit comprises 4 side-arms, each comprising an RBV at the extremity close to the loading ports, and a TV that connects each arm to the main channel, and that simultaneously acts as a CRV. The side arms are preloaded with 4 different reagents that are applied to the respective loading ports, Fig. 6.4B, (t_1-t_2). A filled pipette tip is brought into contact with the chip, and the reagents are spontaneously drawn by capillary pressure into the side-arms up to the TV (t_3). A sample applied to the main loading port flows via a channel, a CRV, fills a short side-conduit stopping at a TV (t_4), and progresses to the reaction chamber. The liquid then flows past the 4 side-arms, through a resistor and flows into the incubation CP that draws a precise volume, flushing it through the reaction chamber. Upon filling the incubation CP (t_5), the sample moves continuously, and activates a TV that is located upstream of the reaction chamber. Following activation, excess sample flows through the TV into the waste CP until the entire excess sample is depleted and the flow stops (t_6). The capillary pressure in the circuit then rises to the level of the waste CP, and triggers the first RBV (t_7) and drains the reagent from the first side-arm, which flows back through the main channel and the reaction chamber to the CP until the CRV stops the drainage. Each arm is drained in sequence according to the threshold of each RBV (t_8-t_{10}). The flow path through the incubation CP remains open but, because the flow

resistance is ~ 55 times higher than that through the reaction chamber, virtually

all reagents flow back through the reaction chamber at a preprogramed flow rate.

This circuit was designed for performing immunoassays.
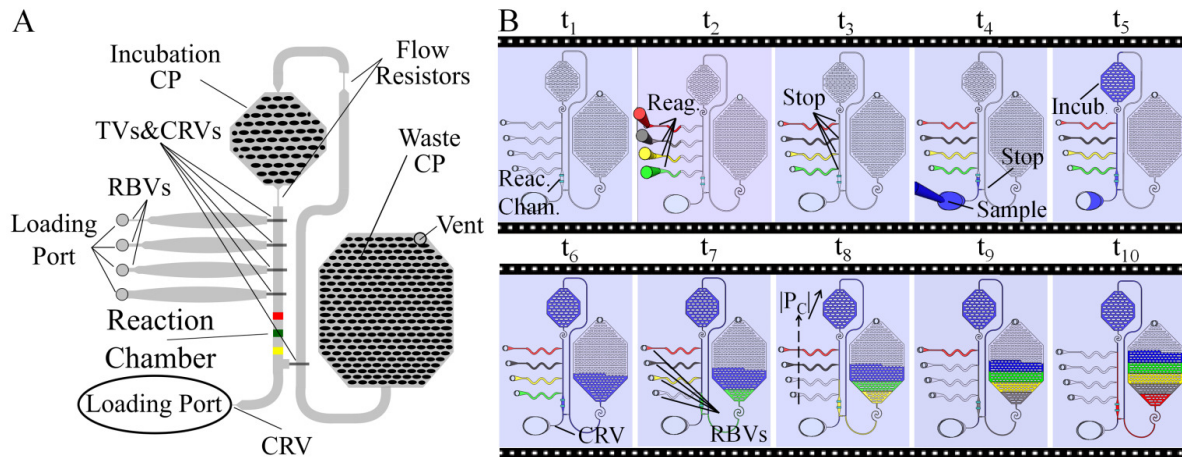
Fig. 6.30: A Capillaric circuit for flowing a metered amount of sample through a reaction chamber followed by flow reversal and sequential flowing of 4 pre-loaded reagents at a different flow rate. (A) Overview of the circuit comprising a reaction chamber, 4 side-arms with RBVs and combined TV/CRVs similar to the ones described in Fig. 6.3, flow resistors, an incubation CP, as well as a waste CP. (B) Schematic drawings outlining the operation of the capillaric circuit step-by-step. Initially, the cover with patterned lines of capture antibodies is sealed orthogonally to the reaction chamber (t_1). Afterwards, various reagents (green, yellow, black and red) are dispensed into the side-arms (t_2), and stop at the TV at the intersection with the main channel (t_3). Next, the sample is introduced through the loading port (t_4), flowing via the main channel to the incubation CP

which draws a predetermined amount at a controlled flow rate (t_5). Subsequently, when the liquid passes the TV at the junction upstream of the reaction chamber, the excess amount of the sample flows through the shortcut directly into the waste CP (t_6).Finally, the side-arms are drained sequentially, and flow in reverse direction through the reaction chamber via the shortcut into the waste CP (t_7-$t1_0$).

The capillaric circuits were made out of PDMS using a two level SU8 mould as a 19 ×21 mm^2 chip. The chips were plasma activated to render them hydrophilic, and a hydrophobic PDMS with vents and loading ports was used as the cover layer, Fig. 6.5.
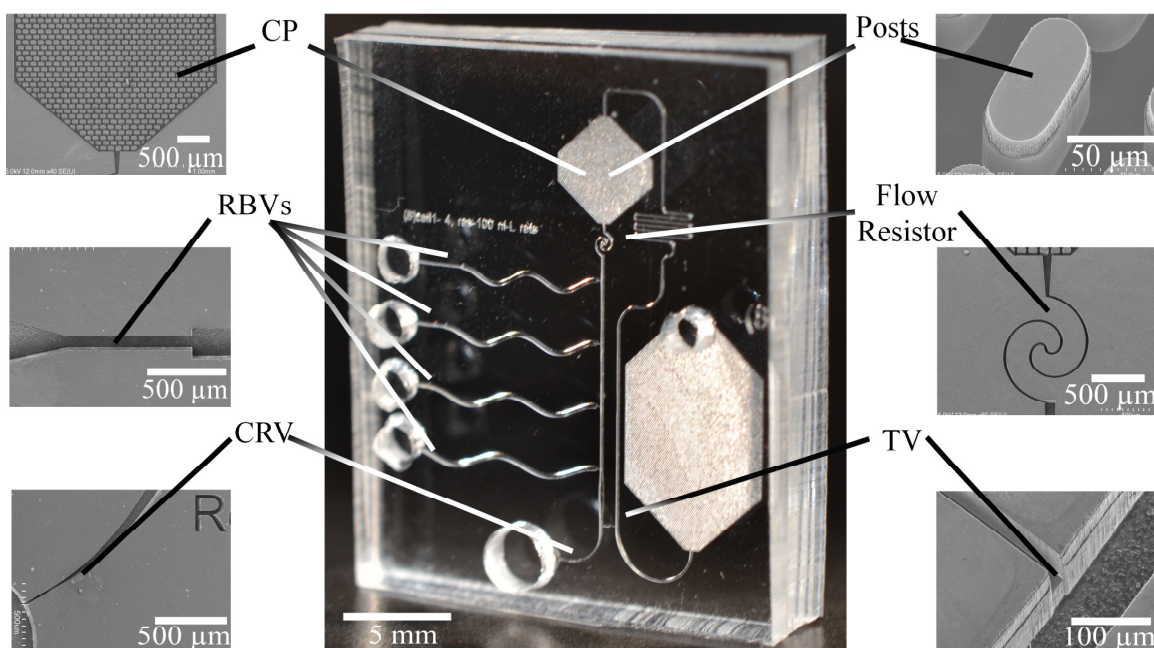
Fig. 6.5: Optical micrograph of a microfluidic capillaric circuit with flow reversal made in PDMS. 19 ×21 mm^2. The PDMS cover includes vents and a loading port.

To validate the design, solutions of food dyes and DI water were filled as outlined in Fig. 6.5, and recorded, Fig. 6.6. The side-arms were filled by simply contacting the extremity of the channel with a pipette tip. 1 µL of a black food dye, serving as a sample, was introduced into the main loading port. The flow pattern replicated the steps outlined above accurately.
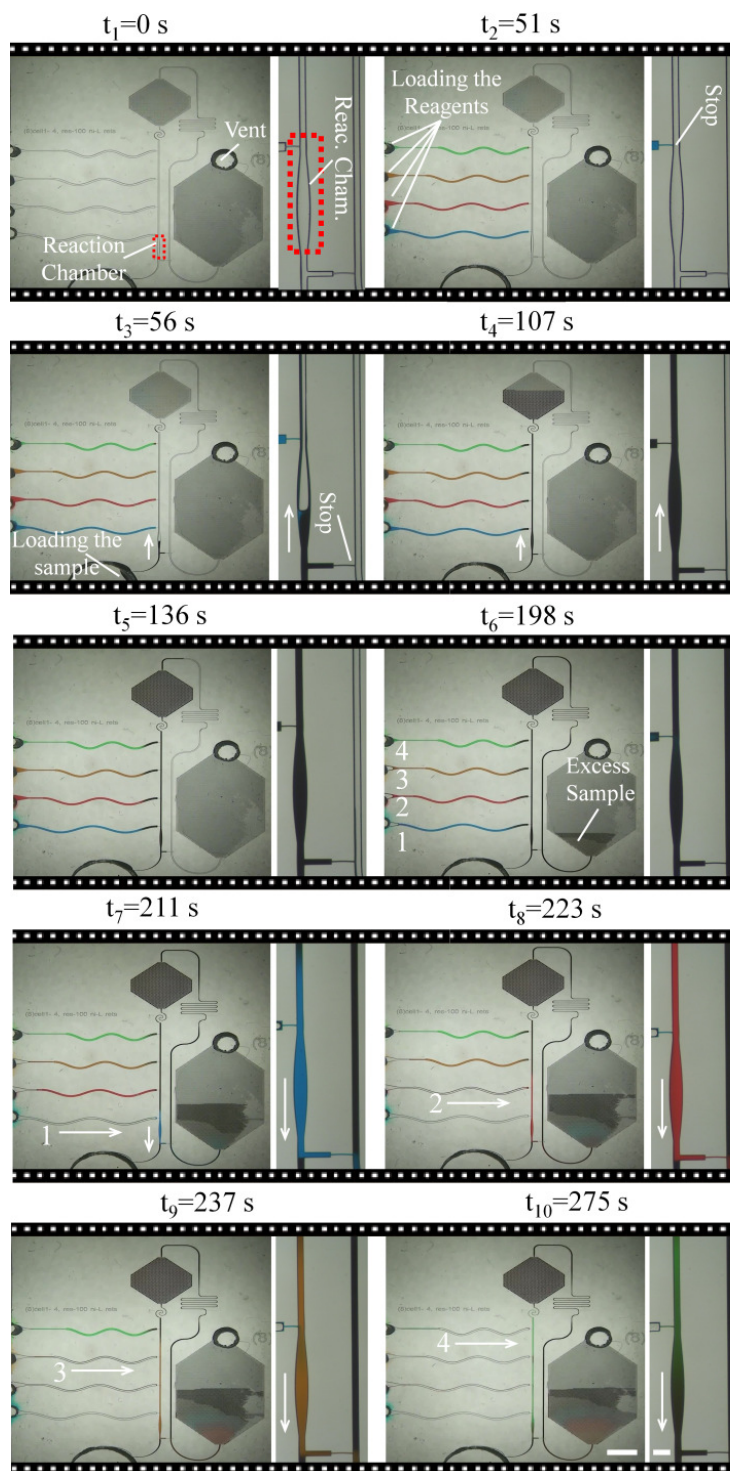
Fig. 6.6: Capillaric circuit with flow reversal and different flow rates. Four food

dyes, blue, red, orange, and green were dispensed to the side-arms using a

pipettte. 1 μL of a black food dye serving as a sample was introduced into the

main loading port. It flowed for ~ 150 s through the metering pump (800 nL), flowed back via the small channel, and activated the TV upstream of the reaction chamber. The excess sample was thus flushed via the shortcut directly into the waste CP (t_6). Next, the reagents in the side-arms are drained sequentially from bottom to top (blue, red, orange, and green) and flow in the reverse direction through the reaction chamber and the shortcut into the waste CP as well. The scale bar is 3 mm in the overviews and 200 µm in the close-up views.

6.5.5 Sandwich immunoassay in a capillaric circuit

To show the potential applications of capillaric circuits, a sandwich immunoassay for CRP was performed as outlined in Fig. 6.7A. We first patterned anti-CRP capture antibody on the cover of the chip using a CS perpendicular to the reaction chamber.[31] Later on, biotinylated anti-CRP antibody was filled into side-arm 1, washing buffer in side-arms 2 and 4, and streptavidin conjugated to Alexa Fluor 488 in side-arm 3. Next, a 1 µL of phosphate buffer saline spiked with CRP was applied to the main loading port, flowing and triggering the flow of all the other reagents. Fig. 6.7B shows the assay results for triplicate measurements of the CRP concentrations between 0.01 and 10 µg/mL as well as a negative control. Two fluorescence micrographs (vertical stripes) in a reaction chamber, corresponding to the signals of 10µg/mL concentration of CRP antigen

171

were also illustrated as an inset of the graph. The scale bar of the micrograph is 100 μm. To achieve higher sensitivity, it will be necessary to increase the incubation time of the sample, and optimize the flushing time for the reagents, while also improving the stability of the surface, because the PDMS used slowly reverted to a hydrophobic state.
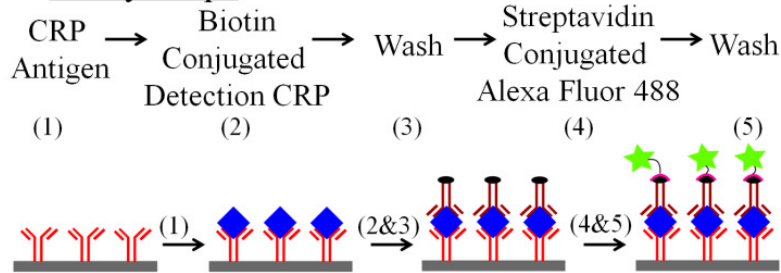
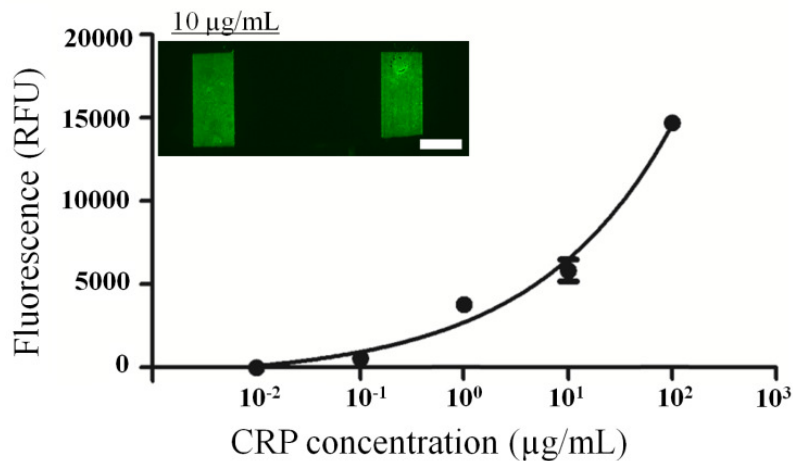Fig. 6.7: Sandwich immunoassay for CRP carried out using a capillaric circuit. (A) The sandwich assay consists of five steps. First, CRP antigen is captured on the reaction chamber by the pre-immobilized capture antibodies . Next, biotinylated detection CRP, washing buffer, fluorescent streptavidin, and second

washing buffer were flushed from the side channels sequentially. Finally, the stamp was imaged with a fluorescence microscope. (B) Standard curves of the fluorescent signals obtained from three independent sets of experiments. In each experiment, we tested six chips and measured the average intensities of the fluorescent signals in two patterned reaction zones in each chip. We then fitted a curve the set of data. The inset illustrates fluorescence micrographs (vertical stripes) correspond to the signals of 10µg/mL concentration of CRP antigen. The scale bar is 100 µm.

6.6 Conclusion

We introduced the concept of capillarics, in analogy to electronics, as a more complex form of capillary systems introduced a decade ago. Whereas one can draw a general conceptual analogy to electronics, there are also deep differences, because with capillaric circuits the fluid logic is realized with the advancement, and retreat, of the wetting front of the liquid in different parts of the circuit in a time and space dependent manner. We demonstrated that capillaric circuits can be made from a number of capillary and capillaric elements including CRVs, RBVs, resistors, vents, TVs, and CPs. We notably designed side channels with RBVs at the extremity and a combined TV/CRV at the intersection with the main channel, so that reagents filled in each side channel would be

drained according to a pre-programmed sequence, regardless of the of the order with which they were filled. These elements were integrated into a capillaric circuit for a one-step immunoassay with flow reversal implementing distinct flow rates for the sample and subsequent reagents, and comprising two CPs for sample metering, and one acting as a final waste collector. The combination of various elements allows creating new fluidic logic operations and circuits, which may be designed at an abstract level, and then realized physically according to design rules yet to be established. We believe that many more fluidic circuits may be built both as microfabricated structures that afford great control, but also using porous supports such as paper that are inexpensive, or possibly by combining the best of both worlds so as to obtain a better control at a reduced cost. However, challenges remain and for example the number of RBVs that can be reliably operated in parallel is limited by imperfections and hysteresis in wetting, which commands the use of significant differences in retention pressure, while requiring CPs with significantly higher capillary pressure than the highest RBV to ensure its drainage. Scaling up of capillaric circuit will depend on overcoming such limitations, but as the examples shown here demonstrate, circuits with moderate complexity can already be designed and built. Whereas we demonstrated a one-step immunoassay, improvement such as long term reagent storage are still needed to permit pre-filling of chips independently of usage

Furthermore, a more convenient assay readout is also needed, and may be implemented using for example silver amplification,[34] permitting assay readout using a cell phone, or an electrochemical detection using simple electronics only. We thus believe that capillarics will be useful for point-of-care diagnostic applications, as well as for many chemical and biochemical processes that require the sequential addition and removal of multiple reagents.

6.7 Acknowledgement

6.8 References

1. Safavieh, R., Roca, M.P., Qasaimeh, M.A., Mirzaei, M. & Juncker, D. Straight SU-8 pins. *Journal of Micromechanics and Microengineering* **20** (2010).
2. Moorthy, J., Burgess, R., Yethiraj, A. & Beebe, D. Microfluidic based platform for characterization of protein interactions in hydrogel nanoenvironments. *Analytical Chemistry* **79**, 5322-5327 (2007).

3. Yager, P., Domingo, G.J. & Gerdes, J. Point-of-care diagnostics for global health, *Annual Review of Biomedical Engineering* **10**, 107-144 (2008).

4. Gervais, L., de Rooij, N. & Delamarche, E. Microfluidic Chips for Point-of-Care Immunodiagnostics. *Advanced Materials* **23**, H151-H176 (2011).

5. Unger, M.A., Chou, H.P., Thorsen, T., Scherer, A. & Quake, S.R. Monolithic microfabricated valves and pumps by multilayer soft lithography. *Science* **288**, 113-116 (2000).

6. Choi, K., Ng, A.H.C., Fobel, R. & Wheeler, A.R. Digital Microfluidics. *Annual Review of Analytical Chemistry*, **5** 413-440 (2012).

7. Haeberle, S. & Zengerle, R. Microfluidic platforms for lab-on-a-chip applications. *Lab on a Chip* **7**, 1094-1110 (2007).

8. Li, X., Ballerini, D.R. & Shen, W. A perspective on paper-based microfluidics: Current status and future trends. *Biomicrofluidics* **6**, 11301-1130113 (2012).

9. Noh, H. & Phillips, S.T. Fluidic Timers for Time-Dependent, Point-of-Care Assays on Paper. *Analytical Chemistry* **82**, 8071-8078 (2010).

10. Fu, E., Ramsey, S.A., Kauffman, P., Lutz, B. & Yager, P. Transport in two-dimensional paper networks. *Microfluidics and Nanofluidics* **10**, 29-35 (2011).

11. Toley, B.J., Fu, E. & Yager, P. A powerless valving system for fluid flow in paper networks. *Sixteenth International Conference on Miniaturized Systems for Chemistry and Life Sciences*, 305-307 (2012).

12. Safavieh, R., Zhou, G.Z. & Juncker, D. Microfluidics made of yarns and knots: from fundamental properties to simple networks and operations. *Lab on a Chip* **11**, 2618-2624 (2011).

13. Zhou, G., Mao, X. & Juncker, D. Immunochromatographic Assay on Thread. *Analytical Chemistry* **84**, 7736-7743 (2012).

14. Delamarche, E., Bernard, A., Schmid, H., Michel, B. & Biebuyck, H. Patterned delivery of immunoglobulins to surfaces using microfluidic networks. *Science* **276**, 779-781 (1997).

15. Juncker, D., Schmid, H., Drechsler, U., Wolf, H., Wolf, M., Michel, B., de Rooij, N. & Delamarche, E. Autonomous microfluidic capillary system. *Analytical Chemistry* **74**, 6139-6144 (2002).

16. Wolf, M., Juncker, D., Michel, B., Hunziker, P. & Delamarche, E. Simultaneous detection of C-reactive protein and other cardiac markers in human plasma using micromosaic immunoassays and self-regulating microfluidic networks. *Biosensors and Bioelectronics* **19**, 1193-1202 (2004).

17. Zimmermann, M., Hunziker, P. & Delamarche, E. Autonomous capillary system for one-step immunoassays. *Biomedical Microdevices* **11**, 1-8 (2009).

18. Gervais, L., Hitzbleck, M. & Delamarche, E. Capillary-driven multiparametric microfluidic chips for one-step immunoassays. *Biosensors & Bioelectronics* **27**, 64-70 (2011).

19. Hitzbleck, M., Gervais, L. & Delamarche, E. Controlled release of reagents in capillary-driven microfluidics using reagent integrators. *Lab on a Chip* **11**, 2680-2685 (2011).

20. Wang, J. et al. A self-powered, one-step chip for rapid, quantitative and multiplexed detection of proteins from pinpricks of whole blood. *Lab on a Chip* **10**, 3157-3162 (2010).

21. Zimmermann, M., Hunziker, P. & Delamarche, E. Valves for autonomous capillary systems. *Microfluidics and Nanofluidics* **5**, 395-402 (2008).

22. Man, P.F., Mastrangelo, C.H., Burns, M.A. & Burke, D.T. Microfabricated capillarity-driven stop valve and sample injector, *Proceedings MEMS 98. IEEE. Eleventh Annual International Workshop on Micro Electro Mechanical Systems,* 45-50 (1998).

23. Melin, J., Roxhed, N., Gimenez, G., Griss, P., Wijngaart, W. & Stemme G. A liquid-triggered liquid microvalve for on-chip flow control. *Journal of Sensors and Actuators, B* **100**, 463-468 (2004).

24. Zimmermann, M., Schmid, H., Hunziker, P. & Delamarche, E. Capillary pumps for autonomous capillary systems. *Lab on a Chip* **7**, 119-125 (2007).

25. Hitzbleck, M., Avrain, L., Smekens, V., Lovchik, R.D., Mertens, P. & Delamarche, E. Capillary soft valves for microfluidics. *Lab on a Chip* **12**, 1972-1978 (2012).

26. Linder, V., Sia, S.K. & Whitesides, G.M. Reagent-loaded cartridges for valveless and automated fluid delivery in microfluidic devices. *Analytical Chemistry* **77**, 64-71 (2005).

27. Novo, P., Volpetti, F., Chu, V. & Conde, J.P. Control of sequential fluid delivery in a fully autonomous capillary microfluidic device. *Lab on a Chip* (2012).

28. Walker, G.M. & Beebe, D.J. A passive pumping method for microfluidic devices. *Lab on a Chip* **2**, 131-134 (2002).

29. Kim, S.-J., Paczesny, S., Takayama, S. & Kurabayashi, K. Preprogrammed capillarity to passively control system-level sequential and parallel microfluidic flows. *Lab on a Chip* (2013).

30. Papra, A. et al. Microfluidic Networks Made of Poly(dimethylsiloxane), Si, and Au Coated with Polyethylene Glycol for Patterning Proteins onto Surfaces. *Langmuir* **17**, 4090-4095 (2001).

31. Juncker, D. et al. Soft and rigid two-level microfluidic networks for patterning surfaces. *Journal of Micromechanics and Microengineering* **11**, 532-541 (2001).

32. Safavieh, R. & Juncker, D. Serpentine and leading Edge capillary pumps. *Proceedings of the 15th International Conference on Miniaturized Systems for Chemistry and Life Sciences* 245-247 (2011).

33. Ziegler, J., Zimmermann, M., Hunziker, P. & Delamarche, E. High-performance immunoassays based on through-stencil patterned antibodies and capillary systems. *Analytical Chemistry* **80**, 1763-1769 (2008).

34. Chin, C.D., Laksanasopin, T., Cheung, Y.K., Steinmiller, D., Linder, V., Parsa, H., Wang, J., Moore, H., Rouse, R., Umviligihozo, G., Karita, E., Mwambarangwe, L., Braunstein, S.L., van de Wijgert, J., Sahabo, R., Justman, E., El-Sadr, W. & Sia, S.K. Microfluidics-based diagnostics of infectious diseases in the developing world. *Nature medicine* **17**, 1015-1019 (2011).

Chapter 7: Conclusion and outlook

7.1 Summary of findings

This work presented three novel platforms of capillary-driven microfluidic systems. These platforms include: (i) polymer pins for microarray spotting, (ii) cotton yarns as a substrate for making capillary driven microfluidics and (iii) complex circuits for sequential delivery of multiple reagents with precise timing of reactions, and reversal of the flow. The work also showed the use of these systems for microarray spotting and diagnostic applications.

First, we optimized the design and proposed a new fabrication technique for making miniaturized quill pins, which can be used for protein printing. The slit inside the pin is filled with capillary effects, and by contacting a substrate, these pins can print a few thousands of spots in one run. Here we developed an annealing process to release/minimize the residual stress formed during the fabrication process due to the mismatch between the thermal expansion coefficients of SU-8 and that of the substrate. The process made fabrication of long-straight free standing structures out of Epoxy SU-8 possible. (Chapter 3).

Next, we demonstrated examples of using cotton yarns for constructing capillary-driven microfluidic systems. We first modified the surface property of the

cotton to enhance its hydrophilicity, and then measured the flow resistance of the yarns. Subsequently we employed knots for both controlling the flow resistance, and making various microfluidic elements such as passive splitters, blenders and mixers out of yarns. We also quantified the mixing ratios of the proposed knotted mixers, and found that topologically different knots can make different mixing ratios. Finally, we made a web of knots, which can be used as a serial dilutor. (Chapter 4).

We also advanced the functionalities of microfluidic capillary systems at a conceptual level. We named the concept capillarics, in analogy to electronics. We developed a library of capillary elements and demonstrated that similar to electronic circuits, in which complex electronic devices can be made out of a limited number of electric elements, advanced capillary circuits can be made by combining a limited number of capillary elements. The first element we introduced were two novel architectures of capillary pumps that guide the progression of the filling front. Second, we presented other capillary elements including novel architectures of capillary valves for switching between liquids and timing the reactions. We then selectively assembled these elements with other microfluidic capillary elements, which had already been developed including flow resistors and capillary retention valves, to make a capillary circuit, which reverses

the flow and flushes four different chemicals in a predetermined sequence with a different flow rate selectively assembled these elements, and showed that using the circuit, we can measure the concentration of C-reactive antigen down to 100 ng/mL in 5 min. (Chapters 5&6).

The original contributions in this part were mainly the design and fabrication of 1st) two novel capillary pumps to accurately control the liquid filling front 2nd) two level robust capillary trigger valve 3rd) Programmable retention burst valves, 4th) a capillary circuit with liquid flow reversal, allowing to perform rapid one-step sandwich immunoassay with a possibility to have an amplification step.

7.2 Recommendations for future directions

Following these advancements in making capillary systems, a number of challenges remain unsolved. For example, most of the capillary circuits presented in Chapter 6 are made out of plasma-activated PDMS. These chips can keep their hydrophilicity only for ~20 minutes, and cannot be used to perform a long incubation time, which is required to achieve a high sensitive immunoassay. To circumvent this issue the circuits need to be fabricated out of materials that can keep their hydrophilicity over time. Microchips made of silicon with an oxide surface keep their hydrophilicity for a long period of time; however,

their costly fabrication process would prevent their use in making low cost diagnostic devices. Polymers which are either inherently hydrophilic or which can be activated while retaining the hydrophilicity for a long time may be exploited for making low cost capillaric circuits..

For some bioassays, such as fluorescence-linked immunosorbent assay (FLISA),[1] or sample preparation steps required for DNA sequencing methods,[2] it is essential to sequentially flow a large number of reagents over the captured reaction zone. [1,2] However, increasing the number of retention burst valves which can be reliably operated in parallel would be challenging (Chapter 6). This can be improved by introducing novel designs of retention burst valves. Also, portable, inexpensive detection systems such as electrochemical methods[3] can be integrated into capillary circuits for making point of care diagnostics. Upon overcoming these challenges the capillary circuits can be manufactured in high volumes and thus be used as low-cost high-sensitive point of care diagnostic devices.

This work also created various exciting prospects for future research. For example, the functionalities of capillaric circuits can be enhanced by introducing novel capillary elements, some of which are reminiscent of logic elements such

as XOR, XNOR and NAND, and some of which can be unique to the capillaric

circuits such as retention burst valves and the trigger valves.

Additionally, by selectively assembling capillaric elements we may develop

various capillaric circuits for different applications from cell or bacteria detections

to multiplex analysis of proteins with large dynamic range. For example

quantifying the concentrations of multiple proteins in a sample is essential for

precise diagnosis such as the evaluation of the risk of heart attack.[4] As for the

heart attacks, it is crucial to have a rapid point of care device, which can

precisely quantify the concentration of at least four biomarkers simultaneously.[5]

However, considering the large variation in the concentration of each biomarker

in a sample,[6] as well as the problem of cross reactivity[7] it is highly desirable to

perform each reaction in a separate reaction chamber, optimized for its pair.

Microfluidic capillary flow reversal can be arrayed to develop a robust one step

assay to analyze multiple proteins at once, while preventing the cross reactivity.

Overall we believe that the platforms of capillary microfluidics we demonstrated

in this thesis can be a step forward towards enabling these systems in the

context of spotting microarrays or point of care diagnostics.

7.3 References

1. Nwankire, C. E., Chan, D. S., Gaughran, J., Burger, R., Gorkin, R. & Ducrée, J. Fluidic Automation of Nitrate and Nitrite Bioassays in Whole Blood by Dissolvable-Film Based Centrifugo-Pneumatic Actuation. *Journal of Sensors* **9,** 11336-11349 (2013)

2. Shendure, J., Mitra, R.B., Varma, C. & Church, G.M., Advanced sequencing technologies: methods and goals. *Nature Reviews Genetics* **5**, 335-344, (2004)

3. Han, K.N., Li, C. A. & Seong, G. H., Microfluidic Chips for Immunoassays. *Annual Review of Analytical Chemistry* **6**, 119-141, (2013)

4. Vistnes, M., Christensen, G. & Omland, T. Multiple cytokine biomarkers in heart failure. *Expert Review of Molecular Diagnostics* **10**, 147-157 (2010).

5. Extended Dynamic Range on Multiplex panelPlus™ Sensors, Axela Inc., http://www.axelabiosensors.com, Retrieved 01/09/2013, (2013)

6. Araz, M.K., Tentori, A.M. & Herr, A.E. Microfluidic Multiplexing in Bioanalyses. *Journal of Laboratory Automation* (2013).

7. Pla-Roca, M., Leulmi, R.F., Tourekhanova, S., Bergeron, S., Laforte, V., Moreau, E., Gosline, S.J., Bertos, N., Hallett, M., Park, M. & Juncker, D. Antibody colocalization microarray: A scalable technology for multiplex protein analysis in complex samples. *Molecular & Cellular Proteomics* **11** (2012).

APPENDIX I

Commercial pin holder with a collimator
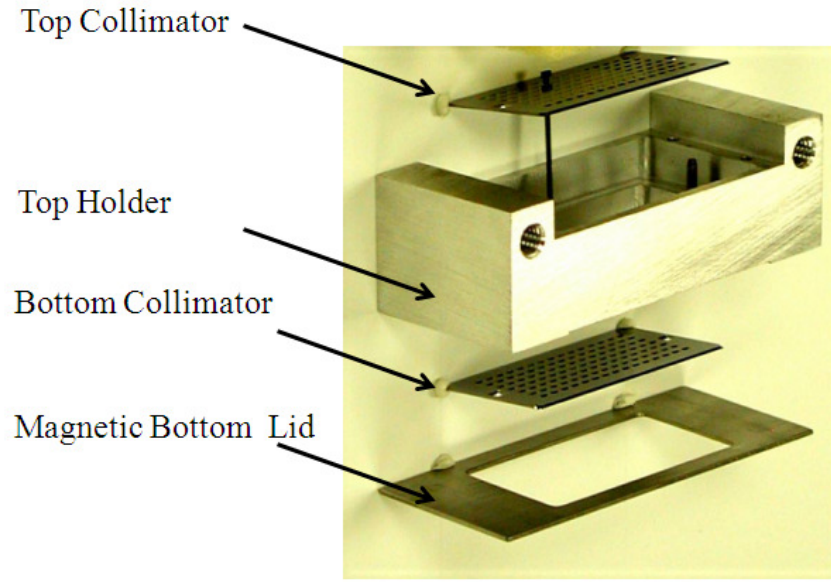
Fig. SI1: A disassembled view of the pin holder. Adapted from Parallel synthesis

Technologies Inc.[1]

Mechanical stability of the pins under applied capillary pressure

To approximate the tip deflection of these pins due to the capillary force, the

stress analysis was performed by a finite element calculation of the set of partial

differential equations (PDEs) for the system geometry using a commercially

available modeling package.[2] The capillary force was applied as a distributed

pressure on the microchannel, which can be calculated as:

$$P = +\frac{2\gamma}{t} - \frac{2\gamma\cos\theta_r}{w},$$ (S.1)

where w is the width of the channel, and $\theta_r=30°$ is the receding contact angle between liquid and the surface.[3] Tetrahedral elements were used to mesh the geometry. 570000 and 1800000 elements were used to approximate the displacement. No substantial changes were observed in the calculated results. So the finer mesh was used as the approximated value. Fig. SI. 1 illustrates the results. It can be observed that for the SU-8 pins, the deformation in the tip due to the capillary pressure is less than 1 µm for the case where the length of the microchannels is 7000 µm.
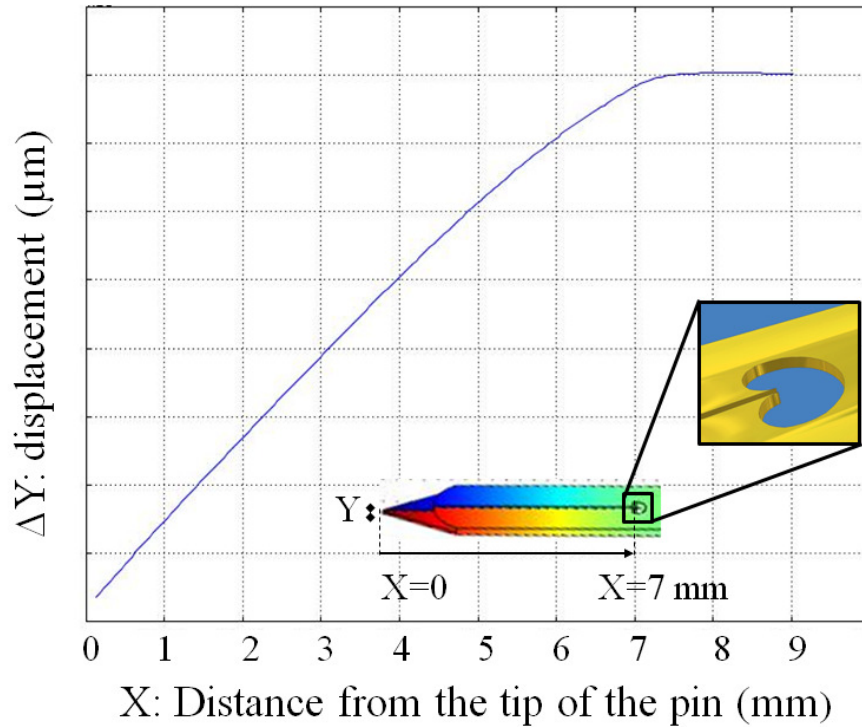
Fig. SI2: The effect of the capillary pressure on the elastic deformation of the microchannel in the polymer pins. Comsol multiphysics 3.4 was used to

approximate the deformation. The modeling is for the case where the length of the microchannel is 7000 μm. The maximum deflection is less than 2% of the size of the tip (i.e. 1 μm over 60 μm tip size)

Surface treatment of the pins
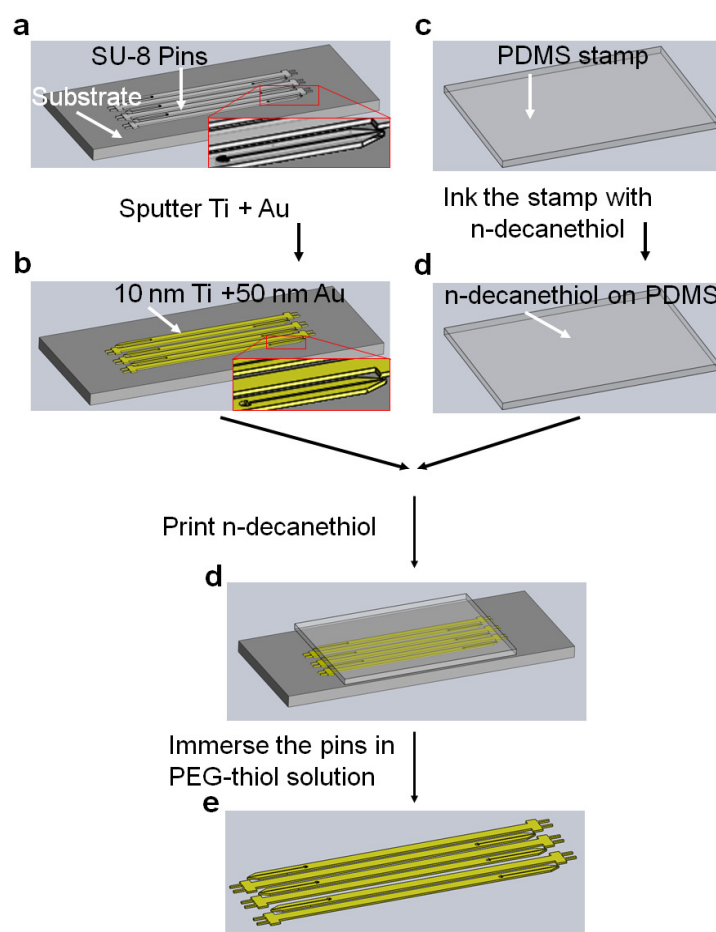
Fig. SI3: Surface treatment of the SU-8 pins. (a) 10 nm of Titanium and 50 nm of Gold were sputtered on the SU-8 pins. (b) To coat the PDMS stamp with a thin layer of n-decanethiol, the stamp was inked with a diluted solution of n-decanethiol in ethanol and blow dried. (c) In order to make the outer surface

hydrophobic the gold coated pins were printed with thiol. (d) The pins were immersed in the dilute solution of PEG thiol in water to make the µchannels hydrophilic.

Pins mounted in a customized ink-jet spotter
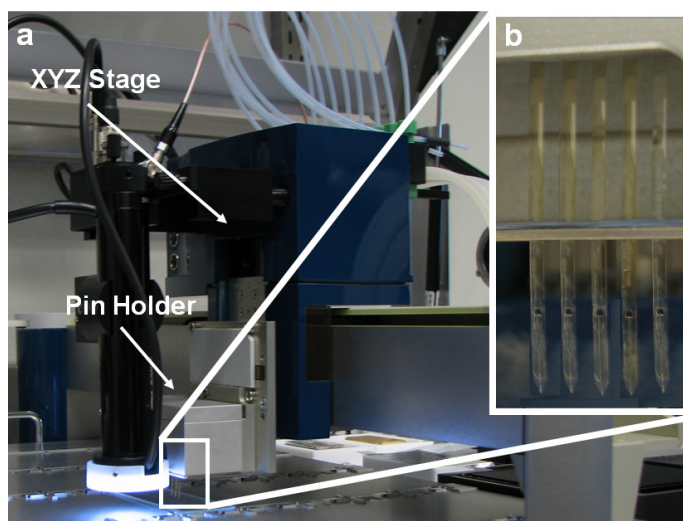
Fig. SI4: Customized ink-jet spotter. (a) Images of the pins mounted in a customized pin spotter (Nanoplotter 2.0, Gesim, Germany). (b) Close-up view of the pins mounted in the holder

Two channel pins
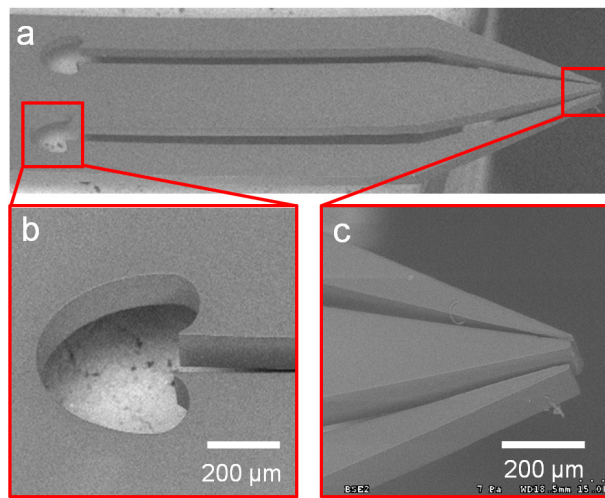
Fig. SI5: SEM images of the two channel pins to transfer larger amount of liquids. (a) Two channel pins. (b) Enlarged view of the stop valve. (c) Enlarged view of the tip of the pin.

Residual stress measurement
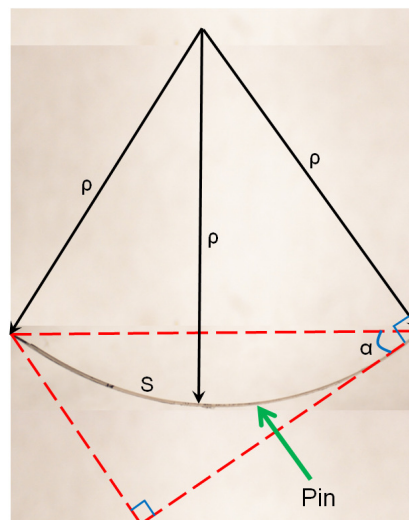
Fig. SI6: Approximating α with respect to ρ, the radius of the curvature of the pin, and *S,* the length of the pin

$$\rho = \frac{S}{2\alpha} \qquad (S.2)$$

Where S is the length of the curvature, which is 30 mm, and α is an angel between the tangent line to the curvature and a line connecting the two ends of the pin.

References

1. Parallel Synthesis Co., http://www.parallel-synthesis.com/, Retrieved 01/12/2008, (2008)
2. Comsol multiphysics 3.4, http://www.comsol.com/, Retrieved 06/06/2009, (2009)
3. Juncker, D., Schmid, H., Drechsler, U., Wolf, H., Wolf, M., Michel, B., de Rooij, N. & Delamarche, E. Autonomous microfluidic capillary system. *Analytical Chemistry* **74**, 6139-6144 (2002).

APPENDIX II

Calculation of the fluid concentration in the outlets of the serial dilutor

With reference to Fig. 4.5C, we perform a nodal analysis to calculate the flow rate ratio and concentration C_4 at outlet 4 (and the complementary concentration C_7 at outlet 7) as a function of the ratio between the resistance of one branch r and the outlet resistance given by nr with n being a proportionality factor. First we write the equations for the current at node A and B based on the unknown potential P_A and P_B:

$$\frac{P_1 - P_A}{(n+1)\times r} + \frac{P_1 - P_A}{n\times r} + \frac{P_B - P_A}{r} - \frac{P_A}{2\times r} = 0 \tag{SII.1}$$

$$\frac{P_1 - P_B}{n\times r} + \frac{P_A - P_B}{r} - \frac{P_B}{r} = 0 \tag{SII.2}$$

The equations can be simplified rewritten as:

$$P_A \times \frac{3\times n^2 + 7\times n + 2}{2\times n^2 + 2\times n} - P_B = P_1 \times \frac{2\times n + 1}{n^2 + n} \tag{SII.3}$$

$$-P_A + P_B \times \frac{2\times n + 1}{n} = P_1 \times \frac{1}{n} \tag{SII.4}$$

Multiplying equation SII.4 by $\dfrac{n}{2\times n + 1}$ and combining equations SII.3 and SII.4 together we obtain:

$$P_A = \frac{10\times n^2 + 10\times n + 2}{4\times n^3 + 15\times n^2 + 11\times n + 2} \times P_1 \tag{SII.5}$$

$$P_B = \frac{14\times n^3 + 25\times n^2 + 13\times n + 2}{4\times n^3 + 15\times n^2 + 11\times n + 2} \times P_1 \tag{SII.6}$$

To identify the concentration of the liquid at the exit 4, and 7, we need to determine the ratio of the flow rates of $K = \dfrac{Q_2}{Q_1}$, where $Q_1 = \dfrac{P_A}{2 \times r}$, and $Q_2 = \dfrac{P_A - P_B}{r}$.

Thus,

$$K = \frac{Q_2}{Q_1} = \frac{3 \times n^2 + n}{5 \times n^2 + 5 \times n + 1} \tag{SII.7}$$

Having the flow ratios, the concentration of fluid 2 in exit 4, C_4, can be approximated using a weighted average of the concentrations of each branch,

$$C_4 = \frac{C_1 \times Q_1 + C_2 \times Q_2}{Q_1 + Q_2} \tag{SII.8}$$

where $C_1 = 0$ and $C_2 = 0.5$

Substituting the concentrations of the liquids and the flow rates in to the eq. SII.8 we have:

$$C_4 = \frac{0.5}{K + 1} \tag{SII.9}$$

and similarly the concentration of fluid at exit 7 is given by the ratios of the mirror flow rates Q_1' and Q_2', and the concentrations C_1' and C_2'. Using the fact that $C_4 + C_7 = 1$ we find:

$$C_7 = \frac{C_1' \times Q_1' + C_2' \times Q_2'}{Q_1' + Q_2'} = \frac{K + 0.5}{K + 1} \tag{SII.10}$$

Fig. SII.4 shows how the concentrations of the liquid in exits 4 and 7 vary with respect to n.
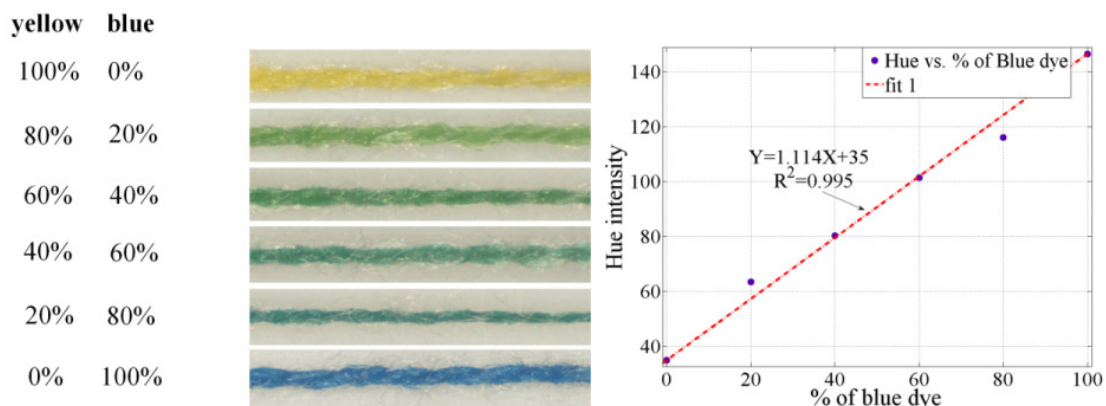
Fig. SII1: Palette of yarns soaked with mixtures of yellow and blue dyes with varying ratios that serve as calibration curve for evaluating the mixing properties of knots. (A) Images obtained from cotton yarns soaked into solutions with different ratios of blue and yellow dyes as indicated on the left; (B) Hue intensities of various concentrations of blue/yellow dyes measured from the pictures in (A). The graph shows that the hue intensities are well approximated by a line with respect to the concentration of blue/yellow dyes.
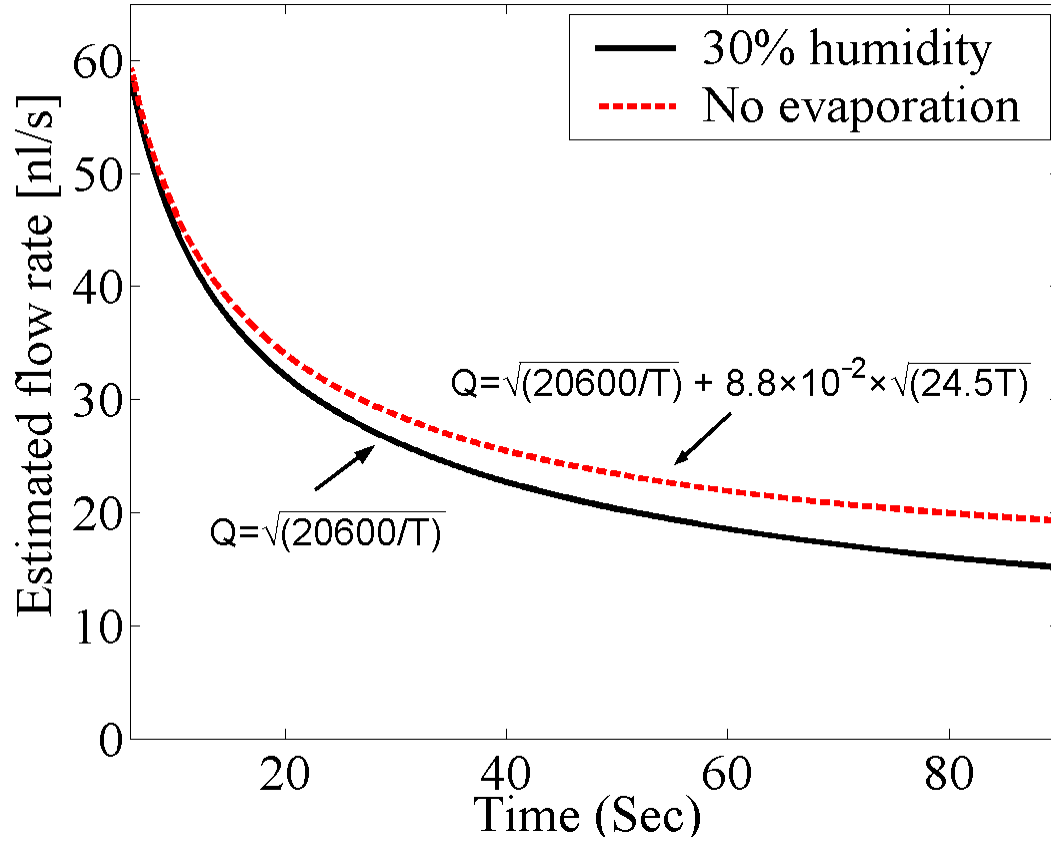
Fig. SII2: Experimental flow rate at the filling front of the yarn measured with a relative humidity of 30% and best fit (black line). The dashed, red line represents the flow rate without evaporation based on the calculations of eq. 2 and a thread diameter of 500 μm and a temperature of 20°C. The flow rate at 40 s is 22.7 nL/s with 30% humidity and 25.4 nL/s without evaporation, corresponding to a difference of ~10 %.
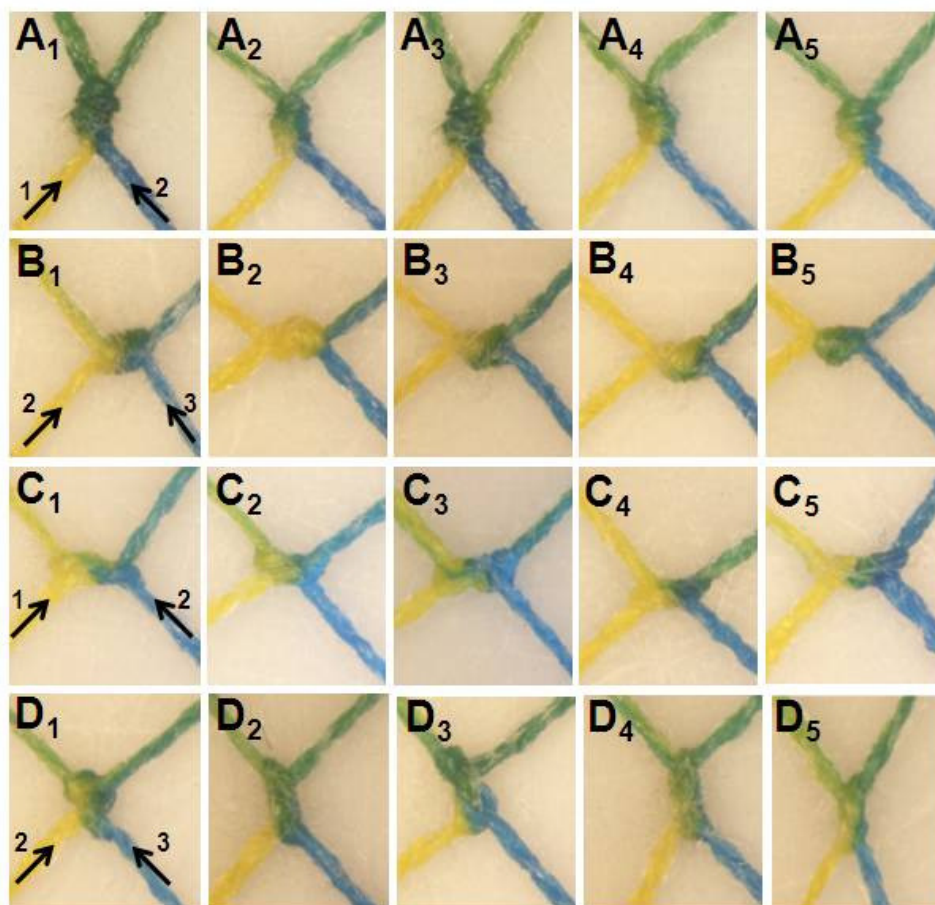
Fig. SII3: Images illustrating the reproducibility of the mixing ratios obtained using topologically different knots to mix a yellow and a blue liquid applied to the two inlets. (A_1- A_5) Five replicates of overhand knots produced mixing ratios of 50.4 % (±6.3%) and 49.6% (±6.2%) concentrations of yellow dye for the left and right outlets respectively. The values in parentheses are SE. (B_1- B_5) mixing of 5 overhand knots rotated 90°, which results in almost complete separation of the dyes in each outlet with 99.1% (± 3.8%) and 0.9% (±0.8%) of yellow dye for the left and right outlets. (C_1- C_5) mixing results for hunter's knot, which lead to almost total separations of the dyes in each outlet with 95% (±5.1%) and 5%

(±4.3%) concentrations of yellow dye for the left and right outlets respectively.

(D_1- D_5) For Hunter's knot rotated by 90°, the mixing ratios are 71.5% (±4%) and

28.5% (±4.7%) of the yellow dye for the left and right outlets, respectively.
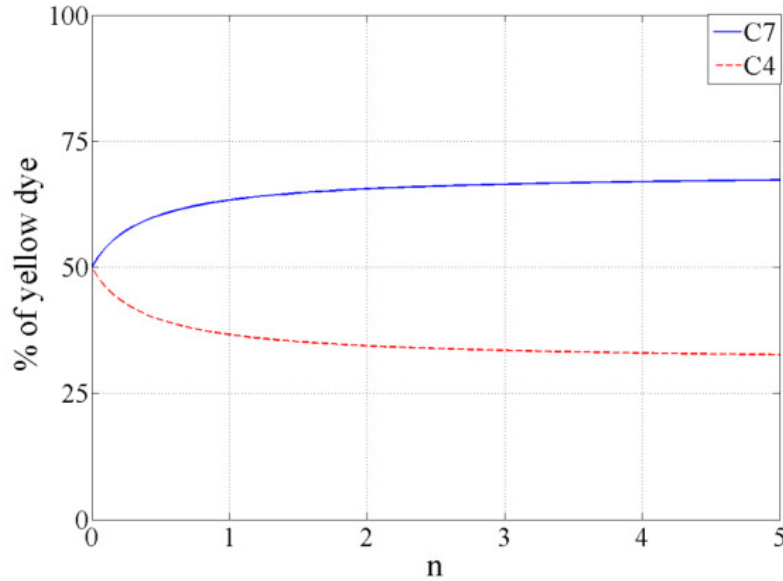
Fig. SII4: Concentrations of blue dyes at outlets 4 and 7 with respect to the ratio

n with the flow resistance of each branch assumed to be r and the flow

resistance of the outlet yarns to be nr. For n=0 (i.e. by placing a capillary paper

on each of the peripheral knots), 50% of blue and 50% of yellow dyes will be

found in each of the outlets. As "n" increases, the value asymptotically converges

68.75% of the ipsilateral solution and 31.25% of the contralateral solution for both

C4 and C7. In the experimental setting, the outlet length was much longer than a

branch and thus n>1.
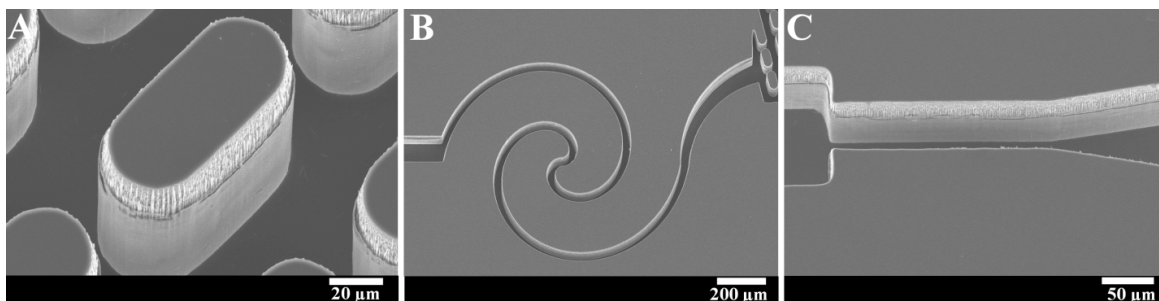
Fig. SIII1: SEM micrographs of a three elements in the capillary system to test the capillary pump. (A) close up view of a pillar in the CPs featuring a rectangular shape with rounded corners with a size of 40×80 µm²; (B) enlarged view of the external flow resistor in the circuit. The width of the resistor is 30 µm and the overall length is 3400 µm; (C) capillary retention valve (CRV) at the end of the loading port, which pins the liquid once the loading port is emptied, and avoids the full drainage of the main channel.

Pore network analysis for calculating the equivalent flow resistance in the pump structures

In pore network modeling, it is postulated that the passing fluid experiences a channel-like flow between posts. The flow resistance in each pore formed by the gap between two neighboring posts can be obtained from Eq. 5.3. Fig. SIII2 illustrates the flow resistance model of the typical serpentine CP.
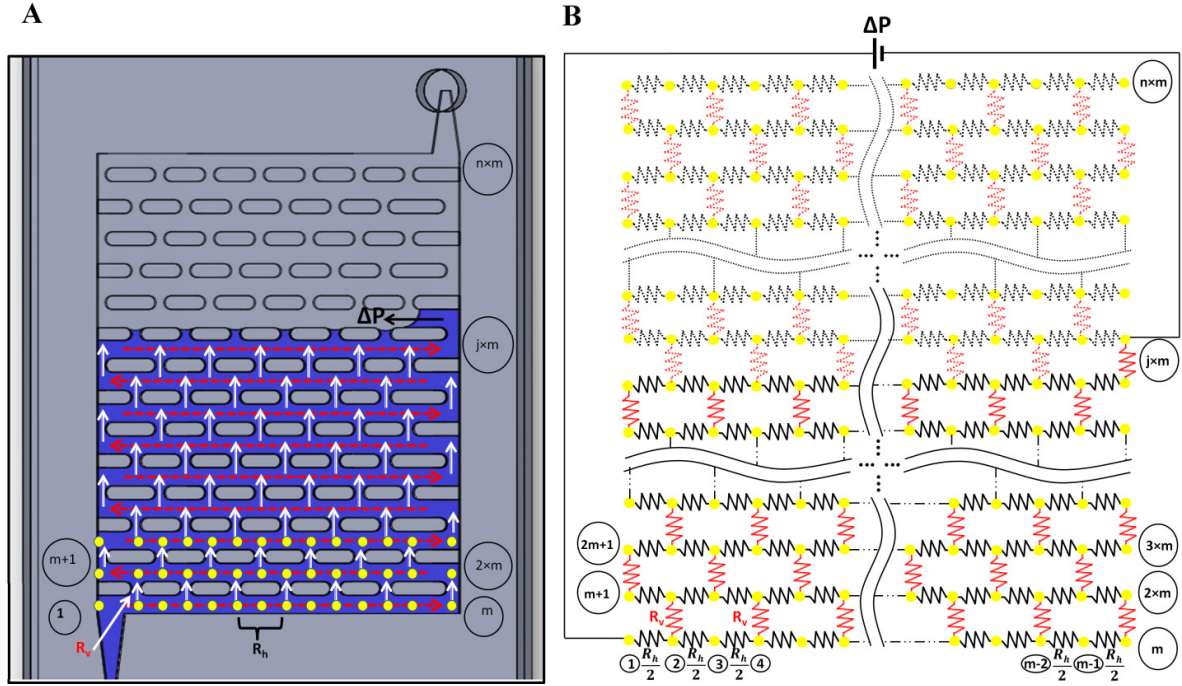
Fig. SIII2: Flow resistance model of the CP. (A) Schematic of the typical serpentine CP with no external resistor; the yellow circles represent the nodes; (B) lumped resistance model of the CP;

The network of the resistors consist of R_v, the vertical flow resistance formed between two neighboring posts in the same row, and R_h, the horizontal flow resistance formed by the gap between the posts in two neighboring rows. Fig. SIII3 illustrates both R_h and R_v.
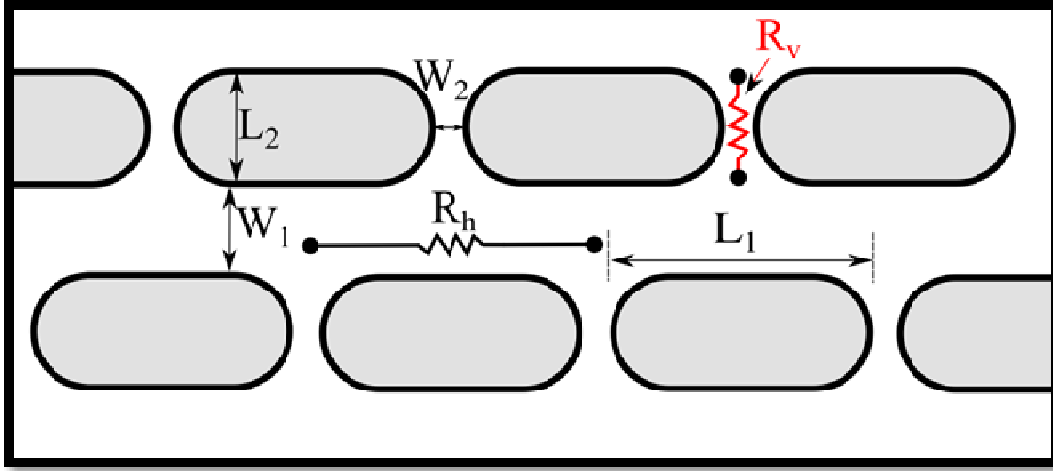
Fig. SIII3: Schematic illustrating the geometry of the CP features used to calculate the flow resistances R_h and R_v. W_1 is the gap between two neighboring rows; W_2 is the gap between two neighboring pillars in one row. The pillars are rectangular shape with rounded corners. L_1, is the length of a pillar, and is used as the effective length to calculate R_h. L_2 is the width of the pillars and is used to calculate as the effective length for R_v.

Tamayol *et al.*[22] have shown that the suitable length scale for determining the pressure drop between adjacent cylinders is the minimum gap size. Thus, W_2 is selected as the width that should be used in Eq. for determining R_v. In the typical serpentine CP, $W_1=35$ µm, $W_2=15$ µm, $L_1=80$ µm, $L_2=40$ µm, $h=100$ µm, and we used water as a working fluid with the viscosity of $\mu=10^{-3}$ Pa s.

Substituting the dimensions in the Eq. 5.3, we have $R_h=3.99\times10^{11}$ Pa s m^{-3} and $R_v=9.90\times10^{11}$ Pa s m^{-3}. Considering that $R_v \gg R_h$, and for the sake of its

simplicity, we assumed that CP is formed with an array of pillars in in-lined configuration rather than the staggered ones. Fig. SIII4 illustrates the simplified lumped resistance model of the CP.
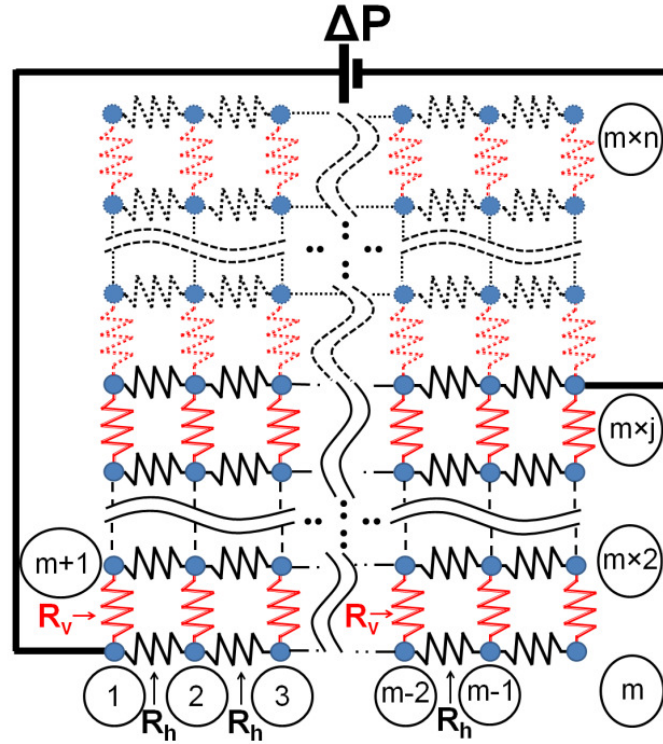

Fig. SIII4: Schematic illustrating the simplified lumped resistance model of the CP. Here we assumed that the pillars in the CP are in the inline configuration.

To calculate the equivalent resistance between two desired nodes in a network of resistances, we used the modified nodal analysis approach. The rationale for the algorithm has been well explained by Ruehli *et al.*.[25] In summary, we first establish the matrix of the flow conductance from kirchoff's circuit law so that for each node:

$$C \times P = Q \qquad\qquad (SIII.1)$$

Afterwards, by assigning a unit value for the current between the two desired nodes (the equivalent of the flow rate, Q), we calculate the P values for those nodes, and by dividing the P over Q, the equivalent of the flow resistance is calculated.

As for the circuit, shown in Fig. SIII4, the calculated conductance matrix, C has the dimension of (j×m)×(j×m), and equals to:

$$(SIII.2)$$

, where $C_h = \dfrac{1}{R_h}$ and $C_v = \dfrac{1}{R_v}$. Also the diagonal elements of the conductance matrix, is a (j×m) matrix and equals to:

$$
\text{Nodes in the first and last columns} \quad M =
\begin{bmatrix}
C_h + C_v & 2\times C_h + C_v \cdots & \cdots 2\times C_h + C_v & C_h + C_v \\
C_h + 2\times C_v & 2\times\left(C_h + C_v\right)\cdots & \cdots 2\times\left(C_h + C_v\right) & C_h + 2\times C_v \\
C_h + 2\times C_v & 2\times\left(C_h + C_v\right)\cdots & \cdots 2\times\left(C_h + C_v\right) & C_h + 2\times C_v \\
\vdots & \vdots \cdots \quad \cdots \vdots & \cdots \vdots & \vdots \\
C_h + 2\times C_v & 2\times\left(C_h + C_v\right)\cdots & \cdots 2\times\left(C_h + C_v\right) & C_h + 2\times C_v \\
C_h + 2\times C_v & 2\times\left(C_h + C_v\right)\cdots & \cdots 2\times\left(C_h + C_v\right) & C_h + 2\times C_v \\
C_h + C_v & 2\times C_h + C_v \cdots & \cdots 2\times C_h + C_v & C_h + C_v
\end{bmatrix}_{(j\times m)}
$$

(SIII.3)

Once we constructed the conductance matrix, we will assign 1 to the $Q_{1,1}$, and -1 to $Q_{j\times m,1}$, and then solve the set of equations to find the value of $P_{1\times1}$ and $P_{j\times m,1}$, as:

$$
\left[C\right]_{(j\times m)\times(j\times m)} \times
\begin{bmatrix}
P_{1,1} \\
P_{2,1} \\
\vdots \\
P_{j\times m-1,1} \\
P_{j\times m,1}
\end{bmatrix}_{(j\times m,1)}
=
\begin{bmatrix}
+1 \\
0 \\
\vdots \\
0 \\
-1
\end{bmatrix}_{(j\times m,1)}
$$

(SIII.4)

Finally, the resistance between the node 1 and j×m, can be calculated as

$$
R = \frac{P_{1,1} - P_{(j\times m),1}}{Q_{(j\times m),1}} = P_{(j\times m),1} - P_{1,1}
$$

(SIII.5)

Static and advancing contact angle between DI water and different surfaces of the CP
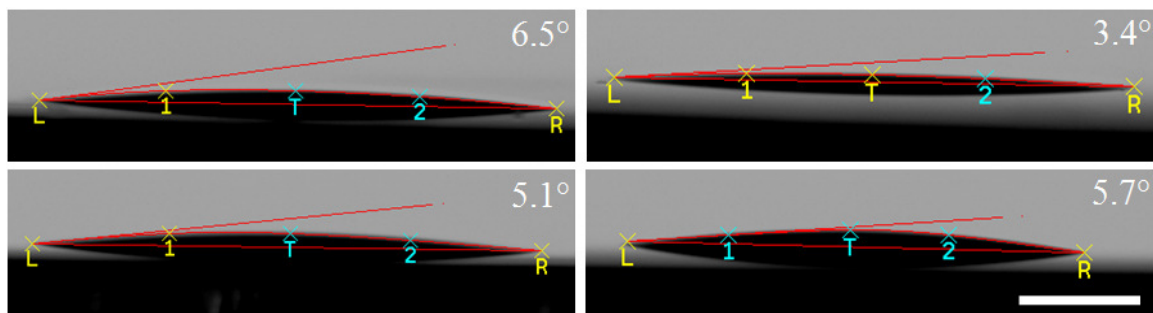

Fig. SIII5: Static contact angle between DI water and flat Si, which was rendered hydrophilic by flaming them for ~45 s until they became glowing red. Each image illustrates an independent measurement. The measured static contact angle is 5.2°±0.6°. The scale bar is 500 µm.
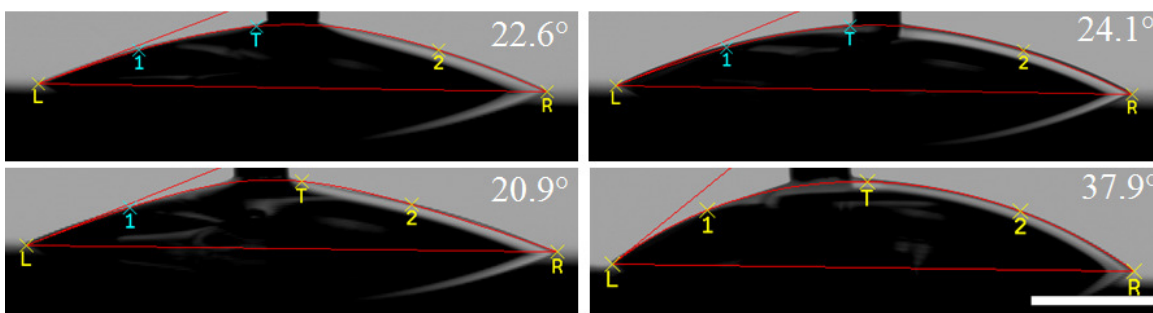

Fig. SIII6: Advancing contact angle between DI water and a flat Si, rendered hydrophilic by flaming. The advancing contact angle measured from four independent experiments is 26.4°±3.3°. The scale bar is 500 µm.
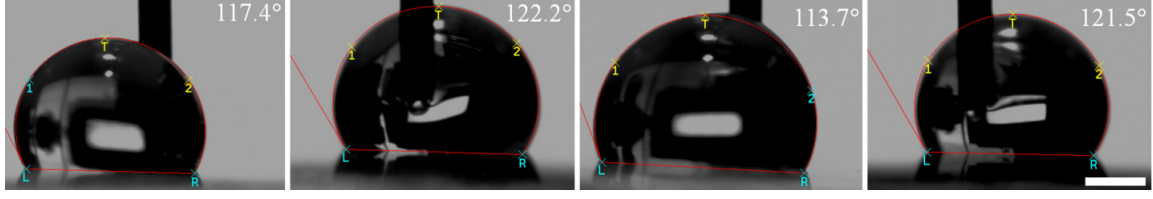
Fig. SIII7: Advancing contact angle between DI water and a flat PDMS. The advancing contact angle measured from four independent experiments is 118.7°±1.7°. The scale bar is 300µm.

Calculation of the relative change in the capillary pressure with respect to the liquid progression in the advanced CP (with variable capillary pressure):

Variation of the free surface energy of a liquid, known as the Gibbs free energy, between two known states is expressed as:

$$\Delta G = \sum_{i=t,b,l,r} \left(\gamma_{LV_i} \times \Delta A_{LV_i} + \gamma_{SV_i} \times \Delta A_{SV_i} + \gamma_{SL_i} \times \Delta A_{SL_i} \right) \qquad \text{(SIII.6)}$$

where ΔA_{LV}, ΔA_{SV}, and ΔA_{SL} are the respective changes of interfacial areas between liquid, solid, and air (i.e. L,S and V).Also , γ_{LV}, γ_{SV}, and γ_{SL} are the surface tensions associated between two phases (i.e. L, S, and V). The subscripts i=t,b,l, and r indicate the associated area and the surface tension of the top, bottom, left, and right walls.

Considering that in our CP, the liquid fills the pump row by row, if we define the unit cells in the CP, as the space between two rows, which is illustrated in Fig. SIII7.

$$\sum_{i=t,b,l,r}\left(\Delta A_{LV_i}\right)=0 \tag{SIII.7}$$

$$\Delta A_{LV_t}=-\Delta A_{SV_t} \tag{SIII.8}$$

$$\Delta A_{SL_b}=-\Delta A_{SV_b} \tag{SIII.9}$$

$$\Delta A_{SL_l}=\Delta A_{SL_r}=-\Delta A_{SV_l}=-\Delta A_{SV_r} \tag{SIII.10}$$

Thus, the energy gain between a filled and no filled row can be calculated as:

$$\Delta G_j=\left((\gamma_{SV}-\gamma_{SL})\times\Delta A_{SV}\right)_t+\left((\gamma_{SV}-\gamma_{SL})\times\Delta A_{SV}\right)_b+2\times\left((\gamma_{SV}-\gamma_{SL})\times\Delta A_{SV}\right)_r \tag{SIII.11}$$

On the other hand, the partial change of Gibbs free energy with capillary pressure can be obtained from Leverett *et al.*[31] as:

$$\frac{\Delta G_j^L}{\Delta P_j}=V_j^L \tag{SIII.12}$$

where ΔP_j is the average capillary pressure in the unit cell, j, and V_j^L is the volume of the liquid transferred in the unit cell.

Also from Young's law, we have:

$$\left(\gamma_{SV}-\gamma_{SL}\right)_i=\gamma_{LV}\times\cos\theta_i \tag{SIII.13}$$

, where γ_{LV} is the surface tension of the liquid (i.e. water) and θ_i is the dynamic contact angle of the liquid-air meniscus in the desired surface.

Combining eqs. (SIII.11) and (SIII.13) result in:

$$\Delta G_j = \gamma_{LV} \times \left(\cos\theta_t \times \Delta A_{SV_t} + \cos\theta_b \times \Delta A_{SV_b} + 2 \times \cos\theta_r \times \Delta A_{SV_r} \right) \qquad \text{(SIII.14)}$$

By replacing eq. (SIII.14) in eq. (SIII.12), the average capillary pressure of a post can be obtained as:

$$\Delta P_j = \frac{\gamma_{LV} \times \left(\cos\theta_t \times \Delta A_{SV_t} + \cos\theta_b \times \Delta A_{SV_b} + 2 \times \cos\theta_r \times \Delta A_{SV_r} \right)}{V_j^L} \qquad \text{(SIII.15)}$$

The unit cell in the typical serpentine CP in Fig. 5.4 has the width of 75 µm and the length of 95 µm, thus the generated capillary pressure is calculated as:

$$\Delta P = \frac{7.2 \times 10^{-2} \times \begin{pmatrix} \cos(118.7^o) \times (75 \times 95 - 2856) \times 10^{-12} + \\ \cos(26.4^o) \times (75 \times 95 - 2856) \times 10^{-12} + \\ 2 \times \cos(26.4^o) \times 100 \times 10^{-6} \times 102.8 \times 10^{-6} \end{pmatrix}}{(75 \times 95 - 2856) \times 10^{-12} \times 100 \times 10^{-6}} = 3375 \quad Pa$$

The value of the estimated capillary is based on the measured advancing contact angles in Figs SIII6 & SIII7. If we consider the effects of the dynamic contact angles the capillary pressure decreases to ~3100 Pa.

The advancing and dynamic contact angles between water as the working liquid and surfaces of the CP are illustrated in Table SIII1. The dynamic contact angles were calculated from eq. 5.8 in the paper.

Table SIII1: contact angle between water and the surfaces of the CP

	Advancing Contact angle	Dynamic contact angle at filling front speed of 5 mm/s	Dynamic contact angle at filling front speed of 2 mm/s
Top surface	118.7°	119.1°	118.8°
Bottom, Right and Left surfaces	26.4°	29°	27.3°

Having the contact angles and geometry of the unit cell in the CP, the average

capillary pressure in row 8 and 34 of the advanced CP can be calculated as:

$$\Delta P_8 = \frac{7.2\times10^{-2}\times\left(\begin{array}{c}\cos\left(119.1^o\right)\times6489\times10^{-12} + \cos\left(29^o\right)\times6489\times10^{-12} + \\ 2\times\cos\left(29^o\right)\times100\times10^{-6}\times102.8\times10^{-6}\end{array}\right)}{6489\times10^{-12}\times100\times10^{-6}} = 2078 \quad Pa$$

$$\Delta P_{34} = \frac{7.2\times10^{-2}\times\left(\begin{array}{c}\cos\left(118.8^o\right)\times14994\times10^{-12} + \cos\left(27.3^o\right)\times14994\times10^{-12} + \\ 2\times\cos\left(27.3^o\right)\times100\times10^{-6}\times102.8\times10^{-6}\end{array}\right)}{14994\times10^{-12}\times100\times10^{-6}} = 1046 \quad Pa$$

Having, ΔP_8 and ΔP_{34}, the ratio of the average capillary pressure generated in

row 8th over that in row 34th is $\frac{\Delta P_8}{\Delta P_{34}} = 2$. Also, since the width of the unit cells in

each row of the CP equals to 105 µm, $\frac{\Delta P_8}{\Delta P_{34}}$ gives the ratio of the average

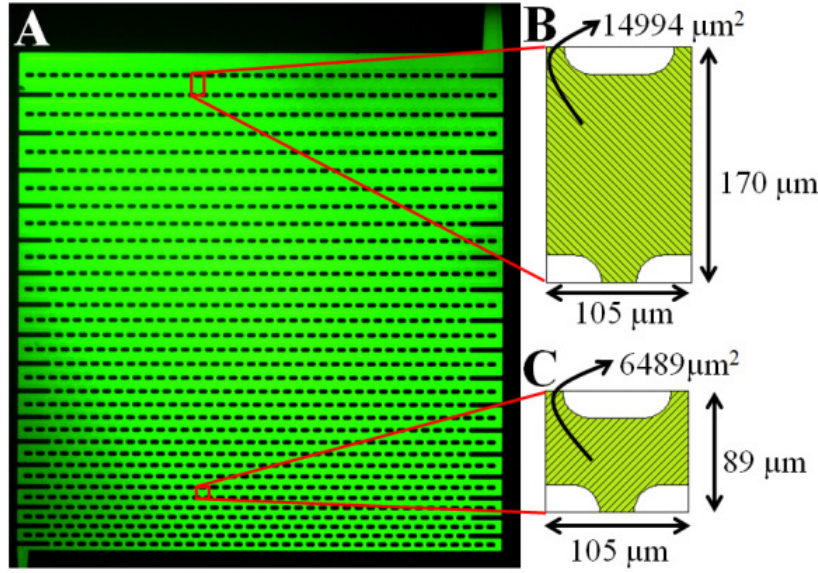capillary pressure generated in row 8 over that in row 34.

Fig. SIII8 illustrates the geometrical parameters of the unit cells in rows 8th and 34th respectively.

Fig. SIII8: CP with variable capillary pressure, and the unit cells defined to calculate the ratio of the capillary pressures from one row to the other. (A) The CP shown in Fig. 5A with two unit cells defined on the 34th row and the 8th row; (B) enlarged schematic of the unit cell in the 34th row. The cell is rectangular shape with the dimensions of 170×105 μm^2 in which a pillar has been subtracted from. The overall area of the cell is 14994 μm^2; (C) the cell in the 8th row, with the area of 6489 μm^2.